Bicyclo[3.3.1]nonanes as Scaffolds in Supramolecular Chemistry

From Host-Guest Systems to Hydrogen-Bonded Aggregates

Lidskog, Anna

2023

Document Version:
Publisher's PDF, also known as Version of record

Bicyclo[3.3.1]nonanes as Scaffolds in Supramolecular Chemistry

From Host-Guest Systems to Hydrogen-Bonded Aggregates

ANNA LIDSKOG | CENTRE FOR ANALYSIS AND SYNTHESIS | LUND UNIVERSITY

Printed by Media-Tryck, Lund 2021 NORDIC SWAN ECOLABEL 3041 0903

ISBN 978-91-7422-988-2

Centre for Analysis and Synthesis
Department of Chemistry
Faculty of Science
Lund University

LUND UNIVERSITY

Bicyclo[3.3.1]nonanes as Scaffolds in Supramolecular Chemistry

Bicyclo[3.3.1]nonanes as Scaffolds in Supramolecular Chemistry

From Host-Guest Systems to Hydrogen-Bonded Aggregates

Anna Lidskog

LUND
UNIVERSITY

DOCTORAL DISSERTATION
Doctoral dissertation for the degree of Doctor of Philosophy (PhD) at the Faculty of Science at Lund University to be publicly defended on November 24th, 2023, at 09.00 in Lecture Hall KC:A, Kemicentrum

Faculty opponent
Assoc. Prof. Sophie Beeren, DTU, Department of Chemistry

Organization: LUND UNIVERSITY

Document name: Doctoral dissertation **Date of issue:** 2023-10-31

Author: Anna Lidskog

Title and subtitle: Bicyclo[3.3.1]nonanes as Scaffolds in Supramolecular Chemistry:

From Host-Guest Systems to Hydrogen-Bonded Aggregates

Abstract:

This thesis describes the use of bicyclo[3.3.1]nonane and its heteroanalogue 1,5-diazabicyclo[3.3.1]nonane as scaffolds in different supramolecular systems. The thesis is divided into two parts, with the first part (chapter 2–4) focusing on the development and applications of a synthetic receptor based on a Tröger's base motif fused with 18-crown-6 moieties. In chapter 3, NMR titration methodology was used to determine relative association constants and binding energies of the binding between the receptor and differently substituted bisammonium ligands. A small but evident discrimination based solely on the substituent was found, with phenyl- and methyl-substituted ligands forming stronger receptor-ligand complexes than ligands with no or larger substituents. By combining the estimated relative binding energies with results from conformational analyses of the receptor-ligand complexes, the free binding energies between a methyl or a phenyl group and an aromatic cavity were estimated to -0.40 and -0.80 kcal/mol, respectively, which is comparable to previously reported values for similar CH-π and π-π interactions.

In chapter 4, the consecutive binding of potassium ions to the same ditopic receptor in water is studied. ITC experiments revealed a counterintuitive result: that the binding of the second potassium ion is enthalpically favored compared to the binding of the first. A combination of experiments and simulations were employed to investigate how different factors influence the thermodynamics of the binding process, resulting in the finding that both the counterion and intrinsic favorable interactions between the two potassium-bound crown-ethers contribute to the observed thermodynamic trends. Although further investigations are needed to fully elucidate the different contributions, the herein presented study offers valuable insights into factors affecting receptor/ligand interactions in water.

The second part of the thesis (chapter 5–6) describes hydrogen-bonding monomers capable of self-assembling into cyclic and tubular aggregates. With the aim of developing amphiphilic monomers, polyethylene glycol (PEG) chains were introduced to the bicyclic backbone of the monomers. The synthesis and self-assembly of two new PEGylated monomers is described and compared to previously reported alkylated analogues. Both new monomers were capable of forming hydrogen-bonded cyclic aggregates. The effect of the PEG chains on the aggregate stability was found to depend on the hydrogen bond strength. One of the monomers exhibited the desired amphiphilicity and could be extracted from an aqueos solution into a chloroform solution, where self-assembly into cyclic tetramers occurred.

Key words: supramolecular chemistry, host-guest chemistry, non-covalent interactions, hydrogen bonding, aromatic interactions, electrostatic interactions, synthetic receptors, self-assembly, nanotubes

Language English

ISBN: 978-91-7422-988-2 (printed)

978-91-7422-989-9 (electronic) **Number of pages**: 110

Bicyclo[3.3.1]nonanes as Scaffolds in Supramolecular Chemistry

From Host-Guest Systems to Hydrogen-Bonded Aggregates

Anna Lidskog

LUND
UNIVERSITY

Front and back cover by Samuel Lidskog

Faculty of Science
Department of Chemistry
Centre for Analysis and Synthesis

ISBN 978-91-7422-988-2
ISSN 978-91-7422-989-9

Printed in Sweden by Media-Tryck, Lund University
Lund 2023

Table of Contents

Populärvetenskaplig sammanfattning

Supramolekylär kemi kan beskrivas som ”kemi bortom molekylen”. Det är ett forskningsområde som fokuserar på strukturer som består av flera molekyler som hålls samman av icke-kovalenta interaktioner så som vätebindningar och hydrofoba effekter. Till skillnad från kovalenta bindningar, som uppstår genom att atomer delar elektronpar mellan sig och bildar molekyler, så består icke-kovalenta interaktioner av svagare, reversibla interaktioner mellan molekyler. Även om icke-kovalenta interaktioner oftast är betydligt svagare än kovalenta bindningar så spelar de en väldigt viktig roll i naturen, till exempel för DNA-molekylens dubbelhelixstruktur och interaktioner mellan läkemedelsmolekyler och deras avsedda receptorer.

Forskning inom supramolekylär kemi handlar både om att studera och försöka förstå dessa icke-kovalenta interaktioner och om att utveckla nya supramolekylära system och material. Sådana system kan till exempel bestå av syntetiska receptorer (värdar) som innehåller bindningsställen där molekyler (gäster) kan bindas in med hjälp av icke-kovalenta interaktioner. Detta kallas också för värd-gästkemi eller molekylär igenkänning. Syntetiska receptorer kan till exempel användas som förenklade modeller för mer komplicerade biologiska system eller som sensorer för specifika substanser. En annan typ av supramolekylära system består av flera mindre komponenter (monomerer) som spontant associerar och bildar större strukturer, till exempel kapslar eller rör.

Den här avhandlingen handlar om utvecklingen av nya supramolekylära system baserade på en liten bicyklisk molekyl, bicyklo[3.3.1]nonan. Bicyklo[3.3.1]nonan består av två ringar som sitter ihop på ett sätt som ger en stel, böjd molekyl. Den vinklade molekylen är en bra bas för supramolekylära komponenter som kräver en specifik tredimensionell form. I första delen av den här avhandlingen har den bicykliska molekylen använts för att utveckla en syntetisk receptor som kan binda in olika positivt laddade joner. I en första studie användes receptorn för att studera icke-kovalenta interaktioner mellan olika grupper och en opolär del av receptorn, liknande vad som kan återfinnas mellan korta peptidkedjor och proteiner i naturen. I en andra studie användes samma receptor för att binda in kaliumjoner, där olika termodynamiska trender observerades och undersöktes. Båda dessa studier syftar till att ge ökad förståelse för hur olika faktorer kan påverka icke-kovalenta interaktioner i värd-gästkomplex.

Den senare delen av avhandlingen beskriver utvecklandet av monomerer som kan självassociera via vätebindningar och bilda supramolekylära ringar och nanorör. Genom att sätta fast polyetylenglykolkedjor på monomererna så kan deras löslighet i mer polära lösningsmedel, till exempel vatten, ökas. Målet var att utveckla monomerer som kan lösas i vatten, där vattenmolekylerna kommer hindra dem från att bilda vätebindningar och självassociera, och sedan överföras till ett organiskt lösningsmedel, där de kan självassociera och bilda till exempel rör. En framtida

förhoppning är att den här typen av system ska kunna infogas i cellmembran, där de självassocierade nanorören kan fungera som kanaler för transport av olika substanser genom membranet.

List of papers

This thesis is based on the following papers, referred to by their Roman numerals:

I. Experimental and Computational Models for Side Chain Discrimination in Peptide-Protein Interactions

A. Lidskog, S. Dawaigher, C. Solano Arribas, A. Ryberg, J. Jensen, K. E. Bergquist, A. Sundin, P.-O. Norrby, K. Wärnmark

Chem. Eur. J. **2021**, *27*, 10883-10897

Contributions: I synthesized and characterized most of the ligands and all of the receptor-ligand complexes. I performed MM and DFT calculations, as well as MD simulations. I performed the conformational analysis of the ligands and the receptor-ligand complexes. I wrote and compiled the supporting information. I wrote and revised the manuscript with input from the coauthors.

II. Counterintuitive Electrostatics upon Metal Ion Coordination to a Receptor with Two Homotopic Binding Sites

V. Aspelin, A. Lidskog, C. Solano Arribas, S. Hervø-Hansen, B. Stenqvist, R. Chudoba, K. Wärnmark, M. Lund

J. Am. Chem. Soc. **2022**, 144, 2921-2932

Contributions: I synthesized the receptor and performed the ITC experiments. I contributed to analyzing the data. I co-wrote the revised version of the manuscript.

III. Design and Synthesis of Amphiphilic Monomers for Cyclic and Tubular Hydrogen-Bonded Self-Assembly

A. Lidskog, A. Neniškis, S. Edin, Z. Takacs, E. Orentas, K. Wärnmark

Manuscript

Contributions: I synthesized and characterized the majority of the compounds. I performed the NMR studies of the monomers/aggregates. I participated in the DOSY experiments. I performed the solubility studies. I performed the modelling and molecular dynamics simulations. I wrote the manuscript and the supporting information.

Publications not included in the thesis:

IV. Enantiotopic Discrimination by Coordination-Desymmetrized meso-Ligands

Y. Li, A. Lidskog, H. Armengol-Relat, T. H. Pham, A. Favraud, M. Nicolas, S. Dawaigher, Z. Xiao, D. Ma, E. Lindbäck, D. Strand, K. Wärnmark

ChemCatChem, **2020**, *12*, 1575-1579

V. Asymmetric Ring-Opening of Epoxides Catalyzed by Metal-Salen Complexes

A. Lidskog, Y. Li, K. Wärnmark

Catalysts **2020**, *10*, 705

Abbreviations

A	Hydrogen bond acceptor
AFM	Atomic force microscopy
AIBN	Azobisisobutyronitrile
BTA	Benzene-1,3,5-tricarboxamide
CIS	Complexation-induced changes in chemical shift
COSY	Correlation spectroscopy
D	Hydrogen bond donor
DFT	Density-functional theory
DLS	Dynamic light scattering
DMF	Dimethyl formamide
DMSO	Dimethyl sulfoxide
DOSY	Diffusion-ordered spectroscopy
ESI	Electrospray ionization
GPC	Gel permeation chromatography
HPLC	High-performance liquid chromatography
ITC	Isothermal Titration Calorimetry
MD	Molecular dynamics
MM	Molecular mechanics
NDI	Naphthalenediimide
NOE	Nuclear Overhauser effect
NOESY	Nuclear Overhauser enhancement spectroscopy
PCA	Principal component analysis
PEG	Polyethylene glycol
PUPy	Pyrrole-fused ureidopyrimidinone
REMD	Replica exchange molecular dynamics
ROESY	Rotating-frame Overhauser enhancement spectroscopy
rt	Room temperature
SEI	Secondary electrostatic interaction

THF	Tetrahydrofuran
TMSCl	Trimethylsilyl chloride
T-ROESY	Transverse rotation-frame Overhauser enhancement spectroscopy
UPy	Ureidopyrimidinone
VT	Variable temperature

1 Introduction

1.1 Background

Supramolecular chemistry is an area of chemistry focused on molecular assemblies formed by the association of two or more chemical species through non-covalent interactions such as electrostatic and van der Waals forces, π-π stacking interactions, solvophobic effects, and hydrogen bonding. These intermolecular forces play an essential role in Nature, for example in substrate-enzyme interactions and the formation of DNA double helices. The field of supramolecular chemistry is concerned both with the study of these interactions in order to increase our understanding of them, as well as with the design and synthesis of new non-natural systems. Supramolecular systems based on non-covalent interactions can be used to construct complex chemical architectures that would be difficult to prepare by traditional covalent synthesis. In addition, the reversible nature of non-covalent interactions allows for the development of stimuli-responsive systems.

There are several important factors to consider when designing the molecular components of a supramolecular system. The molecular component needs to contain suitable binding sites or recognition motifs. Of equal importance is the geometry (shape and size) of the component, which determines the spatial arrangement of the binding sites needed to enable the desired self-assembly. Bicyclo[3.3.1]nonane and its heteroanalogue 1,5-diazabicycol[3.3.1]nonane (Figure 1.1) are examples of rigid, concave structures that can be used to create cavity-containing compounds for supramolecular systems.

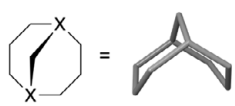

X = C: bicyclo[3.3.1]nonane
X = N: 1,5-diazabicyclo[3.3.1]nonane

Figure 1.1 Structure of bicyclo[3.3.1]nonane and 1,5-diazabicyclo[3.3.1]nonane.

In this thesis, 1,5-diazabicycol[3.3.1]nonane (as incorporated in the Tröger's base motif) and bicyclo[3.3.1]nonane are used as scaffolds in a small synthetic receptor and in monomers capable of forming well-defined cyclic and tubular aggregates, respectively (Figure 1.2). The supramolecular systems described herein utilize aromatic interactions, electrostatic interactions, and hydrogen bonding, and have

been used both to investigate the nature of these interactions and to construct new kinds of supramolecular structures.

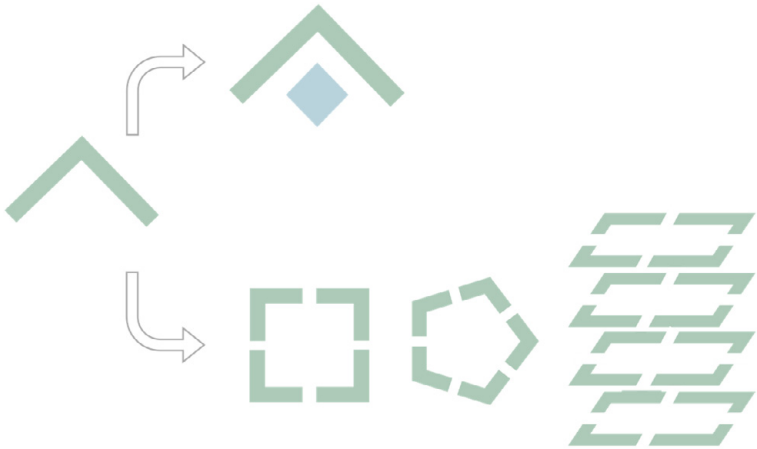

Figure 1.2 Schematic overview of uses of bicyclic compounds: as receptors for host-guest systems (top) and as monomers for the formation of discrete supramolecular aggregates (bottom).

1.2 Thesis outline

This thesis is divided into two parts. The first part (chapter 2–4) focuses on a synthetic receptor based on a Tröger's base motif fused with two crown ethers. Two studies where the receptor is used to investigate non-covalent interactions are described. Chapter 2 gives an introduction to synthetic receptors, with a special focus on receptors based on the Tröger's base motif. In chapter 3, a study where the receptor is used together with differently substituted bisammonium ligands is presented. The receptor-ligand system is used as a model for studying aromatic interactions such as can be found for example between a short peptide sequence and an aromatic cavity of a protein. The binding between the bisammonium ligands and the receptor is studied both quantitatively (binding energies) and qualitatively (conformations) by NMR titrations and 2D NMR spectroscopy. The estimated experimental values are also used to validate a few different computational methods. In chapter 4, a study of the consecutive binding of potassium ions to the ditopic receptor in water is described. A combination of isothermal titration calorimetry experiments and computational simulations is used to measure and explain thermodynamic trends. Different factors such as the counterion, solvation effects and conformational changes and their influence on the binding are investigated.

The second part of the thesis (chapter 5–6) is focused on the design and synthesis of hydrogen-bonding monomers capable of discrete cyclic and tubular self-assembly. Chapter 5 describes different types of hydrogen-bonded aggregates and

gives an overview of previously reported supramolecular aggregates based on the bicyclo[3.3.1]nonane scaffold. In chapter 6, the design, synthesis, and self-assembly studies of new monomers designed to be soluble in water are described. Polyethylene glycol chains are introduced to increase the solubility of the monomers in more polar solvents, with the aim of developing amphiphilic monomers. The hydrogen-bonded aggregation in different solvents is studied by various NMR methods, including ^{1}H NMR spectroscopy, 2D NMR methods, and diffusion-ordered spectroscopy. The solubility and self-assembly behavior of the monomers is compared to previously reported alkylated analogues and the influence of the polyethylene glycol chains is discussed.

2 Synthetic receptors

2.1 Receptors in Nature

In Nature, receptors are proteins located inside or on the surface of cells that can receive and transduce signals. The signals are typically chemical messengers (ligands) released by one cell to signal either itself or a different cell. The binding of a specific signal to a receptor causes a conformational change in the receptor, which in turn activates a physiological response.[1, 2] In most cases, the binding of the ligand to the receptor is governed by the size and shape of the ligand and non-covalent interactions.[3] The ligand must possess appropriate dimensions to interact with the binding pocket of the receptor, and non-covalent interactions between the ligand and the receptor are needed to ensure sufficient binding and prevent unwanted dissociation of the receptor-ligand complex. The binding between a ligand and a receptor typically involves a combination of various interactions, including ionic interactions, hydrogen bonding, dipole-dipole interactions, van der Waals forces, and solvophobic interactions.[4]

Studying the binding of ligands to receptors is an important objective, both for the development of new drugs, as well as for furthering our understanding of different biochemical processes.[5] The investigation of the fundamental thermodynamic factors governing ligand-receptor interactions can also increase our knowledge of related concepts such as entropy-enthalpy compensation[6, 7] and binding cooperativity.[8] Synthetic receptors can be used as models for more complex biological systems and offer a way to study the interactions and factors governing receptor-ligand binding under controlled conditions, both experimentally and theoretically.[9]

2.2 Synthetic receptors

Synthetic molecular receptors are host molecules that contain one or several binding sites for guest molecules or ions. The receptors are typically based on macrocyclic or cleft-shaped scaffolds with a preorganized arrangement of functional groups.[5] Common scaffolds include crown ethers, cyclodextrins and cyclophanes, as well as acyclic, cleft-shaped molecules (Figure 2.1). In most synthetic receptors, the

scaffolds are further modified by covalently introducing features such as linkers for increased solubility, functional groups for enhanced selectivity, or reporter groups for sensing and signaling applications.[5]

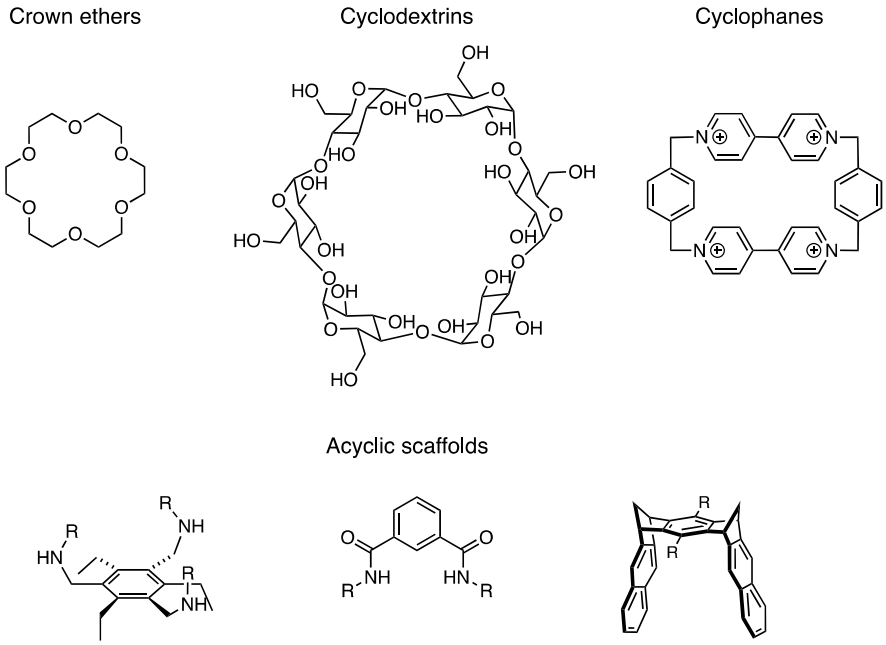

Figure 2.1 Common scaffolds for synthetic receptors.

Synthetic receptors can also be based on metal coordination complexes, where a transition metal with at least one available coordination site is used to bind electron-rich guests.[10, 11] Another strategy is to attach functional groups to larger scaffolds, such as dendrimers or nanoparticles, to form multivalent recognition systems.[12, 13]

In addition to being used as models for more complicated biological systems and for studying non-covalent interactions, synthetic receptors have also found many practically useful applications, for example as probes for imaging and sensing,[14-16] and as ionophores with antibiotic, antimicrobial and anticancer properties (Figure 2.2).[17-19]

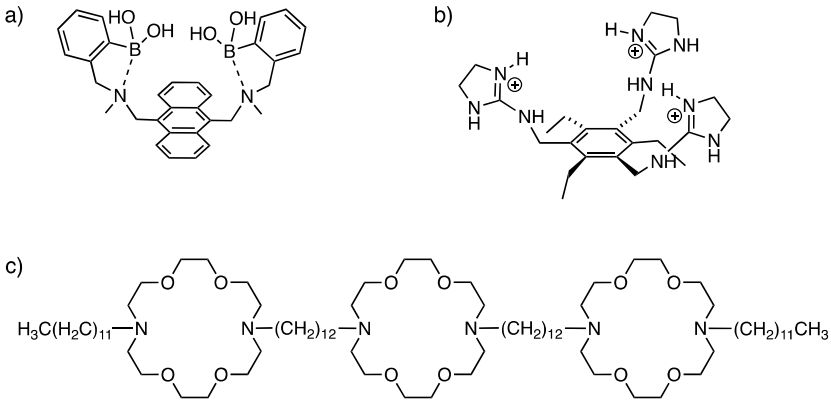

Figure 2.2 Examples of practical applications of synthetic receptors. **a)** Fluorescent receptor for glucose sensing.[14] **b)** Indicator ensemble for sensing of citrate.[15] **c)** Cytotoxic ion channel.[20]

2.3 Tröger's Base as a scaffold for synthetic receptors

Tröger's base (2,8-dimethyl-6*H*,12*H*-5,11-methanodibenzo[*b*,*f*][1,5]diazocine) was first synthesized by Julius Tröger in 1887 by the condensation of *p*-toluidine and methylal in aqueous HCl (Figure 2.3).[21] The C_2-symmetric bicyclic scaffold gives the molecule a cleft shape, with the two aromatic rings arranged nearly perpendicular to each other.[22] The chirality arises from the stereogenic nitrogen atoms, which are configurationally blocked from inversion by the methylene bridge. The resulting relatively rigid shape gives the molecule a well-defined hydrophobic chiral cavity.

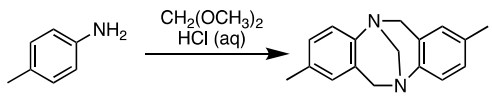

Figure 2.3 Original synthesis of Tröger's base.

Until the 1980s, Tröger's base was mainly used as a model substance for the evaluation of new chiral separation techniques.[23, 24] The use of Tröger's base as a scaffold for molecular recognition was first envisioned by Wilcox and coworkers in 1985.[25] The renewed interest in the molecule resulted in a fast development of new methodologies for the synthesis of Tröger's base analogues. Today, Tröger's base and its analogues have found applications in a number of different fields, including as DNA-interacting probes,[26, 27] in optoelectronic materials,[28, 29] and in catalysis.[30-32]

In synthetic receptors, Tröger's base has been used both as a rigid structural element onto which recognition motifs can be anchored, but also as an aromatic cavity which can interact with unfunctionalized molecules. Since Tröger's base is a chiral

molecule, the resulting receptors can potentially be used for enantiomeric discrimination.[33-35]

One class of synthetic receptors based on Tröger's base are receptors containing hydrogen-bonding motifs. Wilcox and coworkers reported carboxylic acid-substituted receptor **1** (Figure 2.4), which could bind adenine and biotin derivatives.[36] Goswami and Ghosh synthesized receptors with pyridine amide motifs for the complexation of dicarboxylic acids. Receptor **2** (Figure 2.4) was shown to selectively bind suberic acid in the presence of other α,ω-dicarboxylic acids.[37, 38]

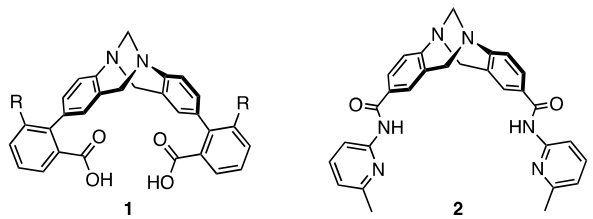

Figure 2.4 Hydrogen-bonding receptors based on Tröger's base.

Crossley and coworkers developed receptors with metal-containing porphyrins (Figure 2.5). Zinc-porphyrin receptor **3a** exhibited strong affinity towards diamine guests, and the enantiopure receptor bound histidine esters with good enantioselectivity.[35, 39, 40] Porphyrin receptor **3b** containing dihydroxytin was found to bind a number of α,ω-dicarboxylic acids.[41] Manjula and Sastry synthesized a Tröger's base receptor with monoaza crown ethers and studied its host-guest interactions with primary bisammonium ions (**4**, Figure 2.5).The incorporation of a flexible linker between the Tröger's base motif and the crown ethers resulted in a preferential binding of bisammonium ions with shorter alkyl chain length.[42]

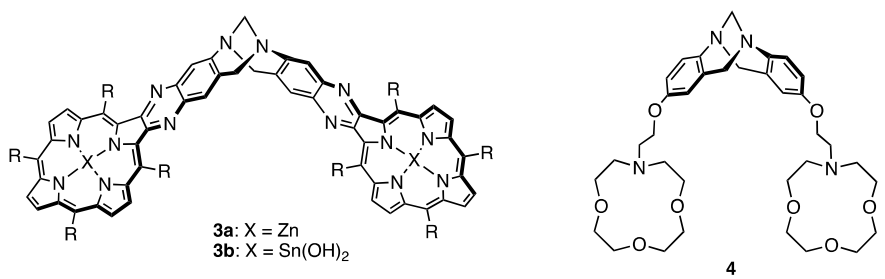

Figure 2.5 Porphyrin- and aza-crown ether-containing receptors based on Tröger's base.

The Tröger's base motif has also been employed in macrocycles. Wilcox and coworkers developed different water-soluble cyclophanes capable of binding benzenoid substrates, menthols, and aromatic phosphates (**5**, Figure 2.6).[43-45] Miyahara and Inazu, as well as Manjula and Nagarajan, combined the Tröger's base motif with polyethylene glycol chains to form macrocyclic compounds (**6**, Figure 2.6).[46, 47] Investigation of the cation-binding properties revealed reasonably high

binding affinities for several organic and inorganic cations, but no selectivity. The lack of selectivity was explained by the highly flexible cavities.[47]

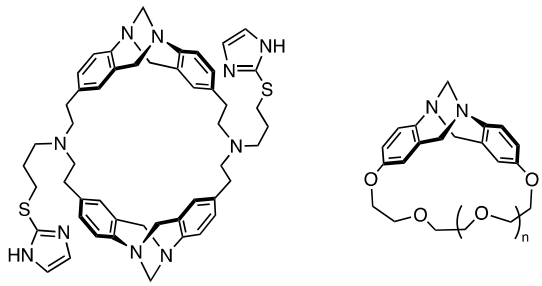

5 **6**

Figure 2.6 Macrocycles based on Tröger's base.

As previously mentioned, another application of the Tröger's base scaffold is to use the aromatic cavity to construct recognition sites for unfunctionalized molecules. The binding of unfunctionalized guests mainly involves non-directional solvophobic effects[48] and van der Waals interactions,[49] and typically take place on a suitable concave surface. If the surface is aromatic, π-π[50, 51] and cation-π[52] interactions may also contribute. One strategy for constructing such recognition sites has been to design receptors containing several fused Tröger's base units. Although synthetically challenging due to the number of possible isomers, cleft-shaped molecules based on linearly fused bis- and tris-Tröger's base analogues have been reported by the groups of Pardo, Král, and Wärnmark, following different synthetic strategies (**7**-**9** in Figure 2.7).[53-56] Experimental and computational studies by Kessler and coworkers have shown that this type of receptor can bind tetracyanobenzene.[57] In work by Král, Havlík, Anzenbacher and coworkers, bowl-shaped receptors were synthesized by fusing three Tröger's base motifs to a central unit (**10** in Figure 2.7).[58-60] In a recent report, receptor **10** was used as a fluorescent sensor for nitroaromatic compounds.[60]

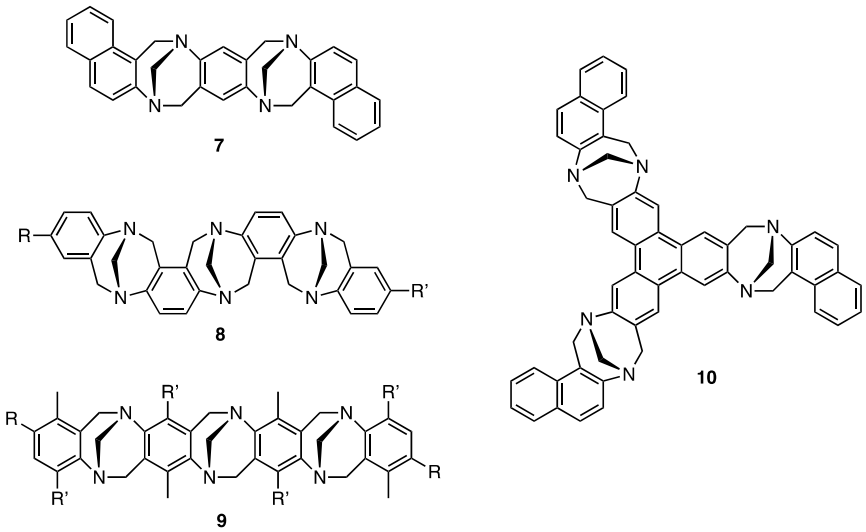

Figure 2.7 Cleft- and bowl-shaped receptors based on fused Tröger's base analogues.

2.3.1 Bis(18-crown-6) Tröger's base receptor

Crown ethers (cyclic oligomers of ethylene oxide) are amongst the most used host compounds in supramolecular chemistry. Their ability to complex cations has been extensively studied and it is well-known that the selectivity for different cations depends on the relative size of the cation and the polyether ring.[61] 18-crown-6 is known to form strong complexes with alkali metal cations, particularly potassium ions. In addition, 18-crown-6 can form inclusion complexes with ammonium and primary alkylammonium ions, where three hydrogen bonds can form between the ammonium hydrogens and alternating oxygens in 18-crown-6 (Figure 2.8).[62, 63]

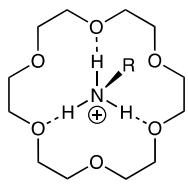

Figure 2.8 Complex between 18-crown-6 and an alkyl ammonium ion. Hydrogen bonds are indicated by dashed lines.

The strength of the binding for the crown ether-cation complex can be measured by the equilibrium constant (K) for the crown ether-cation complex:

$$K = k_{bind}/k_{release} \quad (1)$$

A vast number of equilibrium constants for complexes between different crown ethers and cations have been measured by a number of different methods, including

calorimetric titration techniques,[64] potentiometric measurements,[65] and spectroscopic methods.[66] In general, the stability of the crown ether-cation complex, as measured by the equilibrium constant, depends largely on the solvent, with lower polarity solvents giving more stable complexes. Table 2.1 shows some selected equilibrium constants for 18-crown-6 complexes.

Table 2.1 Equilibrium constants for 18-crown-6 complexes with different cations.

Cation	Method	log*K* (H_2O)	log*K* (CH_3OH)
Na^+	Calorimetric titration	0.80[a]	4.32[b]
	Potentiometry	<0.3[b]	4.36[c]
K^+	Calorimetric titration	2.03[a]	6.10[b]
	Potentiometry	2.06[b]	6.05[d]
NH_4^+	Calorimetric titration	1.23[a]	4.27[c]
	Potentiometry	1.10[b]	-

[a] Ref [64]. [b] Ref [65]. [c] Ref [67]. [d] Ref [68].

Ditopic receptor **11** consists of a Tröger's base motif with 18-crown-6 moieties fused to each end of the aromatic cavity, and can be synthesized in one step from commercially available 4-aminobenzo 18-crown-6 and formaldehyde in the presence of HCl in ethanol (Figure 2.9).[34] The resulting receptor has a rigid aromatic cavity, as well as two flexible crown ether moieties, with an average distance of 10 Å between the latter. In the following chapters, two studies using receptor **11** to investigate different intermolecular interactions are described.

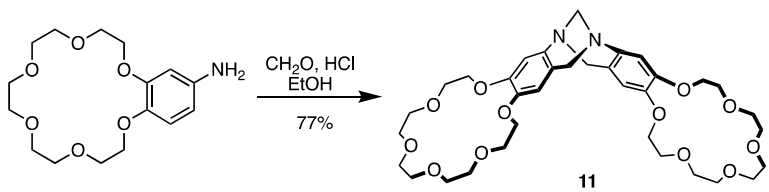

Figure 2.9 Synthesis of bis(18-crown-6) Tröger's base receptor **11**.

3 A model system for interactions between non-polar substituents and an aromatic cavity (Paper I)

3.1 Introduction

Non-covalent interactions involving aromatic rings play an important role in Nature, both for the structure of biological macromolecules such as DNA and proteins, as well as for the interaction between macromolecules and smaller molecules.[69] There are many different types of aromatic interactions, including π-π, cation-π, and CH-π interactions. Although aromatic interactions are generally considered weak non-covalent interactions, their collective strength is significant and they are one of the most prevalent non-covalent interactions in both synthetic and natural systems.[70] Interactions between two aromatic systems (π-π interactions) are amongst the most studied of the aromatic non-covalent interactions. One explanation model for this type of interaction was introduced by Hunter and Sanders in 1990. In their model, an aromatic ring is described as a positively charged σ-framework sandwiched between two negatively charged π-electron clouds. The interaction between two aromatic rings is mainly governed by polar electrostatic interactions.[71] This model can be used to explain the preferred relative orientations of the aromatic rings, where parallel-displaced or edge-to-face arrangements are more energetically favored than a parallel stacked configuration (Figure 3.1).[69, 72] Although this is the most widely used explanation model, other models emphasizing other contributing factors than electrostatic interactions have also been reported.[73-75]

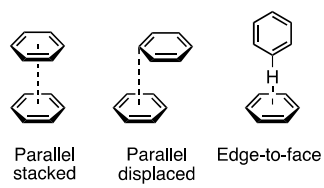

Figure 3.1 Possible arrangements for π-π interactions, exemplified by the benzene dimer.

The CH-π interaction is an attractive force occurring between an aliphatic or aromatic hydrogen (soft acid) and a π-system (soft base) and is considered a weak hydrogen bond. As opposed to classic hydrogen bonds, CH-π bonds are mainly

governed by dispersion forces, with only a small contribution from electrostatics.[76] The interaction shown in the edge-to-face arrangement in Figure 3.1 can also be classified as an aromatic CH-π interaction.

As previously mentioned, aromatic non-covalent interactions are widespread in Nature. Several systematic studies of different databases have identified the role and significance of π-π,[77] cation-π[52] and CH-π[78, 79] interactions in proteins and peptides. Due to their importance in protein structure and protein-ligand recognition, many model systems for the qualitative and quantitative investigation of aromatic interactions have been developed. These model systems typically consist of conformationally restricted molecules or complexes in which non-covalent interactions can affect the conformational equilibrium or binding affinity.[80] Cozzi and Siegel designed several different model systems where the measured barriers to rotation around an aryl-aryl bond were used to investigate parallel π-π interactions (Figure 3.2a).[81, 82] Hunter and coworkers used hydrogen-bonded molecular zippers in a chemical double-mutant cycle to study edge-to-face π-π interactions (Figure 3.2b).[83] Wilcox designed molecular torsion balances based on a Tröger's base motif which can interconvert between a folded and an unfolded conformation through slow rotation around a C-C bond (Figure 3.2c). These torsion balances have been used to study and quantify both aromatic and alkyl CH-π interactions.[84-86]

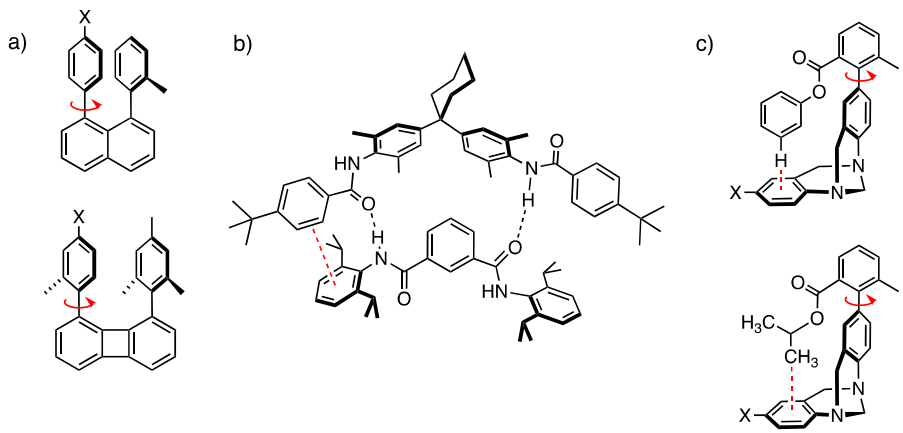

Figure 3.2. Model systems for studying **a)** parallel π-π interactions, **b)** edge-to-face π-π interactions, and **c)** edge-to-face π-π and alkyl CH-π interactions.

In this chapter, a system consisting of receptor **11** and differently substituted bisammonium ligands is used as a model for interactions between an aromatic receptor and an extended linear peptide chain. Interactions between proteins and short peptide sequences are known to play an important role in cellular regulation and signal transduction,[87] and have been identified as a potential drug target.[88, 89] A further aim of the study was to use the obtained experimental data to compare and evaluate different computational methods. The benchmarking of theoretical

methods is an important goal in and of itself, as computational chemistry has become an essential tool for the modeling and prediction of complex systems and non-covalent interactions.[90, 91]

3.2 Description of the model system

The model system is shown in Scheme 3.1. As previously described (chapter 2.3.1), receptor **11** contains a well-defined aromatic cavity, as well as two crown ether moieties capable of complexing primary ammonium ions. Previous studies of the binding of primary bisammonium chlorides of different lengths found that the highest association constant was obtained for the complex between receptor **11** and hepta-1,7-diyl bisammonium chloride **12** and that the heptane chain preferentially adopts an extended (all-*anti*) conformation with the protons of the central methylene group pointing towards the aromatic cavity.[34] Building on this information, we synthesized a number of hepta-1,7-diyl bisammonium ligands with different non-polar substituents in the 4-position.

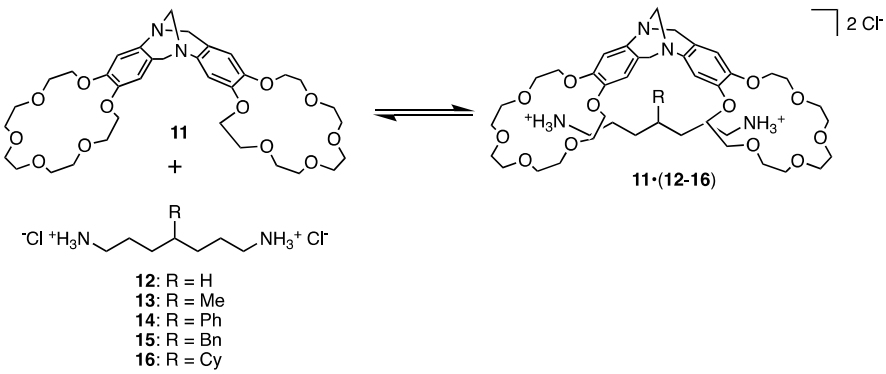

Scheme 3.1 Binding of bisammonium ligands **12-16** to bis(18-crown-6) Tröger's base receptor **11**.

The expected major interactions in receptor-ligand complexes **11•(12-16)** are the hydrogen bonds between the ammonium groups and the crown ethers. Interactions between the substituents and the aromatic cavity are expected to be comparatively weak. However, by measuring the discrimination of the ligands by the receptor relative to unsubstituted ligand **12**, the effect of the substituent and possible conformational changes in the heptane chain can be investigated. If the conformation of the heptane backbone of the ligands were to remain the same within the series of ligands, the measured relative binding energies would represent how strong the interaction of a specific "free" substituent would be with a "free" aromatic cavity. However, the degree of freedom of the aliphatic backbones of the ligands, although a better biological model for an unfolded peptide chains than a less flexible backbone, makes the concept of a "uniform" conformation less likely. A more

correct description in this case is that the relative binding energies sum up the interactions between the substituent and the aromatic cavity, the rearrangement energy of the ligand backbone to fit the receptor, and the solvophobic effect. An obvious drawback of our model is that the individual contributions from different effects to the binding cannot be readily separated. However, unlike many other model systems where the primary goal is to extract information about and quantify a specific interaction, our system offers a more holistic description of the effect of side chains in peptides in their interactions with aromatic receptors.

3.2.1 Synthesis of bisammonium ligands

The synthesis of bisammonium ligands **12-16** is shown in Scheme 3.2. In the first step, a bis-Michael addition between acrylonitrile and a nitro compound is performed. The reaction is catalyzed by 'naked' fluoride, generated by KF and 18-crown-6 in CH_2Cl_2.[92] In the next step, the nitro group is exchanged for a hydrogen using tributyltin hydride and azobisisobutyronitrile (AIBN).[93] In the final step, the nitrile groups are reduced to amines, followed by acidification to obtain the chloride salt. Investigation of different reducing agents found the use of borane-THF complex to give the diamines in acceptable to good yields, and subsequent treatment with hydrochloric acid in 1,4-dioxane afforded the corresponding bisammonium chlorides. Isolation of cyclohexyl-substituted bisammonium salt **16** following the same procedure proved difficult. The reduction was instead accomplished by hydrogenation with Adam's catalyst (PtO_2). Following a procedure reported by Secrist and Logue, the presence of a small amount of chloroform during the hydrogenation led to the direct formation of the corresponding chloride salt **16**.[94]

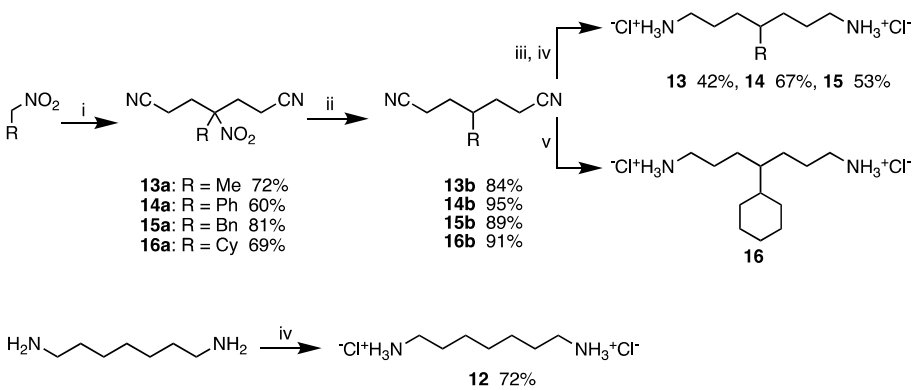

Scheme 3.2 Synthesis of bisammonium ligands **12-16**. i) acrylonitrile, KF, 18-Crown-6, CH_2Cl_2; ii) Bu_3SnH, AIBN, benzene, reflu;. iii) BH_3, THF; iv) HCl (4 M) in dioxane; v) PtO_2, H_2 (50 psi), $CHCl_3$, MeOH.

3.3 Experimental estimations of association constants and binding energies

NMR titration methodology can be used to observe and quantify association processes for host-guest systems that exhibit either a very slow or a very fast exchange rate on the NMR time scale.[95] For our system, previous studies have shown that the exchange rate is fast enough to allow for NMR titration methodology to be used.[34] The binding stoichiometry of the complexes was determined to be 1:1 by a Job plot constructed using chemical shift data from NMR titrations between receptor **11** and ligand **12**, and further corroborated by ESI-mass spectrometry. The experiments were conducted in a 1:1 mixture of methanol and chloroform, as a compromise between a solvent that would allow for similar solvophobic interactions as what is present in living cells (methanol), and a solvent that could dissolve the receptor to a degree needed for the measurements (chloroform).

Previous studies have shown that the association constants for the receptor-ligand complexes are too high for direct determination ($K_{\mathbf{11}\cdot\mathbf{12}} > 10^5$ M^{-1}).[34] Instead, the NMR titrations of the bisammonium ligands were performed in competition with a more weakly binding salt (methylammonium chloride) for which the association constants could be determined by direct measurement. The equilibria between receptor **11**, the bisammonium guest **x**, and methylammonium chloride **M** are described by equations 2–4.

$$\mathbf{11} + \mathbf{x} \rightleftarrows \mathbf{11}\cdot\mathbf{x} \tag{2}$$

$$\mathbf{11} + \mathbf{M} \rightleftarrows \mathbf{11}\cdot\mathbf{M} \tag{3}$$

$$\mathbf{11}\cdot\mathbf{M} + \mathbf{M} \rightleftarrows \mathbf{11}\cdot\mathbf{M}_2 \tag{4}$$

By combining expressions for association constants and total concentration of the different species in the system, equations describing the concentrations of different species can be derived (for further details, see Paper I).

Assuming a fast exchange rate on the NMR time scale, the observed chemical shift of a given resonance in bisammonium ligand **x** (δ_{obs}) can be described as a weighted average of the chemical shift of the resonance in the unbound ligand ($\delta_{\mathbf{x}}$) and the chemical shift of the resonance in the ligand bound to the receptor ($\delta_{\mathbf{11}\cdot\mathbf{x}}$). This is described in Equation 5:

$$\delta_{obs} = x_{\mathbf{x}}\delta_{\mathbf{x}} + x_{\mathbf{11}\cdot\mathbf{x}}\delta_{\mathbf{11}\cdot\mathbf{x}} \tag{5}$$

where $x_{\mathbf{x}} = [\mathbf{x}]/[\mathbf{x}]_{total}$ and $x_{\mathbf{11}\cdot\mathbf{x}} = [\mathbf{11}\cdot\mathbf{x}]/[\mathbf{11}]_{total}$.

The NMR titration experiments were performed by adding specific amounts of a solution of receptor **11** to a solution containing a bisammonium ligand and monomethyl ammonium chloride. After each addition, the ^{1}H NMR spectrum was recorded. The titrations were repeated using different concentrations of bisammonium ligand. The association constants were determined by an iterative process, where chemical shifts were calculated based on assumed association constants. The assumed association constants were then varied to minimize the difference between the calculated chemical shifts and the experimentally observed chemical shifts (for further details, see Paper I). The so-determined association constants (expressed as relative association constants relative to unsubstituted ligand **12**) are shown in Table 3.1.

Table 3.1. Experimentally determined relative association constants $K_{11\cdot x}/K_{11\cdot 12}$ and binding energies $\Delta\Delta G^{\circ}_{11\cdot x\text{-}11\cdot 12}$ (kcal/mol) at 25 °C for the association of ligands **12-16** to receptor **11** in $CDCl_3$/MeOH-d_4 (1:1).

Ligand (**x**)	**12**	**13**	**14**	**15**	**16**
$K_{11\cdot x}/K_{11\cdot 12}$ [a]	1	1.74	5.25	0.74	0.28
$K_{11\cdot x}/K_{11\cdot 12}$ [b]	1	1.96	3.85	0.58	0.35
$\Delta\Delta G^{\circ}_{11\cdot x\text{-}11\cdot 12}$ [c]	0	-0.40	-0.80	0.32	0.62

[a] Values obtained from NMR titrations with methyl ammonium chloride as competitor. [b] Values obtained from pair-wise competitive NMR titrations using ligand **14** as the competitor, recalculated relative to ligand **12**. [c] Calculated using the relative association constants obtained from the pair-wise competitive NMR titrations.

The differences between the estimated relative association constants were comparatively small, so to further validate the data, pair-wise competitive NMR titrations were performed, using ligand **14** as the common competitor. Relative association constants could be obtained directly from the observed chemical shifts and the known chemical shifts of the unbound and bound bisammonium ligands using Equation 6:

$$(\delta_{\mathrm{obs,\,x}}-\delta_{\mathbf{x}})(\delta_{\mathbf{11\cdot 14}}-\delta_{\mathrm{obs,14}})=\frac{K_{\mathbf{11\cdot x}}}{K_{\mathbf{11\cdot 14}}}(\delta_{\mathbf{11\cdot x}}-\delta_{\mathrm{obs,x}})(\delta_{\mathrm{obs,\,14}}-\delta_{\mathbf{14}}) \qquad (6)$$

Gratifyingly, the so-obtained relative association constants were in good agreement with the relative association constants obtained from the NMR titrations with methylammonium chloride as competitor (Table 3.1).

The relative association constants were converted into relative binding energies using Equation (7). The relative binding energy ($\Delta\Delta G^{o}$) is defined as the difference between the standard free binding energy (ΔG^{o}) of the complex between the substituted ligand (**13-16**) and receptor **11**, and the standard free binding energy of the complex between unsubstituted ligand **12** and receptor **11**, and can be calculated directly from the relative association constant.

$$\Delta\Delta G^{o}_{\mathbf{11\cdot x\text{-}11\cdot 12}} = \Delta G^{o}_{\mathbf{11\cdot x}} - \Delta G^{o}_{\mathbf{11\cdot 12}} = -RT\ln\frac{K_{\mathbf{11\cdot x}}}{K_{\mathbf{11\cdot 12}}} \quad (7)$$

The relative association constants and binding energies suggest a weak but evident discrimination in the binding process based solely on the substituent on the ligand (Table 3.1). The strongest binding was observed for phenyl-substituted ligand **14**, followed by methyl-substituted ligand **13**, unsubstituted ligand **12**, benzyl-substituted ligand **15** and cyclohexyl-substituted ligand **16**. Two of the substituted ligands (**13** and **14**) were found to bind more strongly to the receptor than unsubstituted ligand **12**, indicating dominating favorable interactions between the substituents and the aromatic cavity. Rewardingly, the estimated relative binding energies for complexes **11•13** and **11•14** (-0.40 and -0.80 kcal/mol, respectively) are in the same range as values for CH-π and edge-to-face π-π interactions obtained by other synthetic model systems. Wilcox torsion balance (Figure 3.2c) determined the energy of a CH-π interaction to be -0.5 kcal/mol in $CDCl_3$ and -0.72 kcal/mol in D_2O.[86] Hunter and coworkers estimated the energy of the edge-to-face π-π interactions in their system (Figure 3.2b) to -0.33 kcal/mol in $CDCl_3$,[83] which is comparable to the value obtained from Wilcox torsion balance (-0.30 kcal/mol in $CDCl_3$).[85] The comparatively more negative $\Delta\Delta G^0$ value estimated for our phenyl-substituted ligand (-0.80 kcal/mol) could be attributed to the phenyl substituent interacting with both aromatic moieties of receptor **11**, or that the interactions between the substituent and the cavity are a combination of edge-to-face and parallel π-π interactions. Another important factor is the solvent, as it has been shown that the strength of non-covalent aromatic interactions are strongly dependent on the solvent environment.[96] Our measurements were conducted in a 1:1 $CDCl_3$/MeOH-d_4 mixture, while the values for other model systems were obtained in pure $CDCl_3$ (or pure D_2O).

3.4 Computational calculations of binding energies

As previously mentioned, one of the aims of the study was to use the experimental results to evaluate different computational methods. A number of different molecular mechanics (MM) and density-functional theory (DFT) methods were employed to calculate relative binding energies ($\Delta\Delta E_0$) according to Equation 8:

$$\Delta\Delta E_{0,\mathbf{11\cdot x\text{-}11\cdot 12}} = \Delta E_{0,\mathbf{11\cdot x}} - \Delta E_{0,\mathbf{11\cdot 12}} = E_{0,\mathbf{11\cdot x}} - E_{0,\mathbf{x}} - E_{0,\mathbf{11\cdot 12}} + E_{0,\mathbf{12}} \quad (8)$$

where E_0 corresponds to the calculated potential energy of the lowest energy conformation of the ligand or receptor-ligand complex. By calculating the change in binding energy relative to complex **11•12**, the potential energy of the uncomplexed receptor is canceled out. This makes the comparison isodesmic and is

expected to cancel out some of the systematic errors arising from for example neglected entropy terms, as well as deficiencies in the calculation methods.

For the MM calculations, conformational searches were used to generate sets of conformations for each ligand and receptor-ligand complex. The sets of conformations were then minimized using three different force fields (MM3*,[97] MMFFs,[98] and OPLS3e[99, 100]). The minimizations were performed using both a chloroform and a water solvent model. Since the relative binding energies ($\Delta\Delta E_0$) obtained from Equation 8 do not contain any entropic terms, they do not represent free energies. To allow for a better comparison with the experimentally determined $\Delta\Delta G^o$ values, the calculations were also performed with a Boltzmann correction term, which sums up the energy contributions of all conformers within 5 kcal/mol of the lowest energy conformation for each ligand and receptor-ligand complex.

DFT calculations were performed using the M06-2X-D3[101] and the ωB97X-D[102] functionals, with the 6–31G** basis set and a Poisson-Boltzmann (PBF) continuum solvation model[103] for chloroform. The lowest energy conformations of the ligands and receptor-ligand complexes obtained from the MM calculations were used as input structures.

Table 3.2 Calculated $\Delta\Delta E_0$ values (kcal/mol) for receptor-ligand complexes **11**•(**12**-**16**) using MM and DFT calculations. For values from MM calculations, values calculated using Boltzmann correction are included in parentheses. The DFT calculations were performed using the 6-31G** basis set.

Ligand (**x**)		**12**	**13**	**14**	**15**	**16**
Experimental $\Delta\Delta G^o$ values		0	-0.40	-0.80	0.32	0.62
Force field	Solvent model					
MM3*	Chloroform	0	-0.52 (-0.54)	-1.23 (-1.25)	0.29 (0.072)	5.14 (4.53)
	Water	0	-1.06 (-1.04)	-1.54 (-1.61)	-2.10 (-1.19)	3.14 (3.63)
MMFFs	Chloroform	0	-1.00 (-0.84)	-0.59 (-0.34)	-2.27 (-1.69)	2.36 (2.09)
	Water	0	-1.42 (-1.13)	-2.34 (-2.43)	-3.40 (-2.92)	1.63 (1.68)
OPLS3e	Chloroform	0	-0.73 (-0.95)	0.39 (0.44)	-1.39 (-1.32)	1.75 (1.80)
	Water	0	-1.34 (-1.45)	-1.02 (-1.78)	-3.32 (-2.90)	6.14 (6.15)
Functional	Solvent model					
M06-2X-D3	Chloroform	0	-2.28	-4.30	-9.22	-6.73
	Gas phase	0	-2.10	-0.13	1.53	-6.13
ωB97X-D	Chloroform	0	-2.73	-4.97	-11.22	-7.60
	Gas phase	0	-2.37	-3.69	-0.47	-5.68

Table 3.2 shows the calculated relative binding energies ($\Delta\Delta E_0$) obtained from the MM and DFT calculations. In general, it was found that the MM methods predict

the binding affinities significantly more accurately than the DFT methods. Amongst the values obtained from the MM calculations, the MM3* force field with a chloroform solvent model resulted in the most accurate predictions, both in terms of absolute values and in terms of the relative binding affinities of the ligands to the receptor. For all of the employed force fields, the calculations performed with a chloroform solvent model gave more comparable results to the experimental values than the calculations performed with a water solvent model. In most cases, the inclusion of the Boltzmann correction did not significantly improve the overall accuracy of the calculated binding energies. The DFT calculations using either functional resulted in substantially less accurate binding energies and were also unable to predict the relative binding affinity of the ligands to the receptor. This could potentially be explained by the choice of functional and basis set, although the investigated combinations are generally considered sufficiently accurate for applications in organic chemistry. The current results indicate that the chosen combinations might not be suitable for supramolecular interactions of the types found in biomolecules. The differences between the results obtained from MM calculations and DFT calculations are illustrated in Figure 3.3.

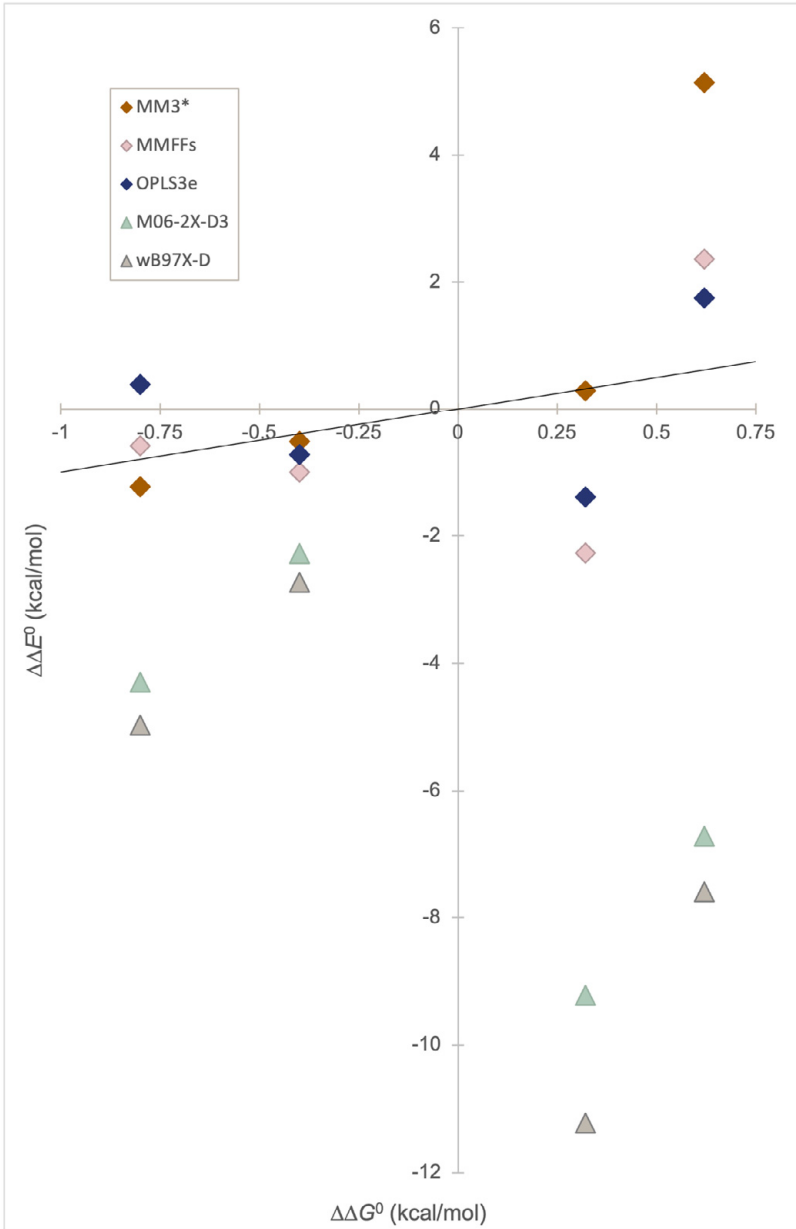

Figure 3.3 Comparison of calculated $\Delta\Delta E_0$ values obtained from MM calculations (diamonds) and DFT calculations (triangles) with experimentally determined $\Delta\Delta G^{o}$ values for receptor-ligand complexes **11**•(**12**-**16**). The included $\Delta\Delta E_0$ values from MM calculations were obtained using a chloroform solvent model and without the Boltzmann correction. The included $\Delta\Delta E_0$ values from DFT calculations were obtained using the 6-31G** basis set and a chloroform solvent model. The diagonal line marks the experimental values.

3.5 Conformational analysis

As the aim of the study was to investigate the interactions between the substituents and the aromatic cavity, conformational analyses of the ligands, both unbound and bound to the receptor, were performed. For each receptor-ligand complex, the position of the ligand substituent relative to the receptor cavity was investigated. In addition, the conformation of the heptane backbone in both the unbound and bound ligand was studied, in order to estimate the potential rearrangement energy required for the ligand to fit the receptor.

Complexation-induced changes in ^{1}H NMR shifts (CIS) obtained from the ^{1}H NMR titrations and cross peaks in the nuclear Overhauser enhancement spectroscopy (NOESY) and rotating-frame nuclear Overhauser enhancement spectroscopy (ROESY) spectra were used to suggest time-average conformations of the ligands. The nuclear- or rotating-frame Overhauser effect (NOE or ROE) is the transfer of nuclear spin polarization from one nuclear spin population to another via dipolar cross-relaxation.[104] NOESY and ROESY can be used to establish through-space correlations between nuclei that are close in space (within 5 Å) to each other. One drawback of NOESY is that for larger molecules (typically 1000–3000 Da), the NOE may be too weak to be detected.[105] In such cases, ROESY can be used as an alternative, as it has a difference dependence between the correlation time and cross-relaxation rate constant.

For all of the ligands, the proton resonances of the heptane backbone were displaced upfield upon complexation with receptor **11**. The largest change was observed for the δ-protons, which were displaced upfield by 0.8–1.2 ppm. The resonances of the α-, β-, and γ-protons were displaced upfield by on average of 0.2, 0.6, and 0.4 ppm, respectively. Taken together, this strongly indicates that all of the ligand backbones adopt all-*anti* conformations when complexed by the receptor, with the β- and δ-protons pointing towards the receptor and thus experiencing the largest shielding effect from the aromatic cavity (Figure 3.4a). Cross peaks in the NOESY spectra of the unbound ligands also suggest that an all-*anti* conformation is preferred for all ligands except cyclohexyl-substituted ligand **16**.

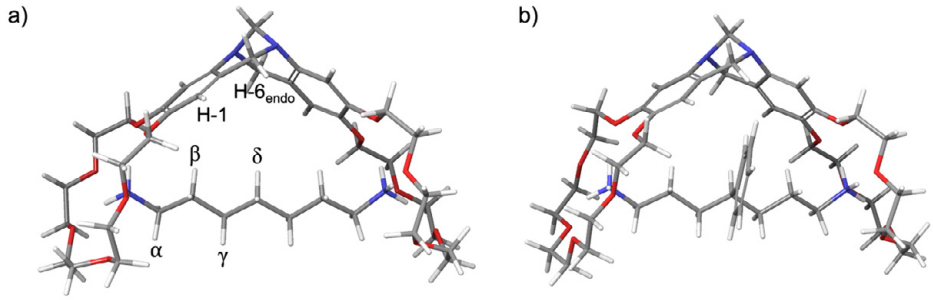

Figure 3.4 Structures of receptor-ligand complex **a) 11•12** and **b) 11•14** (lowest energy conformations obtained from MM calculations with the OPLS3e force field and a chloroform solvent model).

The position of the substituents in the receptor-ligand complexes was proposed based on a combination of CIS of the substituent protons and NOE correlations between the substituent proton resonances and the cavity proton resonances (H-6_{endo} and/or H-1, see Figure 3.4a). Methyl-substituted ligand **13** and phenyl-substituted ligand **14**, which exhibited the highest relative binding energies, appeared to form rigid complexes with the substituent located inside or partially inside the receptor cavity. Conversely, benzyl-substituted ligand **15** and cyclohexyl-substituted ligand **16**, which exhibited lower binding affinities for the receptor, formed more dynamic complexes, with the substituents interacting less with the cavity. For example, in the ROESY spectrum of the complex with benzyl-substituted ligand **15**, the *ortho*-protons of the ligand show cross peaks with H-1 and H-6_{endo} of the receptor, as well as with the crown-ether moieties of the receptor, which shows the dynamic behavior of the substituent on the NMR timescale. In addition, the CIS indicates that at least part of the benzyl group is pointing away from the receptor (as seen by downfield displacement of the resonances of the *meta*- and *para*-protons).

The ligand conformations were also investigated computationally. The lowest-energy conformations obtained from the MM calculations using a chloroform solvent model and the three different force fields (MM3*, MMFFs, and OPLS3e) were compared. In most cases, the three force fields gave similar conformations to what was suggested by NMR data, both in terms of the conformation of the ligand backbone and the position of the substituent. Molecular dynamics (MD) simulations were also performed, which supported the findings from the NMR experiments. The MD simulations of the receptor-ligand complexes showed that ligands **13** and **14** form more rigid complexes with the receptor, while the complexes with ligands **15** and **16** behave more dynamically, with both the ligand backbones and the substituents exhibiting higher conformational flexibility during the simulations. The findings from the NMR experiments, MM calculations, and MD simulations are summarized in Table 3.3.

Table 3.3. Summary of the conformational analysis of receptor-ligand complexes **11•(12-14**) based on NMR spectroscopy, MM calculations and MD simulations. *anti* and *gauche* refers to the conformation around the C-C bonds of the heptane chain of the ligands. I, P, and O refers to the position of the substituent (I = inside cavity, P = partially inside cavity, O = outside cavity). Extended and dynamic refers to the behavior of the ligand during MD simulation (Extended = N-N distance close to 10 Å during most of simulation, dynamic = large variety in N-N distance or substitutent location during simulation).

	NMR		MM			MD [a]
	^{1}H (Δδ) [b]	2D [c]	MM3* [d]	MMFFs [d]	OPLS3e [d]	
11•12	All-*anti*	All-*anti*	All-*anti*	All-*anti*	All-*anti*	Extended
11•13	All-*anti*	All-*anti*	All-*anti*	All-*anti*	All-*anti*	Extended
	I	I	O	O	P	I
11•14	All-*anti*	All-*anti*	All-*anti*	1 *gauche*	All-*anti*	Extended
	P	I	P	P	P	P
11•15	All-*anti*	All-*anti*	All-*anti*	2 *gauche*	2 *gauche*	Dynamic
	P	P	P	P	P	Dynamic
11•16	Inconclusive [e]	Inconclusive [e]	2 *gauche*	2 *gauche*	2 *gauche*	Dynamic
	Inconclusive [e]	P	P	O	P	Dynamic

[a] MD simulation performed with the OPLS3e force field and a methanol solvent model. [b] Based on change in chemical shift (Δδ) of signals corresponding to ligand protons upon complexation. [c] Based on crosspeaks found in NOESY/ROESY spectra. [d] Based on lowest energy conformations obtained with a chloroform solvent model. [e] Cannot be determined due to overlapping NMR peaks.

3.6 Conclusions

A bis(18-crown-6) Tröger's base receptor and a number of 4-substituted hepta-1,7-diyl bisammonium ligands were used to model the interactions between non-polar side chains of peptides and an aromatic cavity of a protein. Relative association constants ($K_{\mathbf{11•x}}/K_{\mathbf{11•12}}$) and binding energies ($\Delta\Delta G^{\circ}_{\mathbf{11•x\text{-}11•12}}$) for the receptor-ligand complexes were estimated using NMR titration methodology. A weak but evident discrimination in the binding process based solely on the ligand substituent was found. The strongest binding was exhibited by phenyl-substituted ligand **14**, followed by methyl-substituted ligand **13**. Rewardingly, the estimated relative binding energies for these complexes (-0.80 and -0.40 kcal/mol, respectively) were comparable to energies for similar CH-π and edge-to-face π-π interactions estimated using other synthetic model systems.[83, 85, 86] Conformational analyses of the ligands, both unbound and bound to the receptor, supported the finding that the phenyl- and methyl-substituents are interacting strongly with the receptor cavity. For both these ligands, the binding to the receptor does not seem to involve any substantial rearrangement energy, as the conformations of the ligands are largely the same in bound and unbound form. Taken together, we can conclude that the estimated relative binding energies for these two ligands can been seen as a measurement of the interactions between the respective substituents and the aromatic cavity of the receptor.

The experimental results were also used to compare and evaluate different computational methods, with the conclusion that in this case, MM calculations gave more accurate predictions of binding affinities than DFT calculations. MM calculations performed using the MM3* force field and a chloroform solvent model resulted in the most accurate predictions, both in terms of absolute values and in terms of relative binding affinities of the different ligands to the receptor.

4 Consecutive binding of potassium ions to a ditopic receptor (Paper II)

4.1 Introduction

Electrostatic interactions play a key role in processes such as protein folding and stability[106] as well as antibody-antigen interactions.[107] While it is typically the electrostatic attraction between two oppositely charged ions that is observed (or the repulsion between ions of similar charge), there are examples of like-charge ion pairing, such as interactions between positively charged amino acids[108] and chloride-chloride pairs in aqueous solution.[109] This apparent attraction is usually attributed to bridging water molecules allowing for stabilizing effects, which are large enough to compensate for the charge-charge repulsion.[108]

One example of a synthetic system used to study cation-cation interactions was reported by Piguet and coworkers, who developed double-stranded helicates based on ligands containing a Tröger's base motif (Figure 4.1).[110] By introducing additional rigid alkynyl groups, the distance between the two Cu^{+} ions could be increased without changing the symmetry or binding sites of the helicate. Spectrophotometric titrations revealed an apparent increased repulsion with increasing intermetallic distance. It was concluded that the increased solvation free energy of the larger helicates dominate over the Coulombic repulsion, resulting in the apparent destabilization of the complexes with larger intermetallic distances.

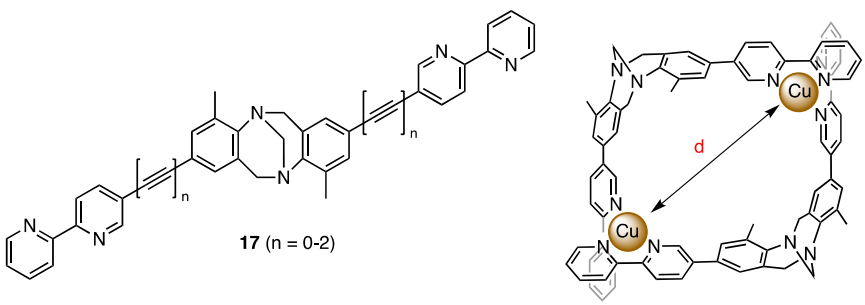

Figure 4.1 Ligand **17** (left) and double-stranded helicate (right). Intermetallic distance d marked in red.

In this chapter, a study of the consecutive binding of potassium ions to receptor **11** in water is described (Scheme 4.1). As previously discussed, receptor **11** contains a

rigid Tröger's base motif which places the two crown-ether moieties (and any potassium ions complexed to them) at a relatively fixed distance. The binding was studied experimentally by isothermal titration calorimetry (ITC). An unexpected observation that the binding of the second potassium ion is *enthalpically* favored compared to the binding of the first was further investigated by a combination of experimental results and computational simulations.

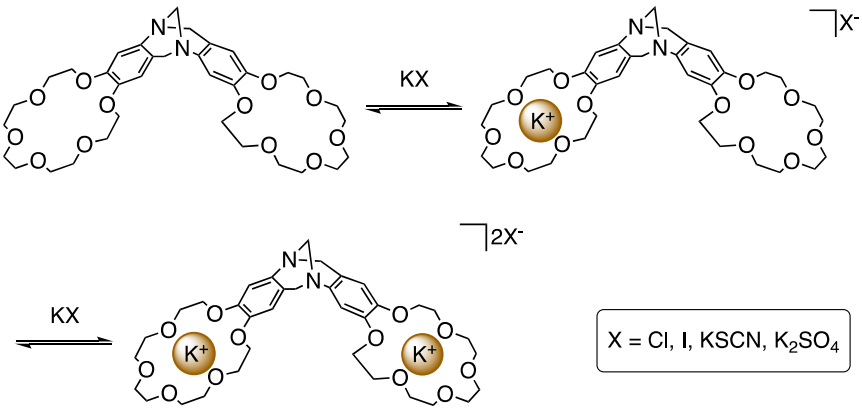

Scheme 4.1 Sequential binding of potassium ions to bis(18-crown-6) Tröger's base receptor **11**.

4.2 Isothermal Titration Calorimetry

ITC is a technique that can be used to quantitatively study binding processes between two or more species in solution. By measuring the heat released or absorbed during changes in the composition of a system, thermodynamic parameters such as association constants and binding enthalpies can be determined directly.[111, 112] A typical ITC experiment consists of additions of aliquots of a ligand solution to a receptor solution, followed by curve fitting of the calorimetric data using a suitable model to obtain the thermodynamic parameters. ITC experiments are preferentially performed on high affinity systems, as this means that the receptor can be saturated by addition of only a few equivalents of ligand. However, it has been shown that ITC experiments can also be used for low affinity systems, as long as a sufficient portion of the binding isotherm is covered, the binding stoichiometry is known, and the concentrations of the ligand and receptor are known with adequate accuracy.[112]

Due to the limited solubility of receptor **11** in water and the comparatively small expected association constants, we performed the ITC experiments by adding a highly concentrated ligand solution into a receptor solution with a much lower concentration, in order to ensure that a sufficient receptor saturation could be achieved. The method was validated by using the same experimental setup to

determine the association constant of a known system (18-crown-6 and potassium ion).

The ITC experiments were performed using four different potassium salts (KCl, KI, KSCN and K_2SO_4). Two different curve fitting models were employed; a sequential binding sites model and a single set of identical sites model. In the former, it is assumed that the binding of the first potassium ion will affect the binding of the second potassium ion and as a result two association constants (K_1 and K_2) are estimated. In the latter, the binding sites are considered identical and independent and only one association constant is estimated. To compare the two models, reduced chi-squared statistics (χ^2/ν) were calculated, which gives the ratio of the fitting error and the measurement error. The closer the χ^2/ν value is to one, the better the fit. A χ^2/ν value significantly less than unity could imply that the model is over-fitting the experimental data or that the estimated measurement errors are overestimated. As can be seen in Figure 4.2, for the ITC experiments with KCl, the sequential binding sites model gave a significantly lower χ^2/ν value than the single set of identical sites model (12.02 compared to 318.80). The same was found for the other salts.

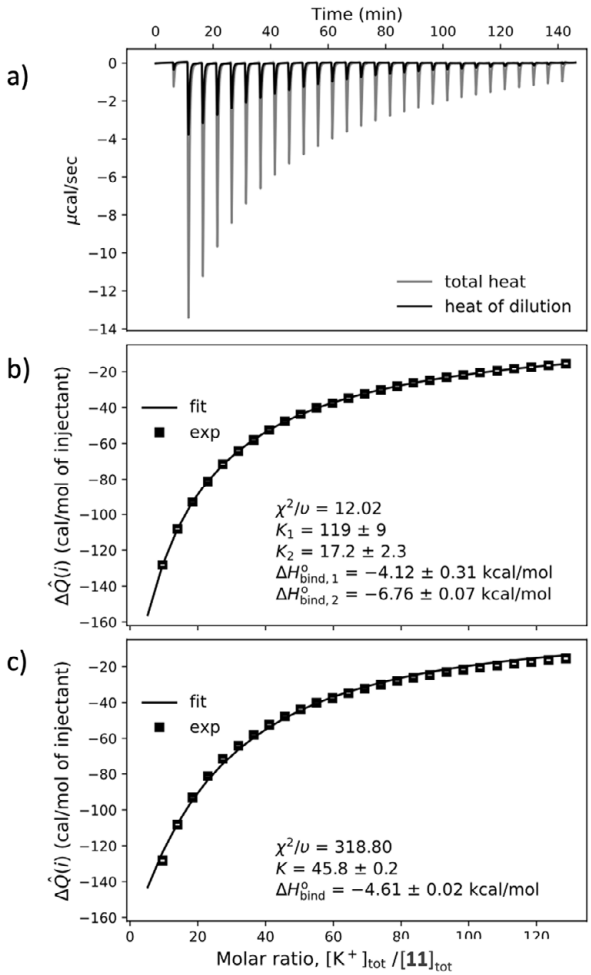

Figure 4.2 a) Heat flow diagram from consecutive additions of potassium chloride solution (247 mM) to a solution of receptor **11** (0.39 mM) in water at 25 °C. **b,c)** Normalized, integrated heats (average from three experiments). The solid lines show the fit of a sequential binding sites model (**b**) and a single set of identical sites model (**c**) to the data. Predicted parameters and reduced chi-squared statistics (χ^2/ν) for each model are included.

Table 4.1 shows the thermodynamic parameters estimated from the ITC experiments with receptor **11** and the different potassium salts using a sequential binding sites model. The estimated association constants for the binding of the first potassium ion (K_1) are similar to reported association constants for the binding of potassium to 18-crown-6 ($K \approx 100$).[64] For a ditopic receptor with two identical non-interacting binding sites, statistical factors dictate that the association constant for the binding of the second ligand (K_2) should be four times lower than the association constant for the binding of the first ligand (referred to as statistical binding).[113] If the relationship between the two association constants deviates from this ratio, the

binding sites are either not identical or exhibit cooperative binding (i.e. the binding of one ligand influences the binding affinity for the second ligand). In our case, the association constants for the binding of the second potassium ion are lower than the statistical binding ($K_2/K_1 < 0.25$), indicating negative cooperativity.

Table 4.1 Association constants, standard free binding enthalpies and standard free energies for the binding process between receptor **11** and potassium ions in water at 25 °C, obtained from ITC experiments using different potassium salts.

	KCl	KI	KSCN	K_2SO_4
K_1	119 ± 9	103 ± 6	139 ± 14	133 ± 6
K_2	17.2 ± 2.3	15.6 ± 0.6	18.1 ± 1.7	15.9 ± 1.4
ΔG^o_1 (kcal/mol)	-2.83 ± 0.05	-2.74 ± 0.03	-2.92 ± 0.06	-2.90 ± 0.03
ΔG^o_2 (kcal/mol)	-1.69 ± 0.08	-1.63 ± 0.02	-1.72 ± 0.05	-1.63 ± 0.05
$\Delta\Delta G^o$ (kcal/mol)[b]	1.14 ± 0.09	1.12 ± 0.04	1.21 ± 0.06	1.26 ± 0.06
ΔH^o_1 (kcal/mol)	-4.12 ± 0.31	-4.54 ± 0.19	-3.61 ± 0.36	-3.83 ± 0.14
ΔH^o_2 (kcal/mol)	-6.76 ± 0.07	-7.35 ± 0.27	-8.88 ± 0.14	-7.62 ± 0.30
$\Delta\Delta H^o$ (kcal/mol)[a]	-2.64 ± 0.31	-2.81 ± 0.33	-5.27 ± 0.39	-3.79 ± 0.34

[a] $\Delta\Delta H^o = \Delta H^o_2 - \Delta H^o_1$. [b] $\Delta\Delta G^o = \Delta G^o_2 - \Delta G^o_1$

Looking at the standard free energies and enthalpies, the binding of the first potassium ion is, as expected, energetically more favorable than the binding of the second potassium ion ($\Delta\Delta G^o > 0$, Table 4.1). However, surprisingly, the ITC experiments showed that the binding of the second potassium ion is enthalpically favored ($\Delta\Delta H^o < 0$, Table 4.1). These trends ($\Delta\Delta G^o > 0$ and $\Delta\Delta H^o < 0$) were reproduced for all potassium salts, indicating that the observed thermodynamic trends are independent of the counterion. While the difference in free energy for the binding of the first and second potassium ion is relatively small and similar for all counterions ($\Delta\Delta G^o$ = 1.14–1.26 kcal/mol), the difference in binding enthalpy is surprisingly large ($\Delta\Delta H^o$ = -2.64 to -5.27 kcal/mol). The estimated positive $\Delta\Delta G^o$ values indicate a large entropic penalty associated with the binding of the second potassium ion, which compensates for the negative $\Delta\Delta H^o$ values. The difference in entropy (for KCl: $T\Delta\Delta S^o = \Delta\Delta H^o - \Delta\Delta G^o$ = -3.78 kcal/mol) shows that the binding of the second potassium ion is associated with an entropy decrease that is 3.78 kcal/mol larger than that of the first. Of these 3.78 kcal/mol, 0.8 kcal/mol can be attributed to the previously mentioned statistical factors associated with binding a second ion to the ditopic receptor ($K_2 = K_1/4$), whereas the rest must be a consequence of additional entropic losses, such as reduced flexibility of the complex or increased ordering of water around the binding sites. Comparing the estimated $\Delta\Delta H^o$ values for different potassium salts, the enthalpic trend ($\Delta\Delta H^o < 0$) is more pronounced with thiocyanate as the counterion than with the other counterions (-5.27 kcal/mol for KSCN, compared to -2.64 kcal/mol for KCl), indicating counterion effects.

4.3 Explaining the observations

The origin of the negative $\Delta\Delta H^o$ values was investigated further by combining the experimental results with continuum electrostatic theory and molecular dynamics simulations. While the counterion appears to contribute largely to the observed negative $\Delta\Delta H^o$ (through stabilization of the positively charged potassium-receptor complex), there also appears to be contributions from favorable intrinsic interactions between the two potassium-coordinated crown-ethers. The investigations are described in more detail below.

4.3.1 The role of the counterion

The first ITC experiments were performed using KCl as the potassium source and, as described above, showed that the binding of the second potassium ion is enthalpically favored. One possible explanation for this could be that either the counterion or water molecules are stabilizing the complex through some kind of bridging interaction between the two cations. To probe the possible role of the counterion, the experiments were repeated with different potassium salts (KI, KSCN, and K_2SO_4). If the observed thermodynamic trend had been completely independent on the counterion, the estimated binding enthalpies and energies would have been similar regardless of what counterion was used. Conversely, if the trend had been dependent on the counterion, results would have varied significantly and the same trend ($\Delta\Delta H^o < 0$) might not have been observed for all counterions. One way to specifically investigate whether the observed stabilization is caused by bridging interactions involving the counterion would have been to use a potassium salt with a non-coordinating counterion. To this end, attempts were made to perform the ITC experiments with KPF_6. Unfortunately, due to the previously mentioned restriction in terms of receptor solubility, we were unable to find experimental conditions that could cover enough of the binding isotherm and give reproducible results.

As previously mentioned, all the investigated potassium salts gave negative $\Delta\Delta H^o$ values, although the absolute values varied somewhat depending on the counterion. While KCl and KI gave similar values (-2.64 and -2.81 kcal/mol, respectively), KSCN gave a more negative $\Delta\Delta H^o$ value (-5.27 kcal/mol). The divalent sulfate ion of K_2SO_4 gave an intermediate $\Delta\Delta H^o$ value of -3.79 kcal/mol. All in all, this indicates that there is a stabilizing counterion effect present, which is more pronounced with thiocyanate ions than with chloride, iodide, or sulfate ions. One explanation of the observed difference could be the solvation of the counterions. The thiocyanate ion is known to be weakly hydrated in water and to possess a higher affinity for nonpolar surfaces than the more hydrated chloride, iodide, and sulfate ions.[114, 115] A higher accumulation of thiocyanate ions around the receptor would stabilize the positive charge that is built-up through the binding of potassium ions

to the receptor, which could explain the additional enthalpic stabilization observed for KSCN. This was also investigated computationally by analyzing the distributing of the counterions around the receptor surface. The calculations showed that chloride, iodide, and thiocyanate are all enriched around the receptor (compared to water). However, amongst the studied anions, thiocyanate showed a significantly higher degree of accumulation around the receptor. Previous studies of the complex between KSCN and 18-crown-6 have shown the thiocyanate ion to either only interact weakly with the complex,[116] or to interact primarily through the nitrogen atom.[117] Interestingly, our calculations found that the thiocyanate ion preferentially orients itself with the sulfur atom pointing towards the receptor, although it should be noted that our analysis looked at the average distance between the counterion and the receptor surface as a whole and not specifically the crown-ether moieties.

4.3.2 Continuum electrostatic theory

The binding of cations to a ditopic receptor includes a contribution from the free energy of interaction between the cations (G_{++}), which depends on the distance between the cations (r) and the temperature (T). This energy can be estimated using Coulomb's law, which for two monovalent ions is described as:

$$G_{++} = \frac{e^2 N_{\mathrm{Av}}}{4\pi\epsilon_0\epsilon_{\mathrm{r}} r} \tag{9}$$

where e is the elementary charge, N_{Av} is the Avogadro constant, ϵ_0 is the vacuum permittivity, ϵ_{r} is the relative dielectric constant of the solvent and r is the distance between the ions. The relative dielectric constant ϵ_{r} is temperature-dependent and $G_{++}(r,T)$ should be regarded as a free energy. The enthalpy of interaction (H_{++}) can be described as:

$$H_{++} = \frac{\partial(G_{++}/T)}{\partial(1/T)} = G_{++}\left(1 + \frac{\partial \ln \epsilon_r}{\partial \ln T}\right) \tag{10}$$

The dielectric constant of water is known to have a significant negative temperature response, with $\frac{\partial \ln \epsilon_{\mathrm{r}}}{\partial \ln T}$ = -1.37 at 25 °C.[118] This means that at 25 °C, the enthalpy of interaction will take the opposite sign compared to the free energy of interaction: $H_{++} = -0.37 G_{++}$ (Figure 4.3).

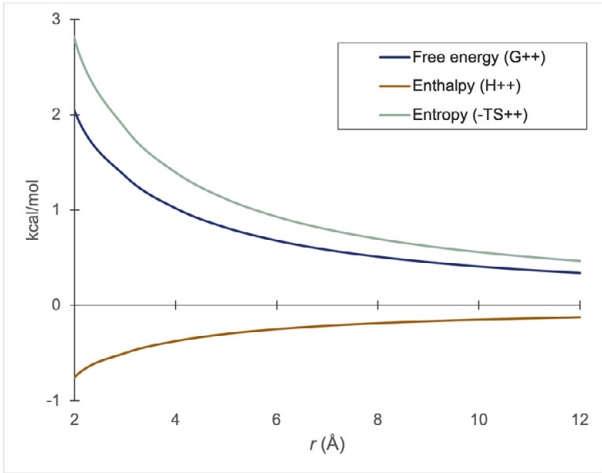

Figure 4.3 Thermodynamic parameters for the interaction of two monovalent cations in water at 25 °C as a function of distance, calculated according to Equation 9 and 10.

Using Equation 9 and 10 with r = 11.5 Å (the average distance between the potassium ions bound to the receptor determined from simulations), G_{++} and H_{++} for our system are calculated to 0.37 and -0.14 kcal/mol, respectively. Although the predicted changes in enthalpy and entropy upon bringing the potassium ions from infinite separation to the average separation in the receptor are comparatively small (H_{++} = -0.14 kcal/mol and $-TS_{++}$ = 0.51 kcal/mol), they can explain parts of the experimentally estimated values (for KCl: $\Delta\Delta H^{o}$ = -2.64 kcal/mol and $-T\Delta\Delta S^{o}$ = 3.78 kcal/mol).

4.3.3 Conformational dynamics of the receptor

For the system with the receptor and KCl, replica exchange molecular dynamics (REMD) simulations were employed to study the conformational dynamics of the receptor during the binding process. Principal component analyses (PCAs) of the simulated conformations of the free receptor and the complexes with one and two potassium ions bound were performed. Four well-defined conformations separated by notable energy barriers were identified: one with both crown ether moieties bent out from the cavity (EXT), one with both crown ether moieties bent in towards the cavity (COL), and two conformations with one crown ether bent in and one bent out (SK1 and SK2) (Figure 4.4).

Probabilities for each conformation obtained from the PCAs showed that with no potassium ion bound, the receptor preferentially adopts the EXT conformation, while the COL conformation is least favored (Figure 4.4). Upon binding of the potassium ions, the probability of the COL conformation increases. The successive stabilization of the COL conformation indicates that there are some favorable interactions introduced when the cations bind, either due to increased solvation or

due to interactions between the binding sites. With one potassium ion bound, one can imagine stabilizing interactions between the bound potassium ion and the opposite free crown ether. The added stabilizing of the COL conformation for the complex with two potassium ions bound indicates potential attractive interactions between the two crown-ether-K^+ moieties. This would be in line with the predictions from continuum electrostatics and could thus partly explain the estimated large negative $\Delta\Delta H^o$ values.

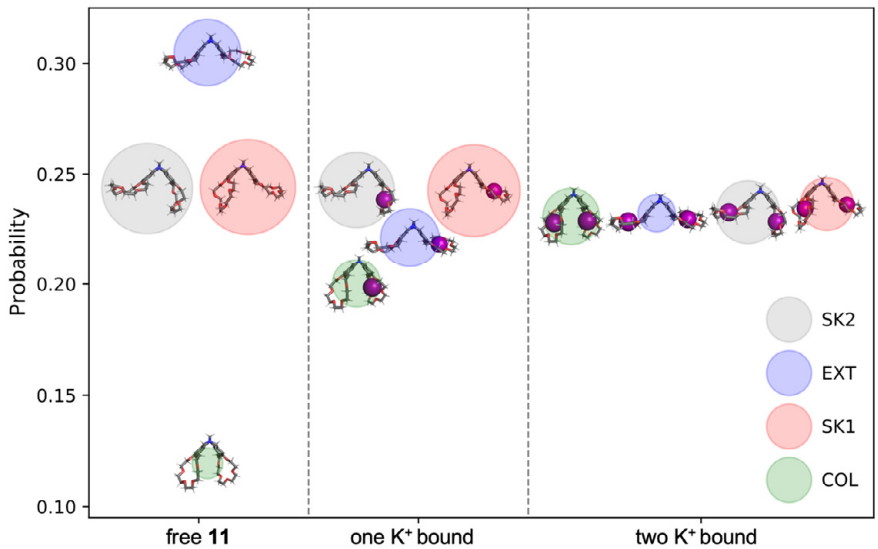

Figure 4.4 Integrated probabilities for the four conformations obtained from the PCAs of receptor **11** with no, one and two potassium ions bound. SK1/SK2 = skewed, EXT = extended, COL = collapsed.

4.3.4 Internal energies of the complexes

The experimentally estimated change in enthalpy (ΔH^o) is also related to a change in the internal potential energy of the system, ΔU_{sys} ($\Delta H_{sys} = \Delta U_{sys} + \Delta PV$). Given the finding that the probability of the COL conformation increases upon the successive binding of potassium ions, while the probability of the EXT conformation decreases (Figure 4.4), the changes in internal potential energies upon binding of the first and second potassium ion were analyzed. The internal potential energies were calculated as average energies of the system obtained from the REMD simulations, excluding water and counterions. As such, the calculated internal potential energies include the bonded and non-bonded interaction within the receptor, and non-bonded interactions between the receptor and the bound potassium ions. Both the energy of adding a first (ΔU_1) and a second (ΔU_2) potassium ion are negative (Table 4.2). The difference between the two changes in energy ($\Delta\Delta U = \Delta U_2 - \Delta U_1$) can be interpreted as a measure of the contribution to the

potential energy solely from interactions between the two potassium-bound binding sites. The negative $\Delta\Delta U$ value indicates that favorable interactions between the two binding sites contribute to the overall negative $\Delta\Delta H^{o}$ value. As opposed to the results obtained from continuum electrostatics, where the enthalpic stabilization is a solvent effect, the $\Delta\Delta U$ is calculated excluding water and thus gives the internal energy within the complex *in vacuo*. Continuum electrostatics predict a positive interaction enthalpy between two positive charges *in vacuo*, so the negative sign of the $\Delta\Delta U$ must be a result of attractive interactions within the complex large enough to overcompensate for the electrostatic ion-ion repulsion.

Table 4.2. Calculated changes in internal potential energy of the complexes upon binding of a first and second potassium ion.

ΔU_1 (kcal/mol)	ΔU_1 (kcal/mol)	$\Delta\Delta U$ (kcal/mol)
-103.75 ± 0.07	-103.94 ± 0.07	-0.19 ±0.13

To understand the origin of the negative $\Delta\Delta U$, it was decomposed into contributions from the four different conformations (EXT, COL, SK1, and SK2). Weighing the internal potential energies of each conformation and bound state (no, one or two potassium ions bound) with their respective probabilities revealed that the negative $\Delta\Delta U$ (and by extension the $\Delta\Delta H^{o}$) stems exclusively from a large negative contribution from the increasingly populated COL conformation, while the other conformations yield positive contributions to $\Delta\Delta U$. This finding points to the presence of intrinsic favorable interactions between the two potassium-bound crown-ethers, which are independent of the solvent and the counterion (as these were excluded from these calculations).

4.3.5 Solvation effects

Previous studies have found the apparent cation-cation attraction to primarily be a result of a change in solvation.[110, 119] To determine the influence of solvation effects in our system, the solvent response upon binding of the first and second potassium ion to receptor **11** was investigated computationally. The calculated distribution of angles between the dipole moment of water molecules in the solvation shell around each binding site was compared for each bound state (with no, one or two potassium ions bound). Only subtle changes in the average angle between the dipoles were observed and it was concluded that solvent reorganization is likely not a significant contributor to the observed enthalpically favorable binding of the second potassium ion.

4.4 Conclusions

The consecutive binding of potassium ions to ditopic receptor **11** was studied by ITC, revealing that, counterintuitively, the binding of the second potassium ion is enthalpically favored over that of the first, despite of the expected electrostatic repulsion between the two cations. The experimentally determined thermodynamic trends ($\Delta\Delta G^{o} > 0$ and $\Delta\Delta H^{o} < 0$) were reproduced with four different potassium salts (KCl, KI, KSCN, K_2SO_4), i.e., the trends are independent of the counterion. However, the magnitude of the enthalpic stabilization was found vary with the counterion, indicating stabilizing counterion-dependent effects. Thiocyanate gave the most negative $\Delta\Delta H^{o}$ value, which could potentially be explained by a comparatively higher affinity of the weakly hydrated thiocyanate ion for the receptor, compared to the more hydrated chloride, iodide, and sulfate ions. To fully elucidate the effect of counterion stabilization, further experiments and analyses are needed. This could include performing the experiments with a broader range of counterions, or more detailed studies into the location of the counterions in relation to the receptor.

In addition to the counterion stabilization, other factors were also found to contribute to the observed negative $\Delta\Delta H^{o}$. In water at 25 °C, continuum electrostatics theory predicts a small enthalpic attraction between two monovalent cations. An analysis of simulated conformations of the receptor revealed that the binding of potassium ions leads to a successive increase of the probability of a more collapsed conformation, where the two crown-ether moieties are closer to each other. The stabilization of the collapsed conformation indicates stabilizing interactions introduced upon binding the ions, either between the two binding sites, or between the solvent (water) and the receptor in its collapsed conformation. While an analysis of the solvation shells around the binding sites showed only a subtle solvent response upon binding of the ions, an evaluation of the internal potential energies within the complexes (excluding water and counterions) found a contribution to the negative $\Delta\Delta H^{o}$ stemming from intrinsic interactions between the two potassium-bound crown-ether moieties in the receptor in the collapsed conformation.

In summary, this study is an attempt to explain an unexpected observation; an enthalpic stabilization of the binding of a second potassium ion to a ditopic receptor. By a combination of experiments and simulations, the influences of a number of different factors were investigated. Although further investigations are needed to fully understand all of the factors contributing to the binding process, the herein described results can hopefully provide valuable insight into the thermodynamic factors governing receptor/ligand interactions in water.

5 Discrete hydrogen-bonded supramolecular aggregates

5.1 Hydrogen bonding in supramolecular assemblies

Hydrogen bonds are ubiquitous in Nature and amongst the most utilized non-covalent interactions in supramolecular systems. The hydrogen bond is defined as an attractive interaction between a hydrogen atom covalently bound to a more electronegative atom (hydrogen bond donor, D) and an electronegative atom (hydrogen bond acceptor, A).[120] Common donor atoms include oxygen, nitrogen or halogens, but also less electronegative elements such as carbon can serve as hydrogen bond donors. The acceptor is typically an electronegative atom bearing a lone pair of electrons, such as a carbonyl oxygen, but can also be an electron-rich π-bond.[121] Hydrogen bonding is primarily considered an electrostatic interaction, but can also include contributions from other factors such as covalent and resonance effects.[122, 123] The bond energy of a hydrogen bond can vary between 1 and 40 kcal/mol and depends on the nature of the hydrogen bond donor and acceptor, and the bond geometry (length and angle). In solution, the strength of the hydrogen bond is strongly affected by the solvent, as polar solvent molecules can also form hydrogen bonds and thus compete with the solute molecules, resulting in a weakening or destruction of the hydrogen bonds between the solute molecules.[121]

In supramolecular assemblies, a single hydrogen bond is usually not enough to ensure the formation of a well-defined construct. Instead, multiple hydrogen bonds arranged in specific motifs, or systems combining hydrogen bonding and other non-covalent interactions, are often employed. Even though a higher number of hydrogen bonds results in a stronger association, the arrangement of the hydrogen bond donors and acceptors also play an important role. The concept of secondary electrostatic interactions (SEI), first introduced by Jorgensen and coworkers, uses the diagonal interactions between adjacent hydrogen bonds to rationalize the preferred arrangement of donors and acceptors (Figure 5.1a).[124, 125] For a triple-bonded array, the strongest association would be obtained with an AAA-DDD motif, which only contains attractive SEIs, while the weakest complex would be obtained with a ADA-DAD motif, in which all of the SEIs are repulsive. This has also been shown experimentally, by comparing the association constants of complexes with different hydrogen-bonding motifs (Figure 5.1b).[125, 126]

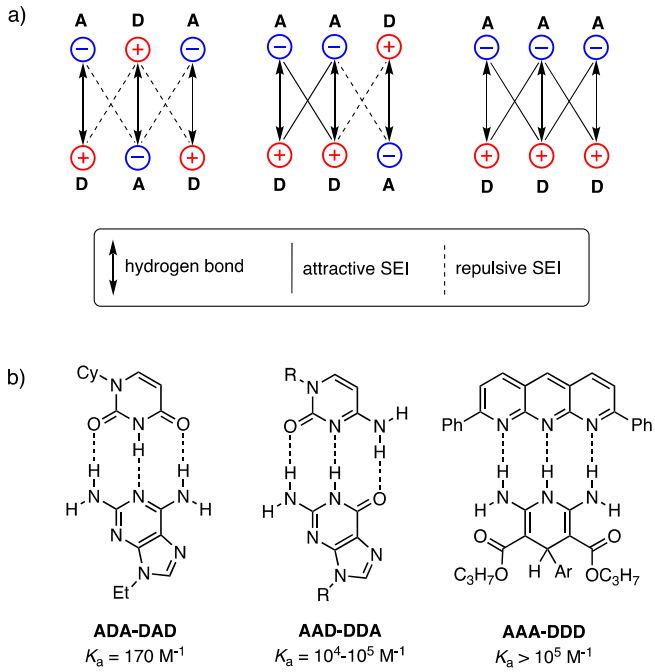

Figure 5.1 a) Schematic representation of secondary electrostatic interactions (SEIs). **b)** Examples of ADA-DAD, AAD-DDA, and AAA-DDD hydrogen-bonded complexes.

In order to achieve a predictable, strong aggregation, a certain level of pre-organization is typically required in the monomers. To this end, hydrogen-bonding monomers often include rigid, flat heteroaromatic systems, where the hydrogen bond donors and acceptors are part of the ring system. Intramolecular hydrogen-bonds can also be used to reduce the flexibility of the system and ensure maximum overlap between the binding sites. The latter was shown experimentally by Meijer and coworkers, who developed self-complementary quadruple hydrogen-bonding monomers. The higher stability of dimer $\mathbf{19}_2$ compared to dimer $\mathbf{18}_2$ was attributed to intramolecular hydrogen bonds fixing the carbonyl groups in the plane of the ring (Figure 5.2).[127, 128]

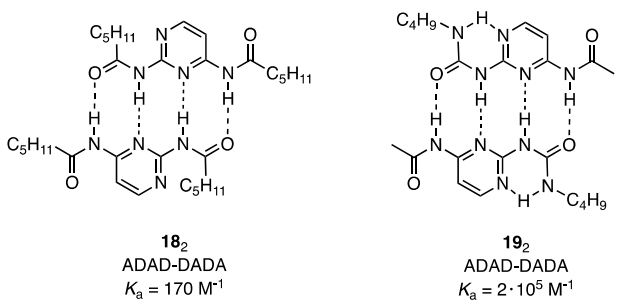

Figure 5.2. Comparison of quadruply hydrogen-bonded dimers without and with preorganizing intramolecular hydrogen bonds.

Compound **19** contains one of the most common hydrogen-bonding motifs, ureidopyrimidinone (UPy). UPy is a versatile building block for hydrogen-bonded self-assembly, owing to its self-complementary nature, ability to dimerize via a strong quadruple hydrogen-bonding motif, and synthetic accessibility.[129] One drawback of UPy as a hydrogen-bonding motif is that it has three tautomeric forms, of which two are self-complementary and can dimerize through AADD or ADAD arrays (Figure 5.3a).[128] The preference for one tautomer over another is governed by the polarity of the solvent and the nature of substituents on the pyrimidinone ring.[130] In polar solvents such as DMSO, where intermolecular hydrogen bonding is suppressed, UPy is present in its 6-[1*H*]-pyrimidinone monomeric form (**6-keto** in Figure 5.3a). In less polar solvents such as chloroform or toluene, a mixture of dimeric 4-[1*H*]-pyrimidinone (**4-keto**) and pyrimidin-4-ol (**enol**) is present. The relative amount of each dimer depends on the electronic properties of the substituents on the pyrimidinone ring, with electron-withdrawing groups in the 6-position favoring the enol tautomer while weakly electron-donating groups favor the keto tautomer.[128] Further strategies to completely control the keto-enol tautomerization by restricting the intramolecular proton transfer include using bifurcated hydrogen bonds [130, 131] (Figure 5.3b) and replacing the ureidopyrimidinone with an *N*-alkylated ureidocytosine[132] (Figure 5.3c).

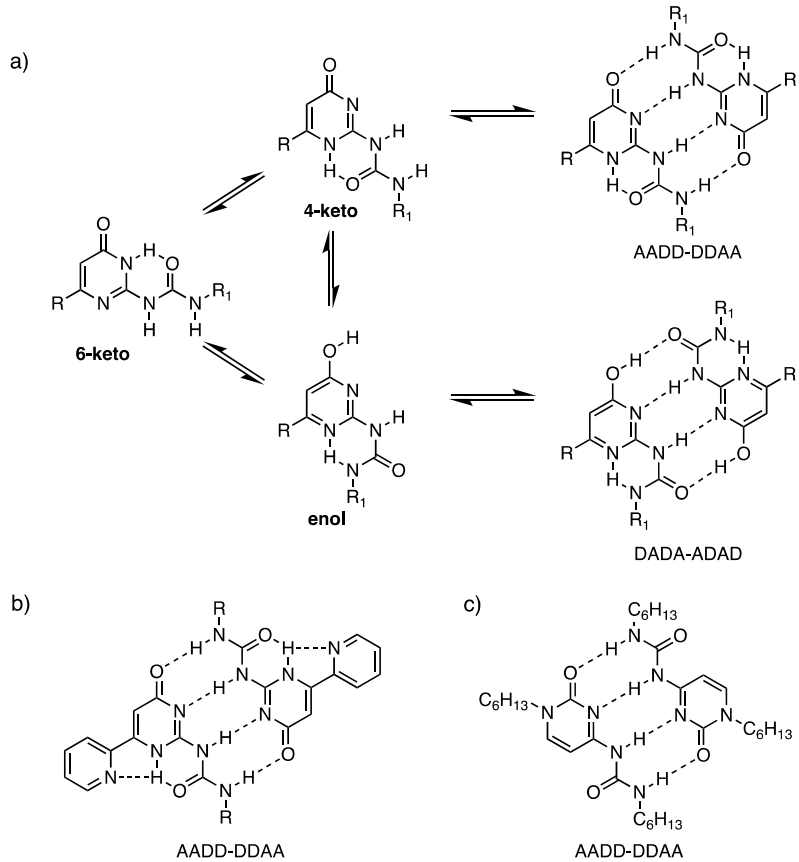

Figure 5.3. a) Tautomeric forms of ureidopyrimidinones (UPys). **b)** AADD-DDAA dimer with bifurcated intramolecular hydrogen bonds. c) AADD-DDAA dimer with *N*-alkylated ureidocytosine.

Although the presence of different tautomeric forms is an issue that needs to be considered when designing supramolecular systems containing UPy units, the tautomerization can also be seen as an asset which could allow for the construction of systems capable of stimuli-responsive switching between different tautomeric forms leading to different self-assembled structures.

5.2 Discrete aggregates

The formation of discrete supramolecular aggregates relies on careful design of the molecular components (monomers). In order to ensure predictable and controlled self-assembly, the monomers have to be encoded with all of the necessary information. Both the choice of binding motif and the shape and geometry of the monomer are important for generating well-defined aggregates. The self-assembly

of monomers into a larger aggregate is associated with an entropic penalty arising from the increased order of the system, which has to be overcome for spontaneous self-assembly to occur. Rigid monomers with a higher degree of preorganization can be used to minimize the reorganization needed for and the strain introduced by self-assembly, making the aggregation more favorable. While the aggregation of more flexible monomers is associated with a larger loss of conformational freedom, they can potentially be used to create more dynamic supramolecular system.

5.2.1 Cyclic aggregates

One type of discrete hydrogen-bonded aggregates are self-assembled macrocycles. This type of aggregate requires a monomer with more than one binding site, where the binding sites are positioned at an angle relative to one another. The preferential formation of cyclic aggregates over linear ones can be attributed to a cooperative effect known as chelate or intramolecular cooperativity, which is caused by the additional binding event taking place in the cyclization process.[133]

The importance of preorganization in self-assembled macrocycles can be illustrated by the two examples in Figure 5.4. Lehn and Mascal reported hexameric macrocycles (rosettes) self-assembled from Janus-type monomers containing two complementary hydrogen-bonding motifs. The relative position of the hydrogen-bonding motifs lead to the exclusive formation of hexameric macrocycles (Figure 5.4a).[134-136] Perrin and coworkers developed a similar system, where the introduction of a central pyrrole unit resulted in monomers with the hydrogen-bonding motifs oriented at a 90° angle. These monomers self-assemble into tetrameric rosettes in solution (Figure 5.4b).[137]

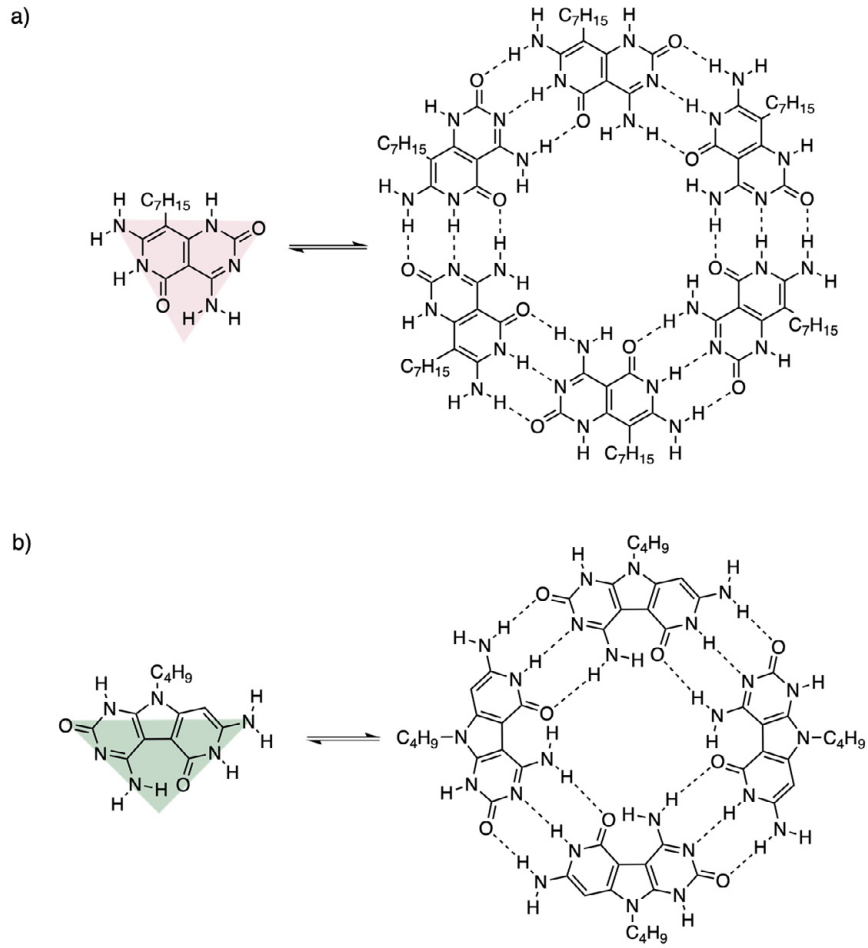

Figure 5.4 a) Hydrogen-bonded hexameric macrocycle. **b)** Hydrogen-bonded tetrameric macrocycle. Angle between hydrogen bonding motifs marked in pink and green, respectively.

5.2.2 Capsules

Another type of discrete hydrogen-bonded aggregates are capsules formed from the self-assembly of concave monomers. The well-defined internal space of capsules makes them interesting for applications in host-chemistry (as nanocontainers) and catalysis (as nanoreactors).[138, 139] The construction of reversible molecular capsules was pioneered by Rebek and coworkers and their "tennis ball": a pseudospherical dimer consisting of two glycoluril-based monomers held together by eight hydrogen-bonds (Figure 5.5a). The small cavity size of capsule $\mathbf{20}_2$ allows for the encapsulation of one small molecule, such as methane or ethane.[140] By extending the backbone of monomer **20**, a dimeric capsule with a cavity large enough to encapsulate two benzene molecules or one molecule of adamantane was

obtained.[141] Rebek and coworkers also reported a dimeric cylindrical capsule based on monomer **21** with a resorcinarene scaffold (Figure 5.5b). The cavity of the capsule is large enough to encapsulate for example two aromatic molecules. Interestingly, when both benzene and *p*-xylene were added to the solution, only capsules containing one benzene molecule and one *p*-xylene molecule were observed. This indicates that the optimal occupancy of the cavity is obtained with the hetero-guest pair, while two benzene molecules leave too much empty space and two *p*-xylene molecules makes the cavity too crowded.[142]

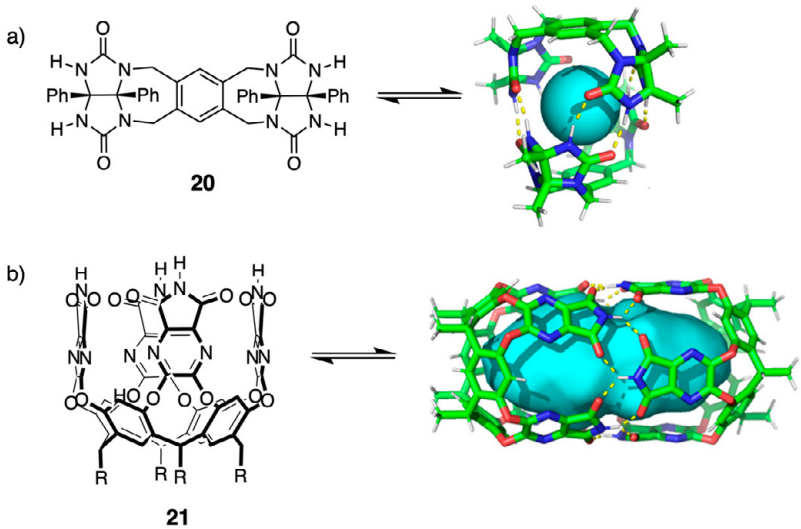

Figure 5.5 Glycoluril-based monomers capable of forming dimeric capsules. **a)** Monomer **20** and "tennis ball" capsule. **b)** Monomer **21** and cylindrical capsule. Adapted from ref[143].

Hydrogen-bonded capsules with larger cavities have also been reported. Mastalerz and coworkers synthesized an octameric capsule with a 2300 Å^3 cavity (Figure 5.6a).[144] Enantiopure tris(isatin) monomer **22** was used to prevent the formation of unwanted oligomeric or polymeric species. The capsule was able to encapsulate several different cationic guests, the largest being the tetrahexadecylammonium cation. The formation of the host-guest complexes was favored by cation-π interactions inside the cavity. The largest cavity size of a hydrogen-bonded capsule reported to date belongs to a hexameric cage reported by Tiefenbacher and coworkers (Figure 5.6b).[145] The capsule, formed from resorcinarene monomer **23** with amide functionalities, has a 2800 Å^3 cavity volume and was shown to encapsulate C_{60} and C_{70} fullerenes through dispersive and π-π interactions between the guest and the cavity. The formation of the hexameric capsule was found to be strongly concentration-dependent, with higher concentrations favoring the hexameric capsule and lower concentrations resulting in mainly smaller species.

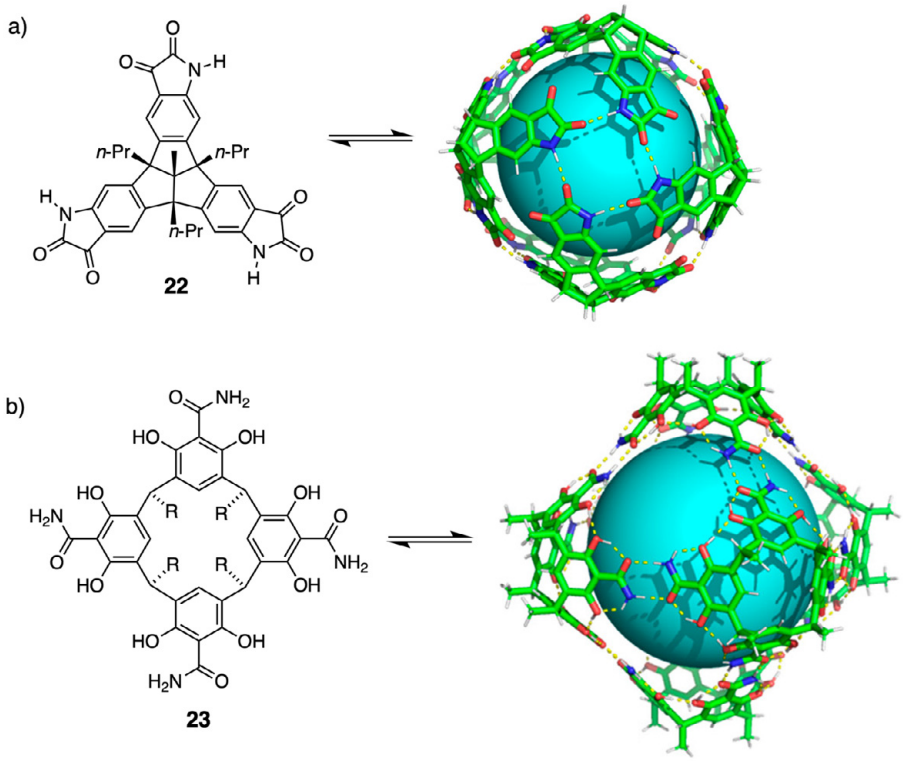

Figure 5.6. **a)** Enantiopure tris(isatin) monomer **22** and octameric capsule. **b)** Resorcinarene-based monomer **22** and hexameric cage. Adapted from ref[143].

5.2.3 Self-assembled nanotubes

In Nature, hollow tubular structures are involved in diverse biological functions, including as channels for the transport of chemicals across cell membranes[146, 147] and as reaction chambers for protein folding[148, 149] and protein degradation[150, 151]. The construction of synthetic open-ended nanotubes has received much attention due to their many potential applications, for example as reaction vessels for flow-through catalysis and for size- and shape-discriminating separation and detection.[152] Several different approaches for the construction of tubular assemblies based on hydrogen bonding have been reported, including helical coiling of a linear precursor and stacking of covalent or non-covalent macrocycles (Figure 5.7). Some selected examples of hydrogen-bonded nanotubes are discussed below.

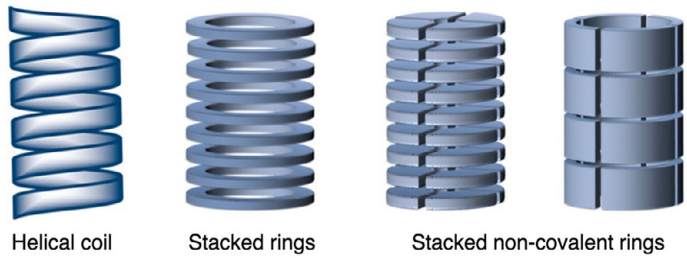

Figure 5.7 Schematic representation of some general strategies for the design of self-assembled nanotubes. Adapted from ref[153].

Gellman and coworkers developed short β-peptides with unnatural backbones which were shown to fold into stable helical nanotubes (**24**, Figure 5.8a). The incorporation of cyclohexyl or cyclopentyl groups into the backbone provided substantial rigidity and facilitated the formation of a specific helix. The helical foldamer is stabilized by multiple intramolecular hydrogen bonds.[154, 155] Sanders and coworkers reported amino acid-functionalized naphthalenediimide (NDI) monomer **25** which could polymerize into helical nanotubes (Figure 5.8b). The monomeric units are held together by hydrogen bonds between the carboxylic acid moieties and the helical structure is reinforced by CH-O hydrogen bonds between aromatic hydrogens and carbonyl groups.[156, 157] The inner diameter of the helical nanotube (12.4 Å) allowed for the encapsulation of C_{60} fullerenes.[158] In a more recent example, Dong and coworkers developed hydrogen-bonded helical nanotubes that could be inserted into lipid bilayers and used to transport glucose across the membrane. A combination of a rigid phenanthroline backbone and robust intramolecular hydrogen bonds was used to control the orientation of the two UPy moieties, ensuring helical self-assembly (**26**, Figure 5.8c).

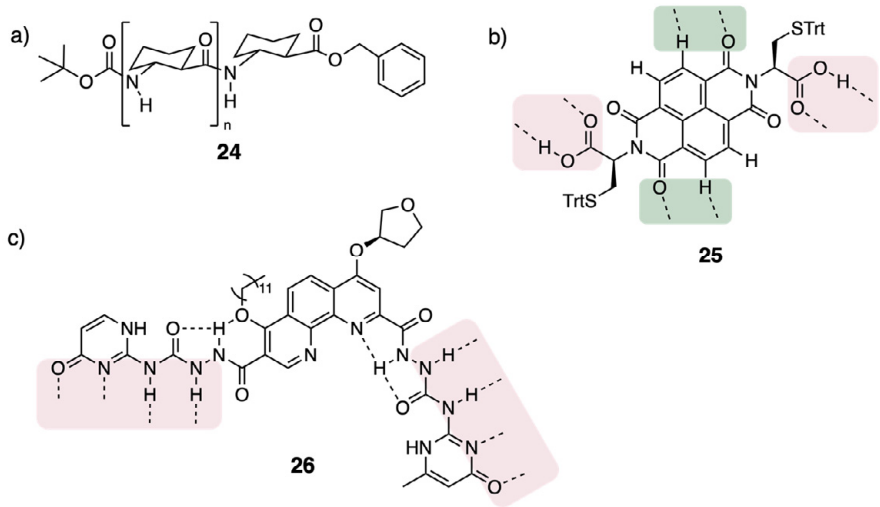

Figure 5.8 a) Linear β-peptide **24** capable of folding into a helical nanotube. **b)** NDI monomer **25** capable of forming polymeric helical nanotube. Hydrogen bonds involved in the polymerization marked in pink, CH-O bonds reinforcing the helical structure marked in green. **c)** Monomer **26** capable of helical self-assembly. AADD hydrogen bonding motifs marked in pink.

An even number of alternating D- and L-amino acids can form cyclic peptides capable of stacking through backbone-backbone hydrogen bonding. This concept, first proposed by DeSantis,[159] has been used by Ghadiri and coworkers to form hollow tubular structures with the amino acid side chains on the outside of the nanotube (Figure 5.9).[152] In their first report, octapeptide cyclo[-(L-Gln-D-Ala-L-Glu-D-Ala)$_2$-] was shown to assemble into a stacked tube by careful acidification of a basic solution.[160] The inner diameter of the tube could be controlled by varying the size of the peptide ring, with octa-, deca-, and dodecapeptides giving structures with an inner diameter of 7, 10, and 13 Å, respectively.[152] Modification of the cyclic peptide also enabled the formation of tubular dimers with functionalized cavities. By attaching different groups to the inside of the tube, the properties of the cavity could be modified, leading to preferential encapsulation of different guests.[161] Nanotubes based on cyclic peptides bearing hydrophobic side chains have also been inserted into lipid bilayers to form transmembrane channels. Self-assembled channels based on an octapeptide displayed ion-transport activities for K^+ and Na^+ rivaling the performance of naturally occurring ion channel gramicidin A.[162] Larger-cavity channels based on decapeptides showed efficient transport of glucose[163] and glutamic acid.[164] Amphiphilic cyclopeptides have also been employed as antibacterial agents, displaying potent in vitro activity against Gram-positive and Gram-negative bacteria by disrupting the cell membrane and causing rapid cell death.[165] Furthermore, specific glycosylation of the cyclopeptides was found to decrease the cell toxicity in mammalian cells while maintaining the bactericidal activity.[166]

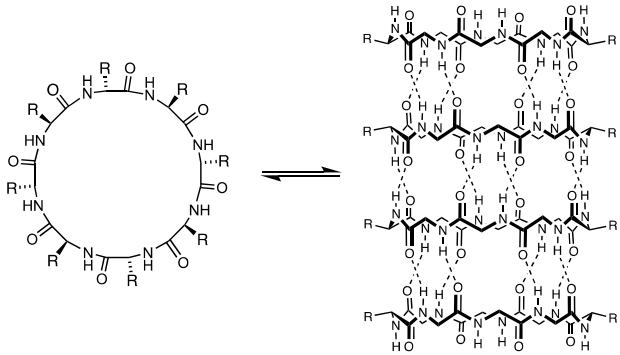

Figure 5.9 Cyclic octapeptide consisting of alternating D- and L-amino acids and self-assembled hydrogen-bonded nanotube.

An interesting example of a nanotube formed through stacking of hydrogen-bonded tetramers was reported by González-Rodríguez and coworkers. Rigid monomer **27** consisting of complementary hydrogen-bonding motifs linked by a linear, π-conjugated spacer self-assembled into tetrameric aggregates in THF (Figure 5.10). When changing the solvent to a less polar THF/cyclohexane or THF/heptane mixture, the tetramers were shown to stack into nanotubes. The stacking into nanotubes was guided by hydrogen bonding between the peripheral amide groups and π-π interactions.[167] The peripheral amide groups play a vital role in the tubular polymerization and the stability of the tube, as an analogous monomer without the amide moieties, while capable of forming tetramers, did not exhibit any tubular stacking.[168]

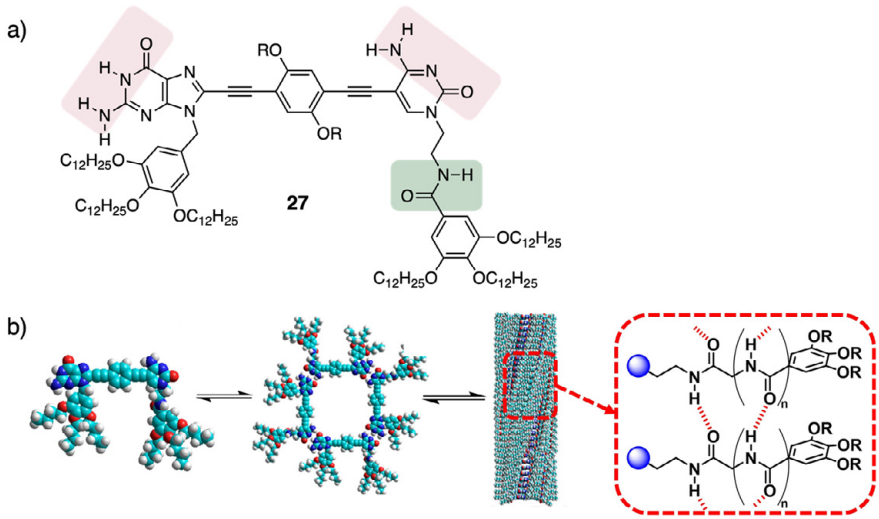

Figure 5.10 a) Monomer consisting of complementary hydrogen-bonding motifs with rigid linker. Hydrogen-bonding motif involved in formation of tetramer marked in pink, hydrogen-bonding motif involved in polymerization and stabilization of nanotube marked in green. **b)** Two-step self-assembly into nanotubes. Adapted from ref[168].

5.3 Supramolecular aggregates based on a bicyclo[3.3.1]nonane scaffold

The design and self-assembly of monomers based on the fusing of different hydrogen-bonding motifs to an enantiopure C_2-symmetric bicyclo[3.3.1]nonane scaffold has been extensively studied by Wärnmark, Orentas and coworkers. The rigid bicyclo[3.3.1]nonane backbone can adopt three different conformations: chair-chair, boat-chair and boat-boat (Figure 5.11). However, by fusing aromatic rings to the cyclohexane rings, the backbone is conformationally restricted, resulting in a structure with the aromatic rings positioned at an ~90° angle. Additionally, the use of an enantiopure bicyclic backbone ensures the exclusive formation of cyclic aggregates over unwanted polymeric species. By incorporating different hydrogen-bonding motifs, systems capable of self-assembling into cyclic tetramers and pentamers,[169-171] capsules,[172, 173] molecular tweezers,[174] and tubular aggregates[153, 173, 175] have been achieved.

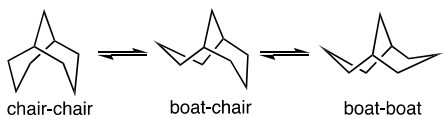

Figure 5.11 Conformations of bicyclo[3.3.1]nonane

In one of the first reported examples, isocytosine units were used as hydrogen-bonding motifs, with branched 3,5-bis(decyloxy)benzyl groups added to the bicyclic scaffold to ensure sufficient solubility (**28**, Figure 5.12a). The design of the monomer is based on the ability of isocytosine to tautomerize. Self-assembly could occur either by hetero-tautoleptic aggregation (i.e., aggregation between two different monomers, each containing only one of the tautomeric forms) or by self-complementary homo-tautoleptic aggregation (i.e., each monomer contains two different tautoleptic forms). A combination of ^{1}H and 2D NMR spectroscopy, diffusion-ordered spectroscopy (DOSY) and gel permeation chromatography (GPC) studies in chloroform indicated the exclusive formation of the homo-tautoleptic tetramer shown in Figure 5.12.[169] In a later study, monomer **28** was found to form a complex decameric capsule in CS_2. NMR spectroscopy studies revealed that the capsule consisted of three different tautomeric forms of the monomer held together by a total of 36 hydrogen bonds (Figure 5.12c). The capsule was able to encapsulate one molecule of C_{60} inside its cavity. [172]

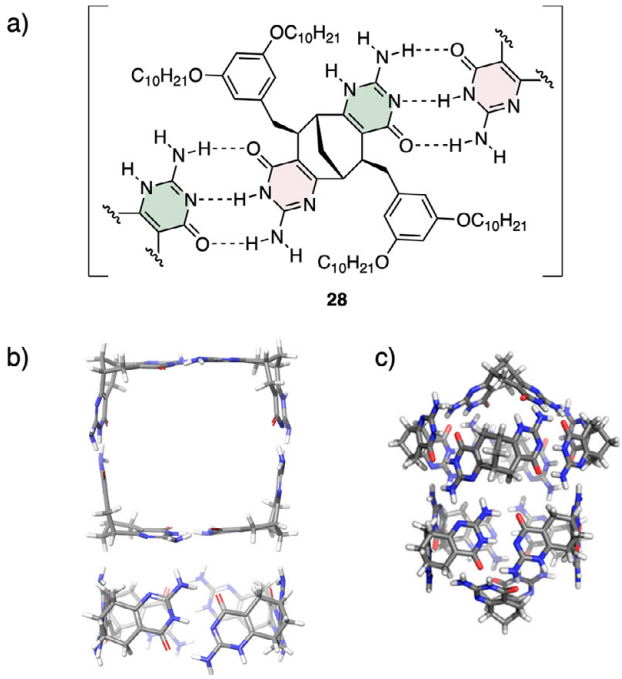

Figure 5.12 a) Structure of isocytosins monomer **28** capable of homo-tautoleptic aggregation. **b)** Molecular model of tetramer $\mathbf{28}_4$. c) Molecular model of decameric capsule formed in CS_2. Solubilizing groups omitted for clarity. Adapted from ref[172].

Extending the hydrogen-bond motif to a UPy unit by adding a urea group resulted in monomer **29** with self-complementary hydrogen-bonding motifs (Figure 5.13a). As previously mentioned, UPy has three tautomeric forms, of which two can participate in self-complementary hydrogen-bonding. For monomer **29**, self-assembly was found to take place solely through the 4-[1*H*]-pyrimidinone tautomer. In chloroform, cyclic tetramers were formed. The high stability of the aggregate was confirmed by dilution and variable temperature (VT) NMR experiments. In toluene and benzene, a mixture of tetramers and pentamers was obtained (Figure 5.13b). It was proposed that the stronger hydrogen bonding in less polar solvents leads to a higher tolerance for distortions of the hydrogen bonding angle, thus allowing the formation of pentameric aggregates. The tetrameric aggregates showed a high affinity for C_{60} and C_{70} in aromatic solvents. Addition of C_{60} to a mixture of tetramers and pentamers in toluene shifted the equilibrium towards the exclusive formation of tetrameric inclusion complexes (Figure 5.13b).[170]

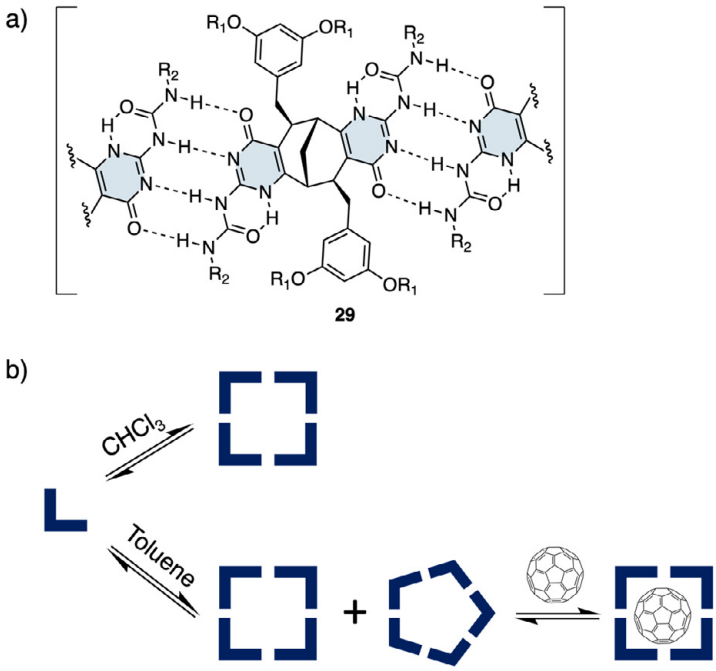

Figure 5.13 a) Structure of UPy monomer **29**. $R_1 = C_{10}H_{21}$, R_2 = Bn or Bu. **b)** Solvent- and guest-controlled self-assembly of **29**.

In an effort to obtain aggregates of a higher degree by the stacking of tetramers into a tube, the bulkiness and position of the solubilizing groups were altered. In monomer **30**, the bulky 3,5-bis(decyloxy)benzyl groups were replaced by linear decyl chains (Figure 5.14a). In monomer **31**, instead of two solubilizing groups in the 4- and 8-position, a single solubilizing group was attached to the bridging methylene. In monomer **32**, flexible linkers were introduced between the bicyclic scaffold and the solubilizing groups. For all three monomers, formation of polymeric aggregates was observed in both chloroform and toluene, as indicated by broad and featureless ^{1}H NMR spectra and high solution viscosity. The tubular polymers were formed by homo-tautoleptic aggregation into cyclic tetramers, analogous to what was observed for monomer **28** with more bulky solubilizing groups, followed by further aggregation through stacking of the tetramers supported by orthogonal hydrogen bonding (Figure 5.14b). Upon increasing the concentration, turbid or transparent gels were obtained. The proposed gelation mechanism involves the initial intertwining of the individual tubular polymer chains, followed by further entanglement into a network. The inner diameter of the tubular polymers (~10 Å) allowed for the encapsulation of C_{60} or C_{70} guest, as could be observed by a gradual change of the color of the gel. The tubular polymers and gelation mechanism were further studied by solid-state NMR and atomic force microscopy (AFM).[153]

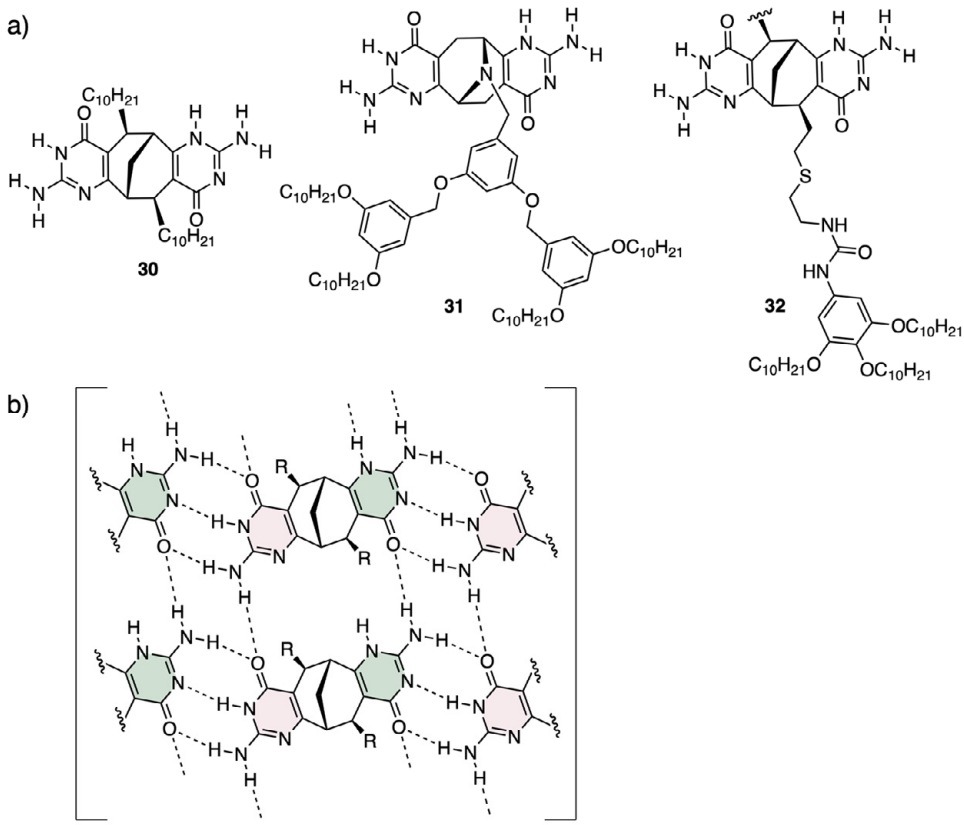

Figure 5.14 a) Structures of isocytosine monomers **30**-**32** designed to reduce steric repulsion between monomers. **b)** Two-dimensional hydrogen bonding leading to tubular monomers.

Linear decyl solubilizing groups were also employed to enable the formation of an octameric tube from an unsymmetrical monomer containing one isocytosine moiety and one UPy moiety (Figure 5.15a). The tubular aggregation relies on the amino group of the isocytosine unit, where one of the protons is involved in the formation of the tetramer and the other in the connection between two tetramers. Despite the existence of several possible aggregation modes, monomer **33** was shown to form the desired octameric tube in several different non-polar solvents. Monomers with 3,5-bis(decyloxy)benzyl groups instead of linear decyl chains showed no octameric aggregation, most likely as a result of the steric repulsion between the bulky groups hindering edge-to-edge interactions between tetramers. Addition of a C_{60} guest resulted in the rearrangement from an octameric tube into a tetrameric inclusion complex with a different hydrogen-bonding mode (Figure 5.15b).[175]

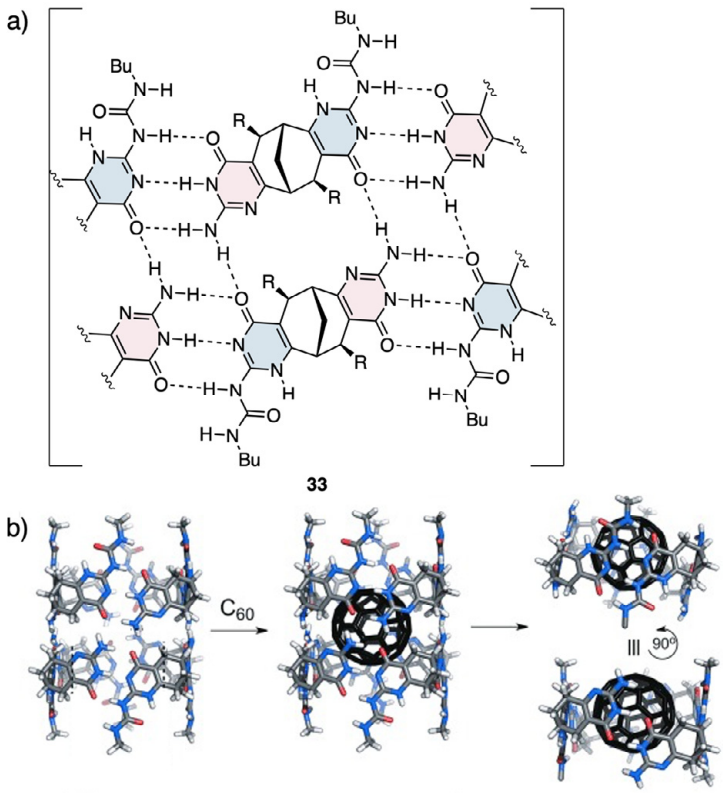

33

Figure 5.15 a) Structure of isocytosine-UPy monomer **33**. R = $C_{10}H_{21}$. **b)** Structural rearrangment from octameric tube to tetramer upon C_{60} complexation. Solubilizing groups omitted for clarity. Adapted from ref[175].

A different strategy for achieving tubular aggregates was to introduce a pyrrole unit between the bicyclic backbone and the UPy motif (here referred to as a PUPy motif). The incorporation of an electron-rich pyrrole results in the 6[1*H*]-pyrimidinone form of the isocytosine unit becoming the most stable tautomer, with one of the terminal urea protons hydrogen-bonded to one of the isocytosine nitrogen atoms (Figure 5.16a). As previously discussed, this tautomer cannot participate in self-complementary quadruple hydrogen bonding, but instead contains several 2H-bonding sites positioned at different angles. The introduction of orthogonal hydrogen bonding motifs was expected to enable aggregation into tubular polymers (Figure 5.16b). In chloroform, the monomer self-assembled into cyclic tetramers, as confirmed by 2D NMR spectroscopy and DOSY. In less polar solvent such as toluene and benzene, extreme broadening or disappearance of the signals in the ^{1}H NMR spectrum indicated the formation of larger aggregates. The formation of polymeric aggregates was confirmed by AFM, GPC and dynamic light scattering (DLS). The polymerization could also be triggered in a more polar solvent (chloroform) by the addition of C_{70} as a templating guest. Interestingly, the addition

of a C_{60} guest resulted in the formation of a single well-defined inclusion complex, which was attributed to a capsule-like structure with the monomers arranged side-to-side rather than end-to-end (Figure 5.16c).[173]

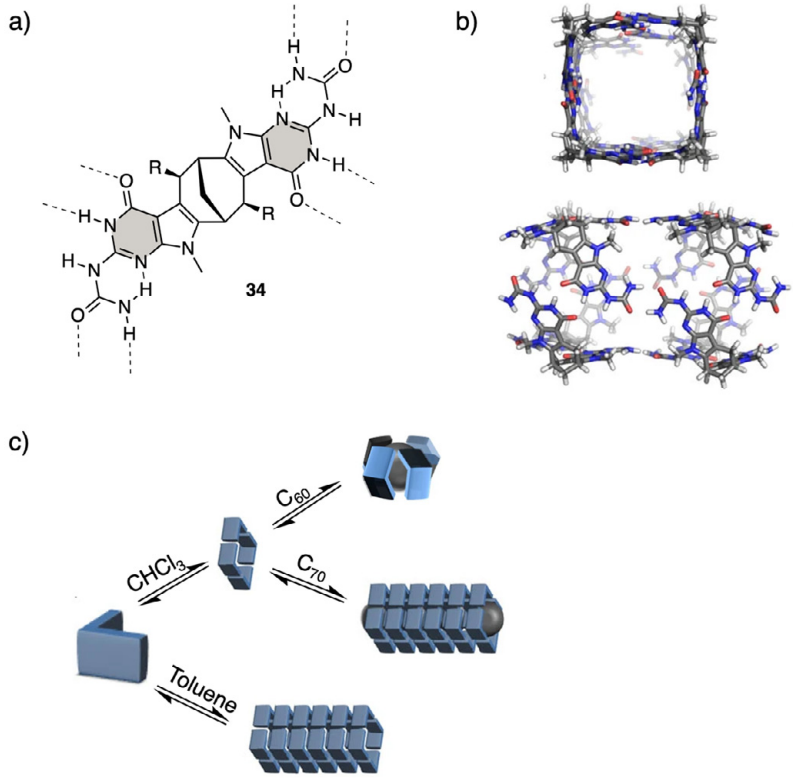

Figure 5.16 a) Structure of PUPy monomer **34**. R = 3,5-bis(decyloxy)benzyl. **b)** Molecular model of tubular aggregate, shown as octamer $\mathbf{34}_8$. Solubilizing groups omitted for clarity. **c)** Solvent- and guest-controlled self-assembly behavior of **34.** Adapted from ref[173].

The following chapter describes the design, synthesis and self-assembly studies of hydrogen-bonding monomers based on monomers **29** and **34**, where polyethylene glycol (PEG) chains were added to improve the solubility of the monomers and their aggregates in more polar solvents.

6 Design and synthesis of amphiphilic monomers (Paper III)

6.1 Introduction

PEG is an amphiphilic polymer consisting of repeating ethylene oxide units, with molecular weights varying between 200 and 20 000 Da depending on the number of repeating units.[176] Due to its high structural flexibility, non-toxicity, and biocompatibility, PEG has been exploited in various industrial and biochemical applications.[177] The introduction of PEG chains is a known strategy for increasing the solubility of compounds and has been employed in areas such as the development of drugs with improved therapeutic effects and biocompatibility,[178-180] carbon nanotubes for applications as therapeutic and imaging tools,[181, 182] and water-soluble supramolecular polymers.[183-185]

This chapter describes the design, synthesis and self-assembly studies of two new PEGylated monomers. Monomers **35** and **36** were designed with the aim of developing amphiphilic hydrogen-bonding monomers with good solubility in both organic solvents and water (Figure 6.1). The structures are based on previously reported UPy- and PUPy-based monomers **29** and **34**, with the decyl chains replaced by tetraethylene glycol monomethyl ether chains. The branched 3,5-substituted benzyl solubilizing groups were chosen to allow for the introduction of a larger number of PEG chains (four PEG chains per monomer, as opposed two PEG chains per monomer if the PEG chains were attached directly to the bicyclic scaffold). In addition, the benzyl groups act as short spacers between the PEG chains and the rest of the monomer, which may benefit the self-assembly. The two monomers contain different hydrogen-bonding motifs, with the UPy motif in monomer **35** enabling the formation of cyclic tetramers through self-complementary 4H-bonding[170] and the PUPy motif in monomer **36** enabling the formation of cyclic tetramers through 2H-bonding, but also the further stacking into tubular polymers through orthogonal 2H-bonding.[173] Monomers **35** and **36** were used to explore how the introduction of PEG chains affects the solubility and self-assembly behavior. In addition, the choice of two different hydrogen-bonding motifs allowed for an investigation into how the hydrogen bond strength affects the stability of PEGylated hydrogen-bonded aggregates.

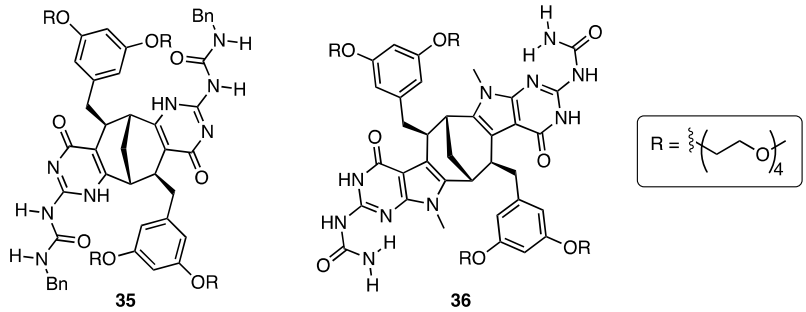

Figure 6.1 Structures of PEGylated monomers **35** and **36**.

6.2 Synthesis of monomers

The syntheses of monomers **35** and **36** are largely based on previously reported procedures by the Wärnmark and Orentas groups and include the construction of the bicyclic scaffold, addition of the PEGylated solubilizing groups and introduction of the hydrogen-bonding motifs.

6.2.1 Synthesis of enantiopure bicyclo[3.3.1]nonane scaffold

The enantiopure bicyclic backbone was synthesized following a reported procedure (Scheme 6.1).[186] Condensation of formaldehyde and dimethyl malonate, followed by treatment with sodium methoxide and acidification with HCl gave Meerwein's ester **37**. The product was collected by filtration after the acidification and required no further workup or purification. The reaction could be performed on a 150 g-scale without loss in yield. Subsequent decarboxylation by refluxing in acetic acid and concentrated HCl gave racemic dione **38**. Enantiomerically pure **38** (*ee* > 99%) was obtained by kinetic resolution using Baker's yeast for sweet dough. Baker's yeast (*Saccharomyces cerevisiae*) selectively reduces one of the enantiomers, leaving the other unreacted. Performing two consecutive fermentations ensured the complete conversion of one of the enantiomers into its reduced form (as determined by chiral HPLC). The workup, which needs to be performed after each fermentation, is a fairly time-consuming process, both due to the large scale of the reaction (50 g) and the presence of remaining sucrose and a complex mixture of yeast cell lysate in the reaction mixture.

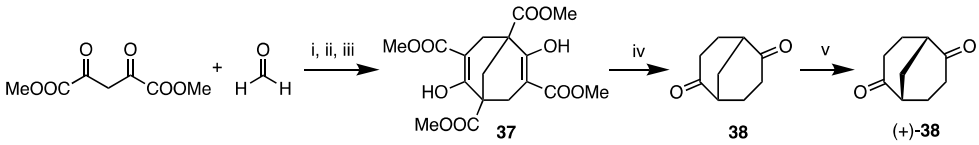

Scheme 6.1 Synthesis of enantiomerically pure dione (+)-**38**. i) benzene, piperidine, reflux; ii) NaOMe, MeOH, reflux; iii) HCl (aq.), 75% over three steps; iv) AcOH, HCl, reflux, 63%, v) Baker's yeast for sweet dough, sucrose, water, 40%.

As the solubilizing groups were introduced by 1,4-addition, dione **38** needed to be converted into a Michael acceptor. For monomers containing UPy units, the dione was first converted into bis-β-ketoester **39** by reaction with dimethyl carbonate and sodium hydride in DMF. The bis-β-ketoester was then oxidized into a Michael acceptor by a stepwise selenation-oxidation-elimination procedure (Scheme 6.2a). The sequential introduction of the double bonds is necessary as direct bis-selenation is not possible due to steric repulsion between the two *endo*-ester groups in the bis-selenated reaction intermediate (**41** in Scheme 6.2).[170, 187] For monomers with the PUPy motif, dienone **42** was synthesized directly from dione **38** by treatment with methyl benzenesulfinate and sodium hydride followed by thermal elimination. (Scheme 6.2b).

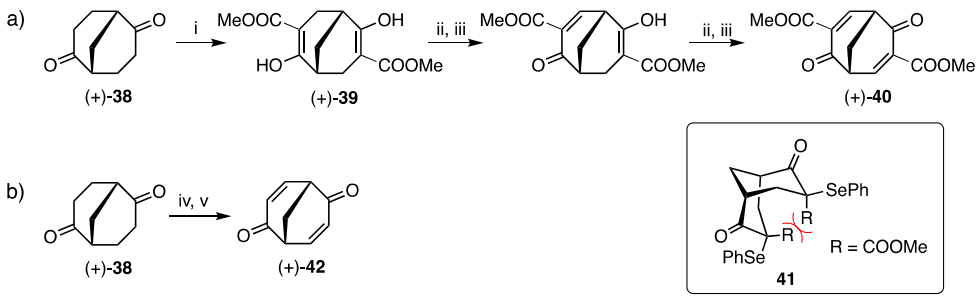

Scheme 6.2 a) Synthesis of unsaturated bis-β-ketoester **40**. i) $(MeO)_2CO$, NaH, DMF, 90%; ii) PhSeCl, pyridine, CH_2Cl_2, 0 °C to rt; iii) H_2O_2, CH_2Cl_2, 0 °C to rt, 39% over two steps. Inset shows sterically hindered intermediate preventing the use of a direct bi-selenation strategy. **b)** Synthesis of dienone **42**. iv) $PhSO_2Me$, NaH, THF, rt; v) Na_2CO_3, toluene, reflux, 30 min, 84%.

6.2.2 1,4-Addition of solubilizing groups

The solubilizing groups were introduced by 1,4-addition to dienone **40** and **42**. Conjugate addition of an organocopper reagent to an α,β-unsaturated carbonyl compound is an important and frequently used reaction for creating carbon-carbon bonds.[188, 189] The organocopper reagent is typically formed in situ by transmetallation between a copper(I) salt and a organometallic reagent. Commonly employed organometallic reagents are Grignard (RMgX) and organolithium (RLi) reagents. Depending on the method of preparation, different types of organocopper

reagents with different reactivities are obtained. Combining a copper(I) halide with two equivalents of an organolithium reagent results in a lower-order organocuprate, also known as a Gilman reagent (R_2CuLi). Two equivalents of organolithium are necessary for the formation of the reagent but only one of them will participate in the C-C bond forming reaction. As a way of avoiding wasting one equivalent of organolithium, mixed organocuprates (R_1R_2CuLi) containing a non-transferable "dummy" ligand (for example an alkynyl group) have been developed.[189] A special type of mixed organocuprates are the cyanocuprates, which are formed by reacting copper cyanide with one or two equivalents of an organolithium reagent and exhibit different stability and reactivity than classical Gilman reagents. Addition of one equivalent of organolithium results in a cyanocuprate containing one R groups and one non-transferable CN ligand (RCu(CN)Li), with the cyano group coordinated to the copper. Organocopper reagents formed from reaction with two equivalents of organolithium were originally believed to be copper(I) dianionic complexes, also referred to as higher-order cyanocuprates ($R_2Cu(CN)Li_2$).[190, 191] It has since then been proven that the cyano group is not bound to copper and that the formed reagent is instead a cyano-Gilman reagent ($R_2CuLi{\cdot}LiCN$).[192, 193] Enantioselective 1,4-additions using Grignard or dialkyl zinc reagents together with a catalytic amount of copper and chiral ligands have also been reported.[194, 195]

Due to their thermal instability and sensitivity to oxygen and moisture, the exact structure and mode of operation of organocuprates, especially in solution, is difficult to study and thus still under investigation.[192] The widely accepted mechanism for the conjugate addition of Gilman reagents to enones involves formation of a reversible π-complex between the copper and the olefin, formal oxidative addition to the β-carbon, and reductive elimination (Scheme 6.3).[192, 194] Addition of Lewis acids such as $BF_3 \cdot OEt_2$ and trimethylsilyl chloride (TMSCl) often results in increased reaction rates and yields.[189, 196]

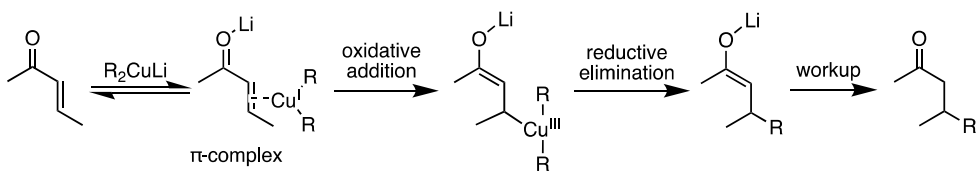

Scheme 6.3 Proposed mechanism for 1,4-addition of Gilman reagents.

In general, the conjugate addition of benzyl groups is known to be more difficult than the addition of alkyl- or aryl groups.[197] Benzylic cuprates are thermally unstable and may decompose below the temperature necessary to effect the 1,4-addition reaction.[198] In addition, the tendency of benzyl anions to form Wurtz coupling products limits which organometallic reagents can be used for the formation of the organocuprate.[199, 200] As an example, treatment of benzyl bromide with *n*-BuLi results primarily in the formation of the cross-coupling product through

rapid reaction between formed benzyl lithium and unreacted benzyl bromide, even at low temperatures (Scheme 6.4).[199, 201]

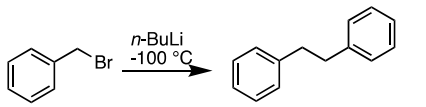

Wurtz-coupling product

Scheme 6.4 Formation of Wurtz-coupling product.

In addition to the above-mentioned aspects, the additions of PEGylated benzyl groups to dienones **40** and **42** are further complicated by the added bulkiness and potential coordinating abilities of the PEG chains, as well as the required bis-addition to the relatively small bicyclic dienones. For the previously reported alkylated analogues of the monomers (**29** and **34**), the 1,4-addition was accomplished by employing an organotin reagent, which was converted into an organolithium reagent by tin-lithium exchange, followed by transmetallation to the desired organocopper reagent.[170, 173] Following the same strategy, PEGylated organotin reagent **43** was synthesized and used in 1,4-additions to dienones **40** and **42** (Scheme 6.5). Organotin reagent **43** was transformed into the corresponding organolithium compound by reaction with *n*-BuLi in THF at -78 °C. A solution of CuCN·2LiCl complex was added to the so-formed organolithium reagent and the temperature was slowly raised to complete the transmetallation. The CuCN·2LiCl complex was used because of its solubility in THF (compared to CuCN which is insoluble). After formation of the organocopper reagent, the dienone was added. THF was the preferred solvent for the reaction as it has been shown to stabilize the cuprate.[200] Owing to the rigid concave shape of the bicyclic dienones, the 1,4-additions is known to proceed exclusively from the external side of the dienone, resulting in the desired *exo*,*exo*-disubstituted products.

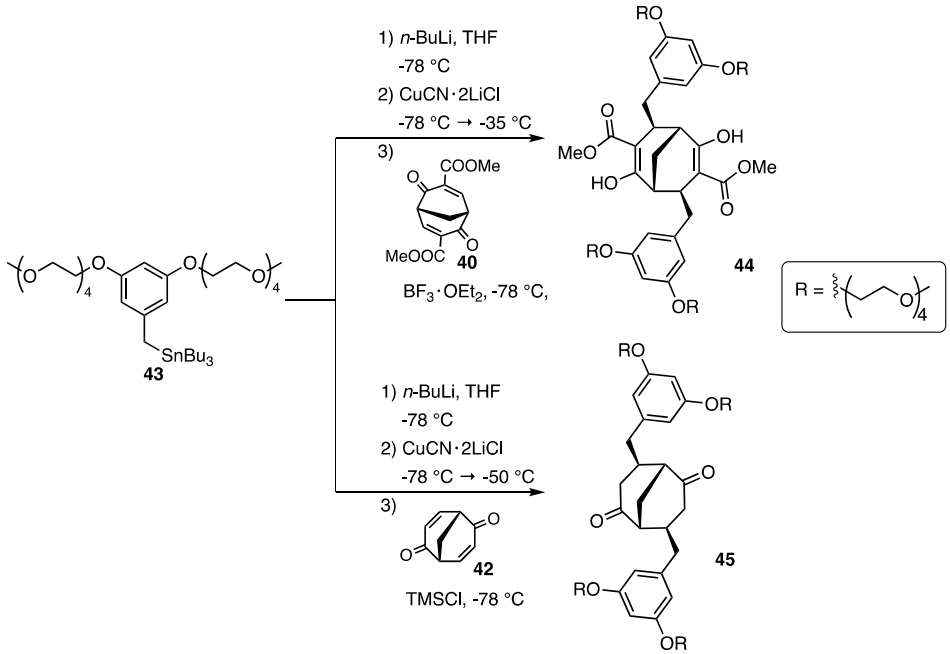

Scheme 6.5 1,4-addition of PEGylated solubilizing groups to dienone **40** and **42** using organotin reagent **43.**

Both 1,4-additions were found to be highly temperature- and moisture-sensitive. Reagents had to be added slowly to avoid temporary increase of the reaction temperature. Dryness of the reagents and solvents was crucial for successful reaction, and had to be ensured either by distillation, use of newly purchased anhydrous reagents, or by drying compounds under vacuum before use. Factors such as the humidity and temperature in the laboratory also affected and sometimes impeded the reaction. After the addition of CuCN·2LiCl, the temperature had to be temporarily raised for the organocopper reagent to form. Optimization of the temperature found that, in general, raising the temperature from -78 °C to somewhere between -50 and -35 °C resulted in the best yields, and that the organocopper reagent seems to decompose at temperatures above - 20 °C. The addition of a Lewis acid together with the dienone was necessary for the 1,4-addition to proceed. For dienone **40**, the best results were obtained with $BF_3 \cdot OEt_2$, while the best results for dienone **42** were afforded with TMSCl. Even with optimization, only poor to moderate yields were obtained (30% for **44** and 61% for **45**).

As a result of these sensitive reaction conditions and varying yields, other methods for the 1,4-additions were also investigated. Organozinc bromide, formed from the direct insertion of zinc into the corresponding bromide, can be used to form a mixed copper-zinc reagent (RCu(CN)ZnX) which can then react in the 1,4-addition. This type of mixed organocopper reagent generally displays similar reactivity and

slightly enhanced stability compared to organocopper reagents prepared from organolithium.[199, 202] Treatment of PEGylated benzyl bromide **46** with zinc (activated with 1,2-dibromoethane and TMSCl[174, 203]) at room temperature afforded the corresponding organozinc bromide (Scheme 6.6). The so-formed organozinc bromide solution was directly added to a solution CuCN·2LiCl at -60 °C. The temperature was raised to -30 °C to ensure formation of the mixed copper-zinc reagent. Addition of dienone **42** and TMSCl to the organocopper-zinc reagent afforded 1,4-addition product **45** in 40% yield. It is expected that further optimization of the reaction conditions would lead to yields comparable to those obtained using the organolithium reagent described above (Scheme 6.5).

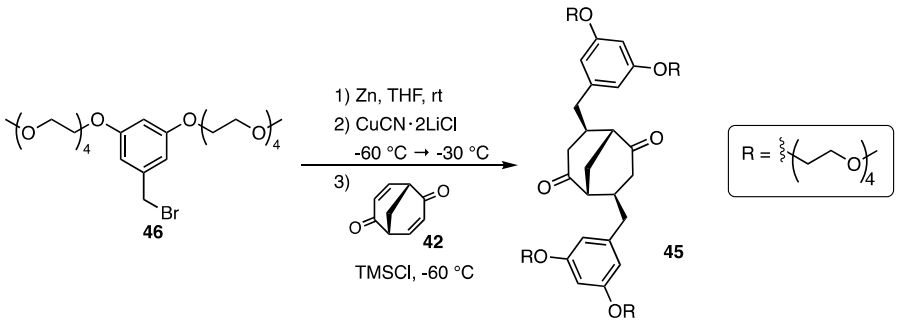

Scheme 6.6 1,4-addition of PEGylated solubilizing groups to dienone **42** using in situ formed mixed copper-zinc reagent.

Other possible strategies for improving the yield include performing the 1,4-addition with a simpler benzyl group and adding the PEG chains in a later step, or introducing an electron-withdrawing bromide in the *para*-position of the benzyl group, which has been reported to aid the formation of the corresponding organocopper reagent.[174] These strategies, as well as further optimization of the reactions described above, are currently being investigated.

6.2.3 Introduction of hydrogen-bonding motifs

*6.2.3.1 UPy monomer **35***

Condensation between PEGylated bis-β-ketoester **44** and guanidinium chloride with potassium *tert*-butoxide in methanol at 100 °C gave isocytosine derivative **47** (Scheme 6.7). Subsequent addition of benzyl-substituted urea moieties by reacting **47** with benzylisocyanate in pyridine under microwave irradiation at 120 °C afforded UPy monomer **35**.

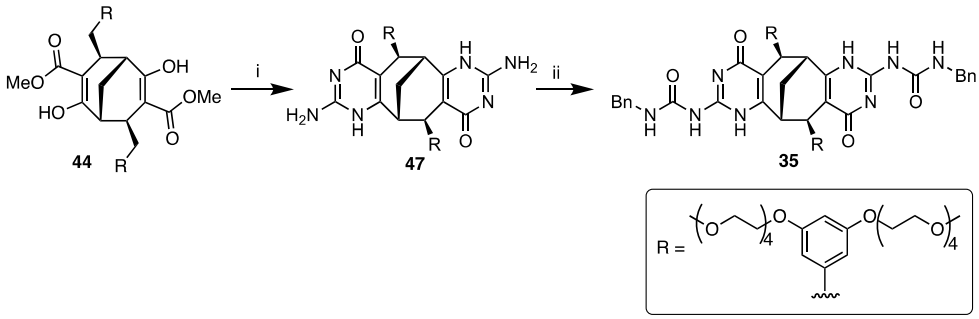

Scheme 6.7 Synthesis of PEGylated UPy monomer **35**. i) Guanidinium chloride, KO*t*Bu, MeOH, 100 °C, 78%; ii) BnNCO, pyridine, 120 °C MW, 76%.

*6.2.3.2 PUPy monomer **36***

The PUPy hydrogen-bonding motifs were introduced by first reacting PEGylated dione **45** with a slight excess of isocytosine hydrazine **48** in acetic acid (Scheme 6.8). The resulting mixture of *E* and *Z* isomers of hydrazone **49** was put through a short silica column to remove unreacted starting materials, then used directly in the next step, where a thermal Fischer indole synthesis was performed by heating hydrazone **49** to 200 °C in diphenyl ether overnight. It is also possible to perform the hydrazone formation and Fischer indolization as a one-pot procedure by refluxing a mixture of hydrazine **48** and the dione in diphenyl ether overnight, although with a slight decrease in yield.[174] In the final step, the terminal urea moieties were added by reacting isocytosine compound **50** with phenyl chloroformate in pyridine for 6 hours, after which aqueous ammonia was added, affording PUPy monomer **36**.

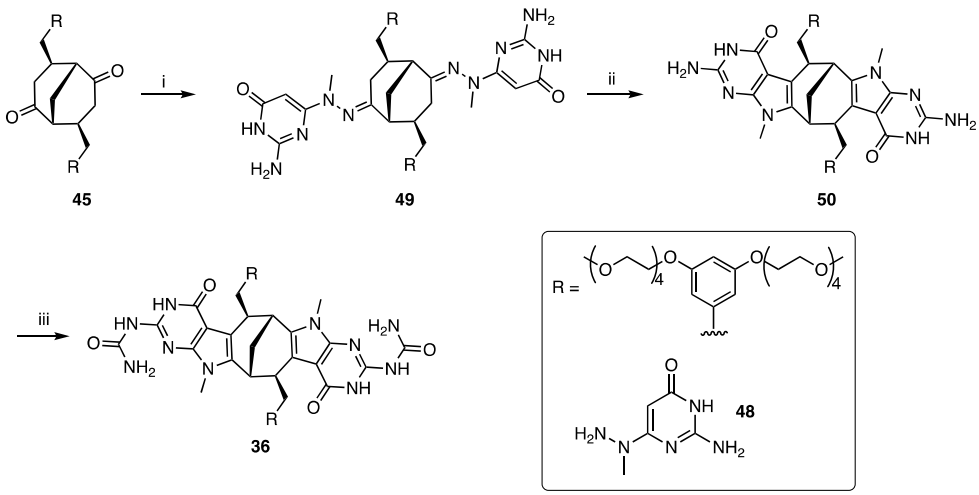

Scheme 6.8 Synthesis of PEGylated PUPy monomer **36**. i) **48**, AcOH, rt; ii) Ph_2O, 200 °C, 55% over two steps; iii) 1) PhCOCl, pyridine, 0 °C to rt, 2) NH_3 (aq), rt, 79%.

6.3 Self-assembly studies

The self-assembly behavior of the PEGylated monomers was studied primarily by NMR spectroscopy methods. In a ^{1}H NMR spectrum, the resonances of hydrogen-bonded protons are expected to be shifted downfield compared to non-bonded protons. The deshielding is believed to be caused by a loss of electron density around the hydrogen-bonded proton.[204] Protons participating in strong hydrogen bonding are also expected to be less prone to exchange with for example solvent molecules. In addition, VT and dilution ^{1}H NMR experiments can be used to investigate the stability of hydrogen-bonded aggregates. Through-space correlation methods such as NOESY and ROESY can aid in determining the conformation and position of hydrogen-bonding motifs within the monomer and in the larger aggregates. DOSY is an NMR method used to determine diffusion coefficients for individual resonances in a ^{1}H NMR spectrum. The diffusion coefficient is inversely related to the hydrodynamic radius of a (spherical) particle through the Stokes-Einstein equation:

$$D = \frac{k_{\mathrm{B}}T}{6\pi\eta r_{\mathrm{H}}} \tag{11}$$

where D is the diffusion coefficient, k_{B} is the Boltzmann constant, T is the temperature, η is the viscosity of the solvent, and r_{H} is the hydrodynamic radius of the solute. The Stokes-Einstein equation is defined for hard, spherical particles. For non-spherical aggregates, the size can be determined by for example performing DOSY experiments at different concentrations and extrapolating to determine a diffusion coefficient at infinite dilution, which can be used to calculate the hydrodynamic radius, or by performing MD simulations and using the simulated conformations to determine the radius of gyration. Previously reported studies of monomers **28** and **29** have shown that for aggregates based on these types of monomers, although not spherical, hydrodynamic radii calculated with the Stokes-Einstein equation were consistent with hydrodynamic radii estimated using MD simulations.[169, 170] To avoid any oversimplification, this chapter discusses the relative sizes of the aggregates in terms of diffusion coefficients, which are determined directly from DOSY experiments and compared with previously reported or calculated diffusion coefficients.

The self-assembly behaviors of PEGylated monomers **35** and **36** were also compared to the self-assembly behaviors of previously reported alkylated analogues **29** and **34**, in order to investigate the potential influence of the PEG chains on the hydrogen-bonded self-assembly.

6.3.1 Self-assembly of UPy monomer 35

The ^{1}H NMR spectrum of **35** in $CDCl_3$ shows three well-defined downfield resonances which were assigned to the three NH protons of the UPy unit in its AADD tautomeric form (Figure 6.2a). A combination of COSY, NOESY and ROESY was used to assign the individual NH resonances (Figure 6.2). The chemical shifts of the NH resonances (12.62, 11.93, and 10.11 ppm) and the high symmetry of the ^{1}H and ^{13}C NMR spectra indicated the formation of a single well-defined cyclic hydrogen-bonded aggregate. This was further supported by a comparison with NMR spectra of alkylated analogue **29**, which is known to form tetrameric species in $CDCl_3$.[170] The high stability of the aggregate was shown by ^{1}H NMR dilution experiments, where no shift or appearance of new resonances was observed upon dilution of the sample. DOSY experiments of **35** in $CDCl_3$ showed that all ^{1}H resonances correlate to a single diffusion coefficient, indicating that a single aggregate is formed. The determined diffusion coefficient ($2.35 \cdot 10^{-10}$ m^2/s) is in good agreement with the reported diffusion coefficient for the tetrameric aggregate of alkylated **29** ($2.93 \cdot 10^{-10}$ m^2/s),[170] taking into account the different size of the solubilizing chains.

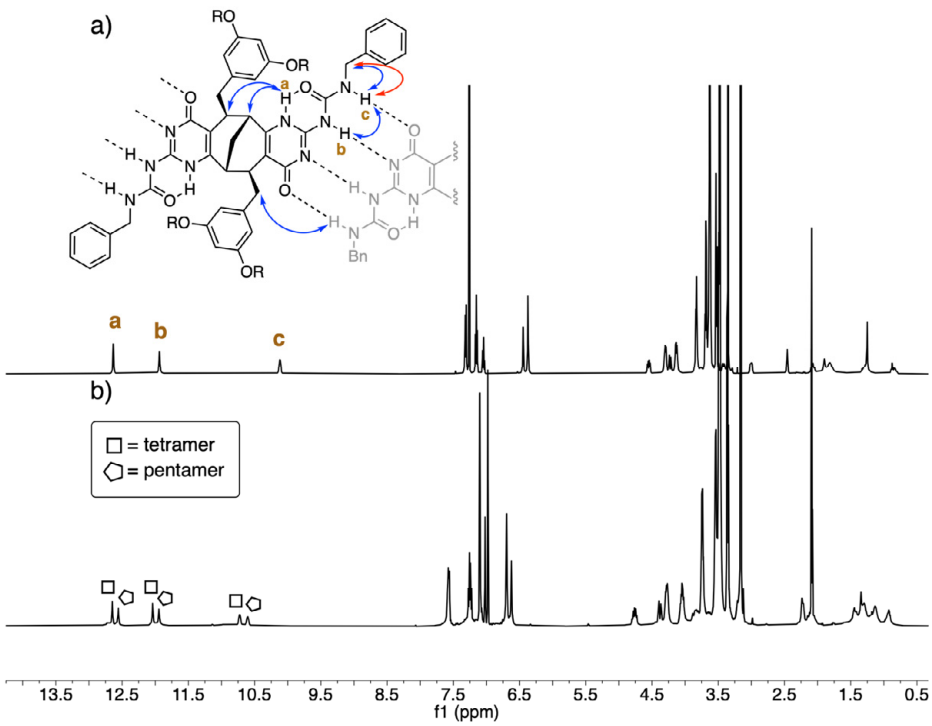

Figure 6.2 ^{1}H NMR spectrum of PEGylated UPy monomer **35** in **a)** $CDCl_3$ and **b)** toluene-d_8. R = $(CH_2CH_2O)_4CH_3$. Arrows in structure show observed cross peaks (red = COSY, blue = NOESY/ROESY).

^{1}H NMR spectra of **35** in less polar solvents (benzene-d_6 and toluene-d_8) show a doubling of the NH resonances, indicating the formation of two different aggregates (Figure 6.2b). This is similar to what has previously been reported for alkylated **29**, where the emergence of new resonances was attributed to the formation of a pentameric aggregate, existing in equilibrium with the tetramer.[170] DOSY experiments of PEGylated **35** in toluene-d_8 confirmed the presence of two differently sized aggregates with diffusion coefficients of $2.28 \cdot 10^{-10}$ and $2.14 \cdot 10^{-10}$ m^2/s, respectively. The determined diffusion coefficients are in good agreement with previously reported diffusion coefficients for tetrameric and pentameric aggregates of alkylated analogue **29** in toluene ($2.13 \cdot 10^{-10}$ and $1.98 \cdot 10^{-10}$ m^2/s, respectively).[170] The T-ROESY spectrum of **35** in toluene-d_8 shows no cross peaks between the two sets of NH resonances, indicating that no or extremely slow exchange between the two aggregates.

All in all, PEGylated monomer **35** exhibits very similar self-assembly behavior to previously reported alkylated analogue **29**, with highly stable cyclic aggregates forming by quadruple self-complementary hydrogen bonding via the AADD tautomeric form of the UPy units. Depending on the polarity of the solvent, either exclusively tetramers or a mixture of tetramers and pentamers are formed.

6.3.2 Self-assembly of PUPy monomer 36

As opposed to PEGylated UPy-based monomer **35**, a comparison of PEGylated PUPy-based monomer **36** with its alkylated analogue **34** revealed large differences. The ^{1}H NMR spectrum of PUPy-based monomer **36** in $CDCl_3$ shows only very broad downfield resonances (Figure 6.3a), which is in stark contrast from what was observed for the alkylated analogue **34** (Figure 6.3b). For previously reported alkylated **34**, the four well-defined downfield peaks were assigned to four different NH protons in a hydrogen-bonded tetrameric aggregate, with proton **d** participating in intermolecular hydrogen bonding, and an intramolecular hydrogen bond between proton **a** and the pyrimidinone nitrogen (Figure **6.3**).[173] The difference in chemical shifts and the broadness of NH resonances in the ^{1}H NMR spectrum of PEGylated **36** (Figure 6.3a) indicates that **36** either does not self-assemble into a well-defined aggregate or that the formed aggregate is not stable on the NMR time scale. The NH resonances in the ^{1}H NMR spectrum of **36** in $CDCl_3$ were assigned based on cross peaks between **c** and **d**, and between **a**/**b** and **c** in the NOESY spectrum. The fact that only one broad resonance is observed for the terminal urea protons (**a**/**b**) indicates that the intramolecular hydrogen bonding observed for alkylated **34** is significantly weakened or not present in PEGylated **36**. The presence of chemical exchange cross peaks between the NH resonances and residual water in the NOESY and ROESY spectra of **36**, which were not observed for UPy-based monomer **35**, also suggests a more dynamic behavior of the PUPy units.

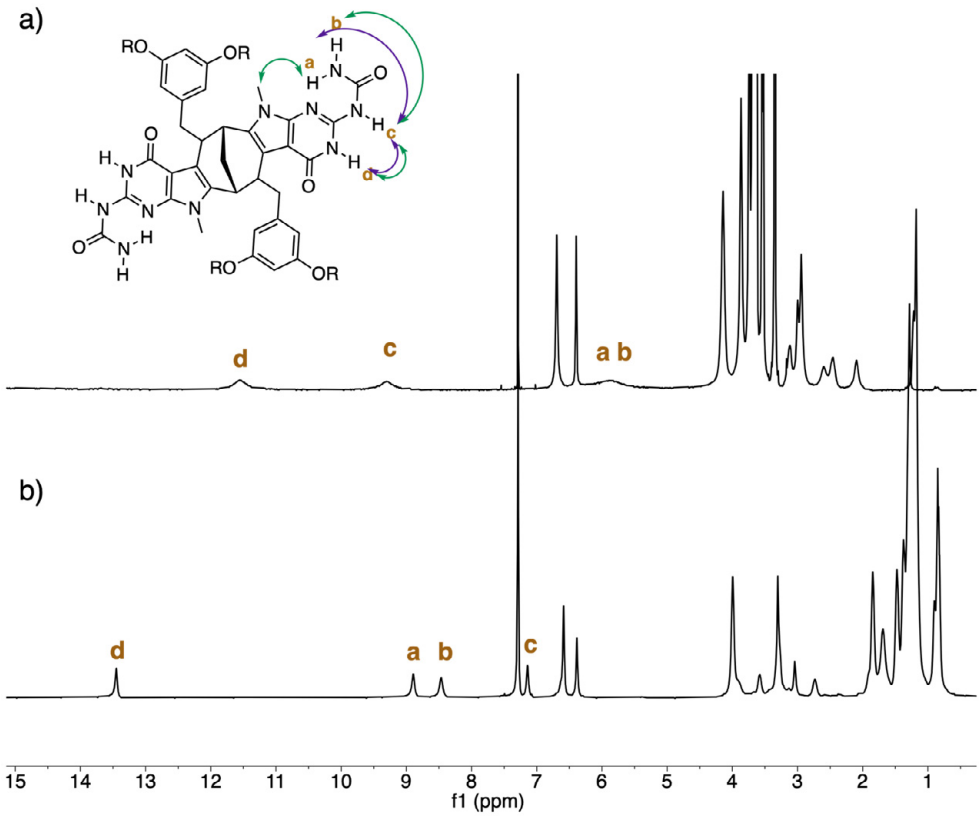

Figure 6.3 a) ^{1}H NMR spectrum of PEGylated **36** in $CDCl_3$. R = $(CH_2CH_2O)_4CH_3$. **b)** ^{1}H NMR spectrum of alkylated **34**. R = $C_{10}H_{21}$. Arrows in structure show observed cross peaks for PEGylated **36** (purple) and alkylated **34** (green).

Interestingly, DOSY experiments revealed that all ^{1}H NMR resonances could be correlated to a single diffusion coefficient, $D = 2.17 \cdot 10^{-10}$ m^2/s. The value of the determined diffusion coefficient is consistent with an aggregate significantly larger than a monomeric species and is similar to what has been reported for the tetramer of alkylated **34** ($2.39 \cdot 10^{-10}$ m^2/s).[173] Comparison of calculated diffusion coefficients for the monomer, dimer, trimer and tetramer of **36** (calculated using the HYDRO software[205, 206]) also supported the formation of a tetrameric aggregate in chloroform ($D_{calc,\ tetramer} = 2.4 \cdot 10^{-10}$ m^2/s). DOSY experiments of **36** in CD_3CN also gave a single diffusion coefficient consistent with a tetrameric aggregate, indicating that even though the hydrogen-bonded self-assembly of **36** appears to be significantly weaker than in alkylated analogue **34**, it is strong enough to afford tetramers even in solvents as polar as acetonitrile.

^{1}H NMR spectra of **36** in less polar solvents (toluene-d_8 and benzene-d_6) showed an extreme broadening and disappearance of signals (Figure 6.4a). This is similar to

what was observed for alkylated **34**, which was reported to stack into tubular polymeric aggregates in aromatic solvents.[173] The similarity of the ^{1}H NMR spectra of **36** and **34** in toluene-d_8 and the DOSY results showing formation of tetramers in $CDCl_3$ and even CD_3CN indicates that PEGylated **36** is also capable of forming tubular aggregates in toluene-d_8 and benzene-d_6. The stronger hydrogen bonding in less polar solvents is expected to both stabilize the tetrameric aggregate and enable stacking of the tetramers into tubular polymers. Further proof for the formation of tubular aggregates was given by the extreme broadening and disappearance of the resonances in the ^{1}H NMR spectrum of **36** in $CDCl_3$ when C_{70} was added, indicating that C_{70} can act as a template and trigger the tubular self-assembly even in more polar solvents (Figure 6.4b). The inner diameter of the PUPy tetramer has previously been shown to be well-suited for the encapsulation of C_{60} and C_{70}, and similar templating effects have been reported for alkylated **34** in $CDCl_3$.[173]

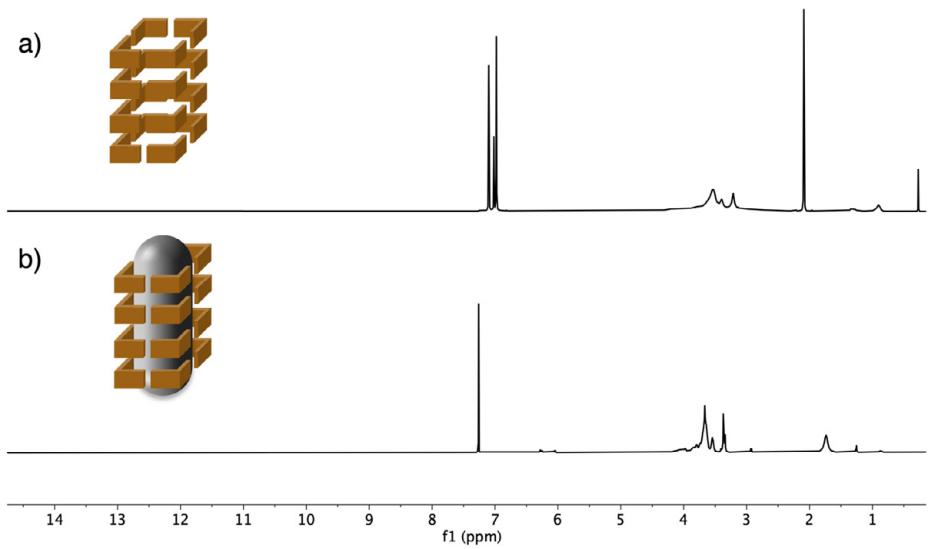

Figure 6.4 a) ^{1}H NMR spectrum of PEGylated **36** in toluene-d_8. **b)** ^{1}H NMR spectrum of PEGylated **36** $CDCl_3$ with 0.25 equiv of C_{70}.

6.3.3 Comparison of PEGylated monomers 35 and 36

In $CDCl_3$, both of the PEGylated monomers (**35** and **36**), as well as their alkylated analogues (**29** and **34**), form tetrameric cyclic aggregates. However, while the introduction of PEG chains in UPy-based monomer **35** does not appear to affect the stability of the formed hydrogen-bonded aggregates compared to alkylated analogue **29**, the tetrameric aggregates of PEGylated PUPy-based **36** exhibit a significantly less stable and more dynamic behavior than tetramers of its alkylated analogue **34**. The reduced stability of the hydrogen-bonded aggregate is assumed to be caused by

interference from the PEG chains. Interactions between ethylene glycol chains and urea groups have previously been investigated by Meijer and coworkers, who found that attaching short ethylene glycol chains directly onto UPys or benzene-1,3,5-tricarboxamides (BTA) resulted in significantly lowered association constants for both the UPy dimerization and the formation of BTA stacks (Figure 6.5).[207-209] The reduction in hydrogen bond strength was attributed to competitive intramolecular hydrogen bonding between the ethylene glycol oxygens and the acidic NH protons of the urea or amide units.

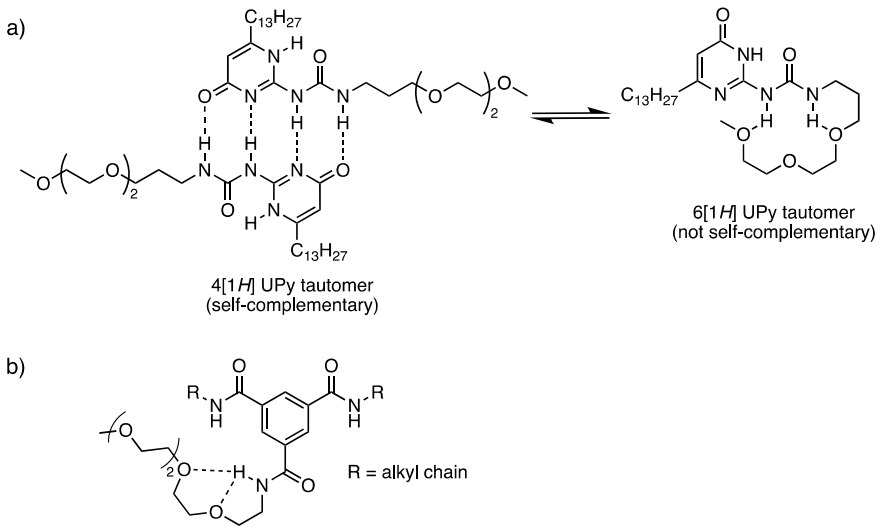

Figure 6.5 Monomers exhibiting intramolecular hydrogen bonding between PEG chains and hydrogen-bonding motif. **a)** Triethylene glycol monomethyl ether-substituted UPy. **b)** BTA containing one tetraethylene glycol monomermethyl ether chain.

In monomers **35** and **36**, the PEG chains are not added directly to the hydrogen-bonding motifs, but rather as 3,5-substituents on benzyl groups which are attached to the bicyclic scaffold (Figure 6.1). The observed self-assembly behavior of **35** and **36** compared to their alkylated analogues indicates that, despite the benzyl spacer between the PEG chains and the hydrogen-bonding motifs, the PEG chains are capable of interfering with the self-assembly. The difference in aggregate stability between the two PEGylated monomers is attributed to the different hydrogen bonding motifs. As previously described, UPys are known to form strong complexes through self-complementary quadruple hydrogen bonding,[128, 170] while the PUPy units preferentially adopt a tautomeric form only containing self-complementary 2H-bonding sites (Figure 6.6).[173] Although the 2H-binding PUPy motif has previously been shown to be sufficient to form tetramers of high stability for alkylated **34**,[173] the introduction of PEG chains is evidently enough to significantly weaken the hydrogen-bonded aggregates. Another difference between **35** and **36** is the benzyl substituents attached to the terminal urea nitrogens in **35**, which can block the hydrogen-bonding sites from the PEG chains (Figure 6.6a). In **36**, the terminal

urea groups are unsubstituted and not involved in the tetrameric hydrogen bonding, which makes them more exposed to the PEG chains (Figure 6.6b). The stability of the tetrameric aggregates and interactions between the PEG chains and the hydrogen-bonding sites were also investigated by MD simulations. For **35**, the tetramer remained stable throughout the 40 ns simulation and the PEG chains, while highly flexible, did not directly interfere with the hydrogen bonding (Figure 6.6a, bottom). For **36**, clear interactions between the PEG chains and the hydrogen-bonding sites could be observed and the tetrameric aggregate was deformed over the course of the simulation (Figure 6.6b, bottom).

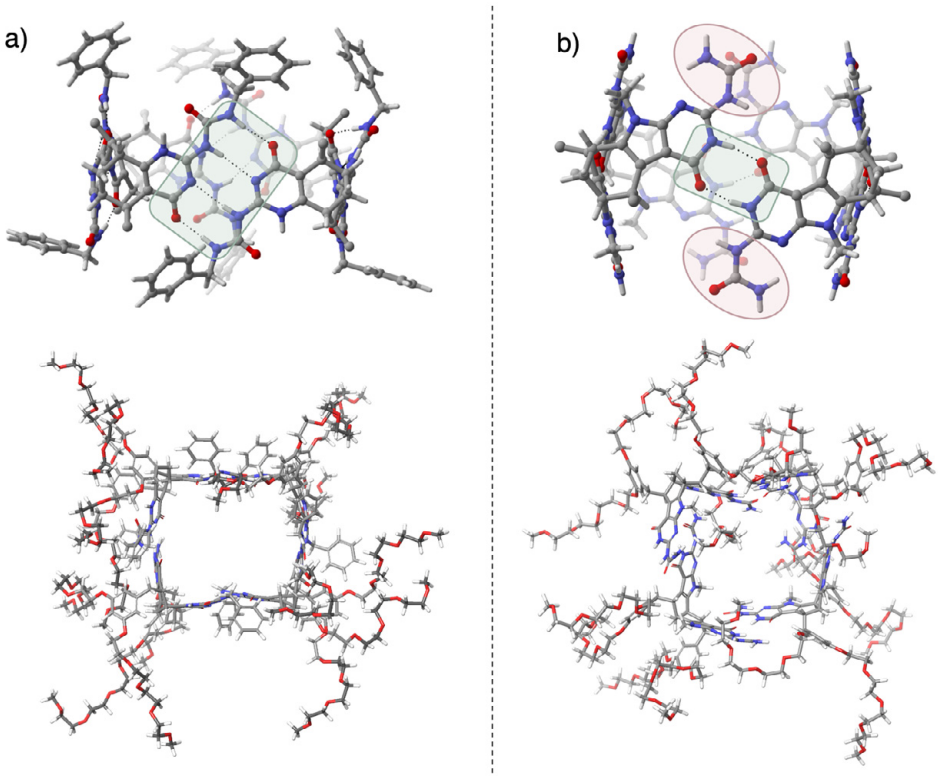

Figure 6.6 a) Molecular model of $\mathbf{35}_4$ with 4H-bonding marked in green (top) and structure after 40 ns MD simulation (bottom). **b)** Molecular model of $\mathbf{36}_4$ with 2H-bonding marked in green and urea moieties not participating in hydrogen bonding marked in pink (top) and structure after 40 ns MD simulation (bottom). MD simulations performed with a chloroform solvent model.

6.4 Solubility of PEGylated monomers

PEGylated **35** and **36** exhibited increased solubility in polar solvents, compared to alkylated analogues **29** and **34**, while still maintaining solubility in less polar

solvents (Table 6.1). Of the two PEGylated monomers, **36** was fully soluble in water, while **35** was insoluble even after extended heating and sonication. The different solubility indicates that either the unsubstituted terminal NH_2 groups on the urea moieties of **36** are needed for water solubility, or the additional benzyl groups on **35** introduce enough of a lipophilic element to inhibit water solubility.

Table 6.1 Solubility of alkylated and PEGylated monomers in different solvents. S = soluble, L = limited solubility (< 10 mg/mL), I = insoluble, n.d. = not determined. Symbols denotes formed aggregates (if known): □ = tetramer, ⬠ = pentamer, ◎ = tubular polymer.

Solvent	Alkylated		PEGylated	
	29	**34**	**35**	**36**
Toluene	L □⬠	L ◎	L □⬠	S ◎
Benzene	S □⬠	S ◎	S □⬠	S ◎
Diethyl ether	I	I	n.d.	S
Dichloromethane	L	L □	S □	S □
THF	n.d.	n.d.	S	S
Chloroform	S □	S □	S □	S □
Methanol	L	L	S	S
Acetonitrile	n.d.	n.d.	S	S □
DMSO	S	S	S	S
Water	I	I	I	S

Water-soluble **36** could be efficiently extracted from an aqueous solution into a chloroform solution (Figure 6.7). The amphiphilicity and self-assembly behavior of **36**, where the monomer is fully soluble in water yet preferentially dissolves in less polar solvents where hydrogen-bonded self-assembly can occur, opens up for future biological applications.

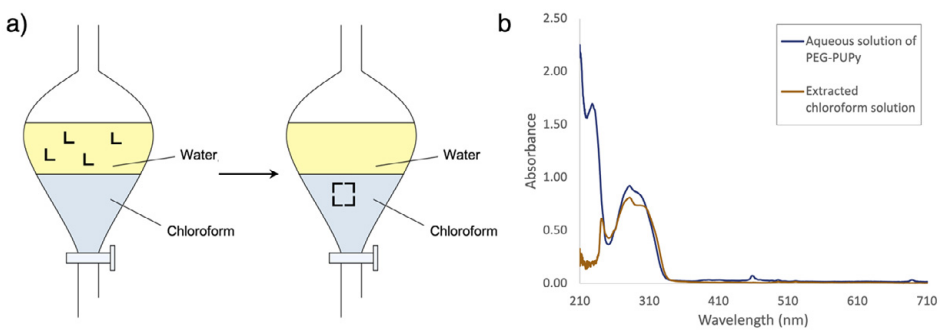

Figure 6.7 a) Schematic representation of extraction of water-soluble monomers into chloroform and the formation of cyclic structures in the less polar environment. **b)** UV/Vis absorption spectrum of aqueous solution of **36** (blue) and extracted chloroform solution (brown).

6.5 Next generation

Monomer **36** containing PUPy units was shown to form tubular aggregates in solvents such as toluene and benzene through orthogonal hydrogen bonding between tetramers. However, as previously discussed, the tetrameric aggregates in chloroform were destabilized by interference from the PEG chains. One strategy for improving the stability of the aggregates is to incorporate alkyl spacers between the PEG chains and the bicyclic backbone. This approach has been successfully employed for the development of water-soluble supramolecular polymers. Bouteiller and coworkers reported monomer **51** which was shown to form hydrogen-bonded polymers in water, acetonitrile and toluene (Figure 6.8). The alkyl spacer was necessary for self-assembly to occur. In water and acetonitrile, the alkyl spacer was assumed to stabilize the aggregation by solvophobic interactions and by creating a low-polarity microenvironment for the hydrogen bonds. In toluene, the alkyl spacer stabilized the aggregate by removing the PEG chains from the bis-urea motif and thus preventing competing intramolecular hydrogen bonding.[183] Another example comes from Meijer and coworkers, who designed BTA monomer **52** which could self-assemble into long fibrillar aggregates in water through a combination of intermolecular hydrogen bonding and solvophobic effects (Figure 6.8).[185]

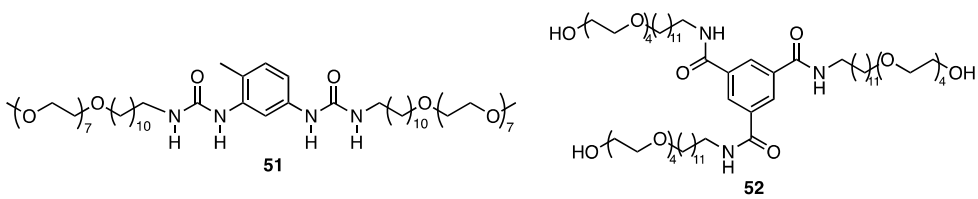

Figure 6.8 Monomers containing alkyl spacer between hydrogen-bonding motif and PEG chains, capable of supramolecular polymerization in water.

Inspired by these reports, new monomers **53** and **54** were designed to improve the stability of the hydrogen-bonded self-assembly (Figure 6.9). In monomer **53**, alkyl spacers are added between the PEG chains and the benzyl groups. The synthetic route would be very similar to the one employed for monomer **36**, with the alkyl-PEG chains introduced in the early steps of the synthesis of the benzyl reagent, before the 1,4-addition. Another option is to add an alkyl spacer between the benzyl group and the bicyclic scaffold, as seen in proposed monomer **54** (Figure 6.9). The design of monomer **54** is based on a reported methodology for the incorporation of ethyl thiol groups on the bicyclo[3.3.1]nonane scaffold via 1,4-addition of a vinyl group, thiol-ene reaction with thioacetic acid, and hydrolysis to obtain the free thiol.[153, 210] Nucleophilic substitution between the thiol and PEGylated benzyl bromide would then afford monomer **54**. The synthesis of these monomers is currently underway.

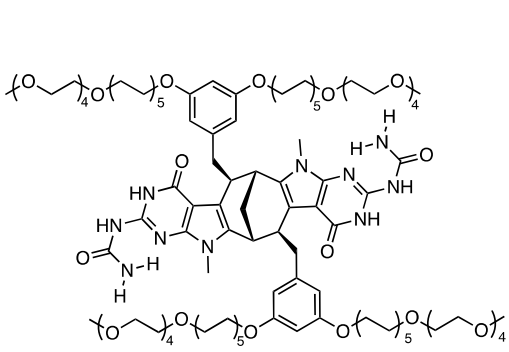

53

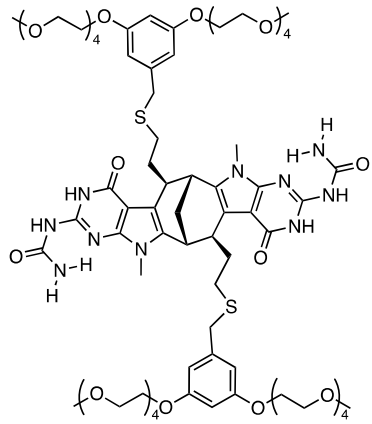

54

Figure 6.9 Proposed monomers with with alkyl spacers for improved stability of hydrogen-bonded aggregates.

6.6 Conclusions

Two new hydrogen-bonding monomers containing PEG chains have been synthesized. The monomers comprise a bicyclo[3.3.1]nonane scaffold appended with either UPy or PUPy hydrogen-bonding motifs, with PEG-substituted benzyl moieties added as solubilizing groups. The monomers were based on previously reported monomers capable of self-assembling into cyclic and tubular aggregates. The aim of introducing the PEG chains was to increase the solubility of the monomers and their aggregates in polar solvents, including water, while still maintaining the solubility in less polar organic solvents where aggregation is expected to occur.

The self-assembly of the monomers was studied by a combination of ^{1}H and 2D NMR spectroscopy methods and DOSY experiments. The UPy-based monomer formed tetrameric aggregates in $CDCl_3$ of similar stability as its previously reported alkylated analogue. Also similar to the alkylated analogue, a mixture of tetramers and pentamers was observed in less polar aromatic solvents (toluene-d_8 and benzene-d_6). In general, the introduction of the PEG chains did not appear to significantly affect the self-assembly behavior of the UPy-based monomer.

For the PUPy-based monomer, the introduction of the PEG chains resulted in significantly weaker tetrameric aggregates in $CDCl_3$ compared to its alkylated analogue, as indicated by a pronounced broadening of the NH resonances in the ^{1}H NMR spectrum and sensitivity to dilution and temperature. Despite the apparent dynamic behavior, DOSY experiments confirmed the formation of a single aggregate of a considerably larger size than the monomeric species. Comparison of

the determined diffusion coefficient with calculated and previously reported values supported the formation of tetrameric aggregate. Interestingly, despite the low stability of the tetramers, further stacking into tubular polymers by orthogonal 2H-bonding could be induced in the less polar solvents toluene-d_8 and benzene-d_6, or by introducing C_{70} as a templating guest. The reduced stability of the aggregates of the PEGylated monomer compared to its alkylated analogue indicates substantial interactions between the PEG chains and the hydrogen-bonding sites.

The level of interference from the PEG chains in the different tetrameric aggregates could be explained either by the strength of the hydrogen bonding (number of hydrogen bonds in the hydrogen-bonding motif) or by the presence of non-polar groups in the vicinity of the hydrogen-bonding motif, as the UPy-based monomer contained benzyl substituents on the terminal urea nitrogens while the PUPy-based monomer had unsubstituted urea groups. Comparison of the two PEGylated monomers could offer useful insights into different factors influencing hydrogen-bonded self-assembly and how PEGylation affects the self-assembly and stability of aggregates. Strategies for improving the stability of the PUPy-based aggregates by introducing alkyl spacers between the PEG chains and the bicyclic scaffold are being investigated.

Both PEGylated monomers exhibited increased solubility compared to their alkylated analogues. Out of the two PEGylated monomers, only the PUPy-based monomer was soluble in water, possibly due to the presence of unsubstituted urea groups. Experiments showed that the PUPy-based monomer could be efficiently extracted from an aqueous solution into a chloroform solution, where it self-assembled into a tetramer. This type of amphiphilicity and self-assembly behavior could be exploited in biological applications, where monomers could be introduced into an aqueous system and subsequently self-assemble into functional aggregates once they reach a less polar environment.

7 Concluding remarks

In the work presented in this thesis, a small bicyclic molecule was utilized as a scaffold to build different supramolecular components. The rigidity and bent shape of the molecule was used to install different binding sites at fixed relative position, which is necessary for reliable molecular recognition or self-assembly.

In the first part of the thesis, the bicyclic core, in the form of a Tröger's base motif, was fused with two 18-crown-6 moieties to form a synthetic receptor. By combining the receptor with differently substituted bisammonium salts, non-covalent aromatic interactions between the substituents on the ligands and the aromatic cavity of the receptor were investigated. The receptor-ligand binding was studied quantitatively and qualitatively by various NMR methods. A weak but evident discrimination in the binding process based solely on the substituent on the ligand, combined with conformational analyses of the receptor-ligand complexes, allowed us to use the system to estimate the free binding energy between a methyl or phenyl group and an aromatic cavity. The experimental results were further used to compare and validate different computational methods.

The same receptor was also used to study the consecutive binding of potassium ions to a ditopic receptor in water by ITC experiments. Based on the counterintuitive observation of an enthalpic stabilization associated with the binding of the second potassium ion, experimental results and computational simulations were combined to investigate how different factors contributed to the binding process. The counterion was found to influence the size of the enthalpic stabilization, with the weakly hydrated thiocyanate counterion resulting in a larger enthalpic stabilization of the binding of the second potassium ion. Favorable intrinsic interactions between the two potassium-bound crown-ethers were suggested based on simulated conformations. Additionally, continuum electrostatics theory predicted a small enthalpic attraction between two monovalent cations in water at 25 °C. Although further studies are needed to fully elucidate and understand the binding process, the presented results should provide valuable insights into host-guest interactions in water.

The second part of the thesis describes the design and synthesis of hydrogen-bonding monomers containing polyethylene glycol solubilizing groups. The aim was to develop amphiphilic monomers, as well as to study the effect of PEGylation on hydrogen-bonded self-assembly. Two monomers were synthesized and

compared to their previously reported alkylated analogues. The comparison, both between the two PEGylated monomers and between the PEGylated and alkylated monomers, offered insights into the relationship between the hydrogen bond strength and the influence of PEGylation on the hydrogen-bonded self-assembly. One of the PEGylated monomers exhibited the desired amphiphilicity and could be extracted from an aqueous solution into an organic solvent, where self-assembly occurred. The next step is to design and synthesized new monomers with improved aggregate stability, with the goal of developing PEGylated monomers and aggregates which can be introduced into biological systems.

Acknowledgements

This thesis and the work presented in it would not have been possible without the help and support of many people.

First and foremost, I would like to thank my supervisor, KENNETH. Your encouragement was a large reason for me deciding to pursue PhD studies to begin with and I have appreciated your continued encouragement throughout my years as a PhD student. Thank you for allowing me to go on this journey and develop as a researcher and a person.

I would also like to thank my co-supervisor OLA and department representative LOTTA, who have offered support when needed and always been available.

I have had the pleasure and privilege to work with several collaborators and co-authors. A special thank you to VIDAR, for a very fruitful and rewarding collaboration on the potassium ion project. ANDERS and PER-OLA, for interesting discussions and teaching me all I know about computational chemistry. KARL-ERIK and ZOLTAN, for NMR expertise and listening to my endless questions. VICKY, ALGIRDAS and SIMON, for invaluable help and support on the PEG project.

The KW group has been a constant source of inspiration and support. I have thoroughly enjoyed my time in the group and am extremely grateful to be able to call you not only colleagues but also close friends. VALTÝR, who is the only current KW member who has been in the group longer than me and who has shared the ups and downs of PhD life and often offered much-needed calm. LISA, we started as PhD students a few months apart and will now finish within a few weeks of each other. Thank you especially for suggesting our thesis writing sessions, which were a huge help in getting this thing started and keeping me on track. ALEKSANDRA, who initially thought I was a serious and scary person but has since learned better. I am very happy to have found someone to join me on my daily trips to the vending machine, constantly trade stupid memes with, and who is always available for venting sessions when things get overwhelming. A huge thank you for proof-reading the thesis and giving me feedback and input. JESPER, who is always up for a fika break and is often the first to step up and take responsibility, be it as the KW group social event coordinator or as my successor in the PhD student network and CAS unit council. SAMUEL, thank you for many interesting lunchroom discussions and for being my trusted cat-sitter. ERIC and CLARA, the new generation, who bring some much-needed youth and energy to the group.

I have spent a significant amount of time teaching. It has been a highly enjoyable, rewarding, and, at times, challenging experience that I am very grateful for. I would like to extend a big thank you to SOPHIE, who has been a continued support in teaching, research, and life in general. I know that I am not the only one at CAS who is very grateful for the care and concern you continue to show. I would also like to thank ULF E for allowing me to try my hand at lecturing this last spring, it was a great experience.

Life at CAS and as a PhD student would not work as well as it does without our amazing supporting staff. MARIA and SARA, you have always been very helpful with any issues or questions I've had, however small or insignificant. Thank you to KORNELIJE for help with instruments and issues in the lab, and SOFIA, ANETTE, and FIONA for all the help with mass spectrometry. I would also like to extend a thank you the whole of CAS, especially all of the PhD students, who make our unit such a fun place to work in.

Finally, and most importantly, to my family: MAMMA, PAPPA, EMMA och GEORGE, och SAMUEL. Ni är de bästa personerna jag vet och utan er hade jag inte varit där jag är idag ♡

References

1. Dow, J.; Lindsay, G.; Morrison, J., *Biochemistry : Molecules, Cells and the Body*. 1996: Addison-Wesley. p. 70.
2. Berg, J. M.; Tymoczko, J. L.; Stryer, L., *Biochemistry*. 7th ed. 2012: Palgrave Macmillan. p. 416.
3. Lehn, J.-M. Supramolecular Chemistry: Receptors, Catalysts, and Carriers. *Science* **1985**, *4689*, 849-856.
4. Adhav, V. A.; Saikrishnan, K. The Realm of Unconventional Noncovalent Interactions in Proteins: Their Significance in Structure and Function. *ACS Omega* **2023**, *25*, 22268-22284.
5. Peck, E. M.; Smith, B. D., *Applications of Synthetic Receptors for Biomolecules*, in *Synthetic Receptors for Biomolecules: Design Principles and Applications*, B. D. Smith (ed.), 2015, Royal Society of Chemistry. p. 1-38.
6. Chodera, J. D.; Mobley, D. L. Entropy-Enthalpy Compensation: Role and Ramifications in Biomolecular Ligand Recognition and Design. *Annu. Rev. Biophys.* **2013**, *1*, 121-142.
7. Peccati, F.; Jiménez-Osés, G. Enthalpy–Entropy Compensation in Biomolecular Recognition: A Computational Perspective. *ACS Omega* **2021**, *17*, 11122-11130.
8. Sackett, D. L.; Saroff, H. A. The multiple origins of cooperativity in binding to multi-site lattices. *FEBS Lett.* **1996**, *1*, 1-6.
9. Klärner, F.-G.; Kahlert, B. Molecular Tweezers and Clips as Synthetic Receptors. Molecular Recognition and Dynamics in Receptor−Substrate Complexes. *Acc. Chem. Res.* **2003**, *12*, 919-932.
10. Leevy, W. M.; Gammon, S. T.; Jiang, H.; Johnson, J. R.; Maxwell, D. J.; Jackson, E. N.; Marquez, M.; Piwnica-Worms, D.; Smith, B. D. Optical Imaging of Bacterial Infection in Living Mice Using a Fluorescent Near-Infrared Molecular Probe. *J. Am. Chem. Soc.* **2006**, *51*, 16476-16477.
11. Zhao, M.; Wang, H. B.; Ji, L. N.; Mao, Z. W. Insights into metalloenzyme microenvironments: biomimetic metal complexes with a functional second coordination sphere. *Chem. Soc. Rev.* **2013**, *21*, 8360-75.
12. Mancin, F.; Prins, L. J.; Scrimin, P. Catalysis on gold-nanoparticle-passivating monolayers. *Curr. Opin. Colloid Interface Sci.* **2013**, *1*, 61-69.
13. Deshayes, S.; Cabral, H.; Ishii, T.; Miura, Y.; Kobayashi, S.; Yamashita, T.; Matsumoto, A.; Miyahara, Y.; Nishiyama, N.; Kataoka, K. Phenylboronic Acid-Installed Polymeric Micelles for Targeting Sialylated Epitopes in Solid Tumors. *J. Am. Chem. Soc.* **2013**, *41*, 15501-15507.

14. James, T. D.; Sandanayake, K. R. A. S.; Shinkai, S. A Glucose-Selective Molecular Fluorescence Sensor. *Angew. Chem. Int. Ed. Engl.* **1994**, *21*, 2207-2209.
15. Metzger, A.; Anslyn, E. V. A Chemosensor for Citrate in Beverages. *Angew. Chem. Int. Ed.* **1998**, *5*, 649-652.
16. Bruemmer, K. J.; Crossley, S. W. M.; Chang, C. J. Activity-Based Sensing: A Synthetic Methods Approach for Selective Molecular Imaging and Beyond. *Angew. Chem. Int. Ed.* **2020**, *33*, 13734-13762.
17. Alfonso, I.; Quesada, R. Biological activity of synthetic ionophores: ion transporters as prospective drugs? *Chem. Sci.* **2013**, *8*, 3009-3019.
18. Gokel, G. W.; Negin, S. Synthetic membrane active amphiphiles. *Adv. Drug Delivery Rev.* **2012**, *9*, 784-796.
19. Yan, T.; Zheng, X.; Liu, S.; Zou, Y.; Liu, J. Ion transporters: emerging agents for anticancer therapy. *Sci. China: Chem.* **2022**, *7*, 1265-1278.
20. Gokel, G. W. Hydraphiles: design, synthesis and analysis of a family of synthetic, cation-conducting channels. *Chem. Commun.* **2000**, *1*, 1-9.
21. Tröger, J. Ueber einige mittelst nascirenden Formaldehydes entstehende Basen. *J. Prakt. Chem.* **1887**, *1*, 225-245.
22. Dolenský, B.; Elguero, J.; Král, V.; Pardo, C.; Valík, M. Current Tröger's Base Chemistry. *Adv. Heterocycl. Chem.* **2007**, 1-56.
23. Sergeyev, S. Recent Developments in Synthetic Chemistry, Chiral Separations, and Applications of Tröger's Base Analogues. *Helv. Chim. Acta* **2009**, *3*, 415-444.
24. Rúnarsson, Ö. V.; Artacho, J.; Wärnmark, K. The 125th Anniversary of the Tröger's Base Molecule: Synthesis and Applications of Tröger's Base Analogues. *Eur. J. Org. Chem.* **2012**, *36*, 7015-7041.
25. Wilcox, C. S. Tröger's base analogs. New structural units for the preparation of chiral hosts and metal ligands. *Tetrahedron Lett.* **1985**, *47*, 5749-5752.
26. Tatibouët, A.; Demeunynck, M.; Andraud, C.; Collet, A.; Lhomme, J. Synthesis and study of an acridine substituted Tröger's base: preferential binding of the (–)-isomer to B-DNA. *Chem. Commun.* **1999**, *2*, 161-162.
27. Valík, M.; Malina, J.; Palivec, L.; Foltýnová, J.; Tkadlecová, M.; Urbanová, M.; Brabec, V.; Král, V. Tröger's base scaffold in racemic and chiral fashion as a spacer for bisdistamycin formation. Synthesis and DNA binding study. *Tetrahedron* **2006**, *36*, 8591-8600.
28. Yuan, C.; Xin, Q.; Liu, H.; Wang, L.; Jiang, M.; Tao, X. Λ-shaped optoelectronic materials based on Tröger's base. *Sci. China: Chem.* **2011**, *4*, 587-595.
29. Braukyla, T.; Xia, R.; Daskeviciene, M.; Malinauskas, T.; Gruodis, A.; Jankauskas, V.; Fei, Z.; Momblona, C.; Roldán-Carmona, C.; Dyson, P. J.; Getautis, V.; Nazeeruddin, M. K. Inexpensive Hole-Transporting Materials Derived from Tröger's Base Afford Efficient and Stable Perovskite Solar Cells. *Angew. Chem. Int. Ed.* **2019**, *33*, 11266-11272.
30. Antonangelo, A. R.; Hawkins, N.; Tocci, E.; Muzzi, C.; Fuoco, A.; Carta, M. Tröger's Base Network Polymers of Intrinsic Microporosity (TB-PIMs) with Tunable Pore Size for Heterogeneous Catalysis. *J. Am. Chem. Soc.* **2022**, *34*, 15581-15594.

31. Wu, H.; Chen, X.-m.; Wan, Y.; Ye, L.; Xin, H.-q.; Xu, H.-h.; Yue, C.-h.; Pang, L.-l.; Ma, R.; Shi, D.-q. Stereoselective Mannich reactions catalyzed by Tröger's base derivatives in aqueous media. *Tetrahedron Lett.* **2009**, *9*, 1062-1065.
32. Cuenú, F.; Abonia, R.; Bolaños, A.; Cabrera, A. Synthesis, structural elucidation and catalytic activity toward a model Mizoroki–Heck C–C coupling reaction of the pyrazolic Tröger's base Pd4Cl8(PzTB)2 complex. *J. Organomet. Chem.* **2011**, *9*, 1834-1839.
33. Webb, T. H.; Suh, H.; Wilcox, C. S. Chemistry of synthetic receptors and functional group arrays. 16. Enantioselective and diastereoselective molecular recognition of alicyclic substrates in aqueous media by a chiral, resolved synthetic receptor. *J. Am. Chem. Soc.* **1991**, *22*, 8554-8555.
34. Hansson, A. P.; Norrby, P.-O.; Wärnmark, K. A bis(crown-ether) analogue of Tröger's base: Recognition of achiral and chiral primary bisammonium salts. *Tetrahedron Lett.* **1998**, *25*, 4565-4568.
35. Crossley, M. J.; Mackay, L. G.; Try, A. C. Enantioselective recognition of histidine and lysine esters by porphyrin chiral clefts and detection of amino acid conformations in the bound state. *J. Chem. Soc., Chem. Commun.* **1995**, *18*, 1925-1927.
36. Adrian, J. C., Jr.; Wilcox, C. S. Chemistry of synthetic receptors and functional group arrays. 10. Orderly functional group dyads. Recognition of biotin and adenine derivatives by a new synthetic host. *J. Am. Chem. Soc.* **1989**, *20*, 8055-8057.
37. Goswami, S.; Ghosh, K. Molecular recognition: Chain length selectivity studies of dicarboxylic acids by the cavity of a new Troger's base receptor. *Tetrahedron Lett.* **1997**, *25*, 4503-4506.
38. Goswami, S.; Ghosh, K.; Dasgupta, S. Troger's Base Molecular Scaffolds in Dicarboxylic Acid Recognition. *J. Org. Chem.* **2000**, *7*, 1907-1914.
39. Crossley, M. J.; Hambley, T. W.; Mackay, L. G.; Try, A. C.; Walton, R. Porphyrin analogues of Tröger's base: large chiral cavities with a bimetallic binding site. *J. Chem. Soc., Chem. Commun.* **1995**, *10*, 1077-1079.
40. Crossley, M. J.; Try, A. C.; Walton, R. Synthesis of accurate distance models of the primary donor - primary acceptor pair of bacterial photosynthetic reaction centres. *Tetrahedron Lett.* **1996**, *37*, 6807-6810.
41. Brotherhood, P. R.; Wu, R. A. S.; Turner, P.; Crossley, M. J. Cavity effect amplification in the recognition of dicarboxylic acids by initial ditopic H-bond formation followed by kinetic trapping. *Chem. Commun.* **2007**, *3*, 225-227.
42. Bhaskar Reddy, M.; Shailaja, M.; Manjula, A.; Premkumar, J. R.; Sastry, G. N.; Sirisha, K.; Sarma, A. V. S. Design and synthesis of Tröger's base ditopic receptors: host–guest interactions, a combined theoretical and experimental study. *Org. Biomol. Chem.* **2015**, *4*, 1141-1149.
43. Wilcox, C. S.; Cowart, M. D. New approaches to synthetic receptors. Synthesis and host properties of a water soluble macrocyclic analog of Tröger's base. *Tetrahedron Lett.* **1986**, *46*, 5563-5566.

44. Cowart, M. D.; Sucholeiki, I.; Bukownik, R. R.; Wilcox, C. S. Molecular recognition in aqueous media. Conformationally restricted water-soluble cyclophanes derived from 6H,12H-5,11-methanodibenzo[b,f][1,5]diazocine. *J. Am. Chem. Soc.* **1988**, *18*, 6204-6210.
45. Miyake, M.; S. Wilcox, C. Design and Synthesis of a Novel Cyclophane as Host for Aryl Phosphate. *Heterocycles* **2002**, *3*,
46. Ibrahim, A. A.; Matsumoto, M.; Miyahara, Y.; Izumi, K.; Suenaga, M.; Shimizu, N.; Inazu, T. Synthesis and properties of a new series of trögerophanes. *J. Heterocycl. Chem.* **1998**, *1*, 209-215.
47. Manjula, A.; Nagarajan, M. New supramolecular hosts: Synthesis and cation binding studies of novel Tröger's base-crown ether composites. *Tetrahedron* **1997**, *34*, 11859-11868.
48. Marmur, A. Dissolution and Self-Assembly: The Solvophobic/Hydrophobic Effect. *J. Am. Chem. Soc.* **2000**, *9*, 2120-2121.
49. Steed, J. W.; Atwood, J. L., *Supramolecular chemistry*. 2000: Wiley. p. 28.
50. Hunter, C. A.; Sanders, J. K. M. The nature of .pi.-.pi. interactions. *J. Am. Chem. Soc.* **2002**, *14*, 5525-5534.
51. Thakuria, R.; Nath, N. K.; Saha, B. K. The Nature and Applications of π–π Interactions: A Perspective. *Cryst. Growth Des.* **2019**, *2*, 523-528.
52. Ma, J. C.; Dougherty, D. A. The Cation−π Interaction. *Chem. Rev.* **1997**, *5*, 1303-1324.
53. Mas, T.; Pardo, C.; Elguero, J. Use of Tröger's Base as a Scaffold for New Chiral Molecular Tweezers: Synthesis of Trimeric, Fused Tröger's Bases. *Helv. Chim. Acta* **2005**, *6*, 1199-1207.
54. Mas, T.; Pardo, C.; Elguero, J. Synthesis of new chiral molecular tweezers with a tris-Tröger's base skeleton. *Mendeleev Commun.* **2004**, *6*, 235-237.
55. Havlík, M.; Král, V.; Dolenský, B. Overcoming Regioselectivity Issues Inherent in Bis-Tröger's Base Preparation. *Org. Lett.* **2006**, *21*, 4867-4870.
56. Artacho, J.; Nilsson, P.; Bergquist, K.-E.; Wendt, O. F.; Wärnmark, K. The Synthesis and Characterization of all Diastereomers of a Linear Symmetrically Fused Tris-Tröger's Base Analogue: New Chiral Cleft Compounds. *Chem. Eur. J.* **2006**, *10*, 2692-2701.
57. Kessler, J.; Jakubek, M.; Dolenský, B.; Bouř, P. Binding energies of five molecular pincers calculated by explicit and implicit solvent models. *J. Comput. Chem.* **2012**, *29*, 2310-2317.
58. Valik, M.; Dolensky, B.; Petrickova, H.; Kral, V. Regio- and stereoselectivity in preparation of benzene bridged bis- and tris-Troger's bases. *Collect. Czech. Chem. Commun.* **2002**, *5*, 609-621.
59. Havlík, M.; Dolenský, B.; Kessler, J.; Císařová, I.; Král, V. A new synthetic strategy to prepare throne and calix diastereoisomers of parallel tris-Tröger's bases. *Supramol. Chem.* **2012**, *2*, 127-134.

60. Mosca, L.; Čejka, J.; Dolenský, B.; Havlík, M.; Jakubek, M.; Kaplánek, R.; Král, V.; Anzenbacher, P. Bowl-shaped Tröger's bases and their recognition properties. *Chem. Commun.* **2016**, *70*, 10664-10667.
61. Pedersen, C. J.; Frensdorff, H. K. Macrocyclic Polyethers and Their Complexes. *Angew. Chem. Int. Ed. Engl.* **1972**, *1*, 16-25.
62. Gokel, G. W.; Leevy, W. M.; Weber, M. E. Crown Ethers: Sensors for Ions and Molecular Scaffolds for Materials and Biological Models. *Chem. Rev.* **2004**, *5*, 2723-2750.
63. Pears, D. A.; Stoddart, J. F.; Fakley, M. E.; Allwood, B. L.; Williams, D. J. Ammonium-Chloride Complexes with 18-Crown-6. *Acta Crystallogr., Sect. C: Cryst. Struct. Commun.* **1988**, 1426-1430.
64. Izatt, R. M.; Terry, R. E.; Haymore, B. L.; Hansen, L. D.; Dalley, N. K.; Avondet, A. G.; Christensen, J. J. Calorimetric titration study of the interaction of several uni- and bivalent cations with 15-crown-5, 18-crown-6, and two isomers of dicyclohexo-18-crown-6 in aqueous solution at 25.degree.C and .mu. = 0.1. *J. Am. Chem. Soc.* **1976**, *24*, 7620-7626.
65. Frensdorff, H. K. Stability constants of cyclic polyether complexes with univalent cations. *J. Am. Chem. Soc.* **1971**, *3*, 600-606.
66. Wong, K. H.; Konizer, G.; Smid, J. Binding of cyclic polyethers to ion pairs of carbanion alkali salts. *J. Am. Chem. Soc.* **1970**, *3*, 666-670.
67. Izatt, R. M.; Izatt, N. E.; Rossiter, B. E.; Christensen, J. J.; Haymore, B. L. Cyclic Polyether-Protonated Organic Amine Binding: Significance in Enzymatic and Ion Transport Processes. *Science* **1978**, *4332*, 994-996.
68. Izatt, R. M.; Lamb, J. D.; Maas, G. E.; Asay, R. E.; Bradshaw, J. S.; Christensen, J. J. Synthesis of two novel cyclic polyether-ester compounds and some comparisons of their reactions with sodium(1+), potassium(1+), and barium(2+) ions with those of 18-crown-6 and valinomycin. *J. Am. Chem. Soc.* **1977**, *7*, 2365-2366.
69. Meyer, E. A.; Castellano, R. K.; Diederich, F. Interactions with Aromatic Rings in Chemical and Biological Recognition. *Angew. Chem. Int. Ed.* **2003**, *11*, 1210-1250.
70. Emenike, B. U.; Spinelle, R. A.; Rosario, A.; Shinn, D. W.; Yoo, B. Solvent Modulation of Aromatic Substituent Effects in Molecular Balances Controlled by CH−π Interactions. *J. Phys. Chem. A* **2018**, *4*, 909-915.
71. Hunter, C. A.; Sanders, J. K. M. The nature of .pi.-.pi. interactions. *J. Am. Chem. Soc.* **1990**, *14*, 5525-5534.
72. Hunter, C. A.; Lawson, K. R.; Perkins, J.; Urch, C. J. Aromatic interactions. *J. Chem. Soc., Perkin Trans. 2* **2001**, *5*, 651-669.
73. Martinez, C. R.; Iverson, B. L. Rethinking the term “pi-stacking”. *Chem. Sci.* **2012**, *7*, 2191-2201.
74. Müller-Dethlefs, K.; Hobza, P. Noncovalent Interactions: A Challenge for Experiment and Theory. *Chem. Rev.* **2000**, *1*, 143-168.
75. Wheeler, S. E.; Bloom, J. W. G. Toward a More Complete Understanding of Noncovalent Interactions Involving Aromatic Rings. *J. Phys. Chem. A* **2014**, *32*, 6133-6147.

76. Nishio, M. The CH/π hydrogen bond in chemistry. Conformation, supramolecules, optical resolution and interactions involving carbohydrates. *Phys. Chem. Chem. Phys.* **2011**, *31*, 13873-13900.
77. Burley, S. K.; Petsko, G. A. Aromatic-Aromatic Interaction: A Mechanism of Protein Structure Stabilization. *Science* **1985**, *4708*, 23-28.
78. Umezawa, Y.; Tsuboyama, S.; Takahashi, H.; Uzawa, J.; Nishio, M. CH/π interaction in the conformation of peptides. A database study††This paper is dedicated to the memory of the late Professor Sir Derek H. R. Barton, the founder of the concept of conformation. The authors sincerely regret the immeasurable loss of an outstanding figure in the world of science. *Biorg. Med. Chem.* **1999**, *9*, 2021-2026.
79. Brandl, M.; Weiss, M. S.; Jabs, A.; Sühnel, J.; Hilgenfeld, R. C-h···π-interactions in proteins. *J. Mol. Biol.* **2001**, *1*, 357-377.
80. Mati, I. K.; Cockroft, S. L. Molecular balances for quantifying non-covalent interactions. *Chem. Soc. Rev.* **2010**, *11*, 4195-4205.
81. Cozzi, F.; Siegel, J. S. Interaction between stacked aryl groups in 1,8-diarylnaphthalenes: Dominance of polar/π over charge-transfer effects. *Pure Appl. Chem.* **1995**, *5*, 683-689.
82. Cozzi, F.; Annunziata, R.; Benaglia, M.; Baldridge, K. K.; Aguirre, G.; Estrada, J.; Sritana-Anant, Y.; Siegel, J. S. Through-space interactions between parallel-offset arenes at the van der Waals distance: 1,8-diarylbiphenylene syntheses, structure and QM computations. *Phys. Chem. Chem. Phys.* **2008**, *19*, 2686-2694.
83. Adams, H.; Carver, F. J.; Hunter, C. A.; Morales, J. C.; Seward, E. M. Chemical Double-Mutant Cycles for the Measurement of Weak Intermolecular Interactions: Edge-to-Face Aromatic Interactions. *Angew. Chem. Int. Ed. Engl.* **1996**, *13-14*, 1542-1544.
84. Paliwal, S.; Geib, S.; Wilcox, C. S. Molecular Torsion Balance for Weak Molecular Recognition Forces. Effects of "Tilted-T" Edge-to-Face Aromatic Interactions on Conformational Selection and Solid-State Structure. *J. Am. Chem. Soc.* **1994**, *10*, 4497-4498.
85. Kim, E.-i.; Paliwal, S.; Wilcox, C. S. Measurements of Molecular Electrostatic Field Effects in Edge-to-Face Aromatic Interactions and CH-π Interactions with Implications for Protein Folding and Molecular Recognition. *J. Am. Chem. Soc.* **1998**, *43*, 11192-11193.
86. Bhayana, B.; Wilcox, C. S. A Minimal Protein Folding Model To Measure Hydrophobic and CH–π Effects on Interactions between Nonpolar Surfaces in Water. *Angew. Chem. Int. Ed.* **2007**, *36*, 6833-6836.
87. Stanfield, R. L.; Wilson, I. A. Protein-peptide interactions. *Curr. Opin. Struct. Biol.* **1995**, *1*, 103-113.
88. Neduva, V.; Russell, R. B. Peptides mediating interaction networks: new leads at last. *Curr. Opin. Biotechnol.* **2006**, *5*, 465-471.
89. Petsalaki, E.; Russell, R. B. Peptide-mediated interactions in biological systems: new discoveries and applications. *Curr. Opin. Biotechnol.* **2008**, *4*, 344-350.

90. Mata, R. A.; Suhm, M. A. Benchmarking Quantum Chemical Methods: Are We Heading in the Right Direction? *Angew. Chem. Int. Ed.* **2017**, *37*, 11011-11018.
91. Řezáč, J.; Hobza, P. Benchmark Calculations of Interaction Energies in Noncovalent Complexes and Their Applications. *Chem. Rev.* **2016**, *9*, 5038-5071.
92. Belsky, I. 'Naked' fluorid-ecatalysed Michael-additions. *J. Chem. Soc., Chem. Commun.* **1977**, *7*, 237-237.
93. Ono, N.; Miyake, H.; Tamura, R.; Kaji, A. A new synthetic method: Direct replacement of the nitro group by hydrogen or deuterium. *Tetrahedron Lett.* **1981**, *18*, 1705-1708.
94. Secrist, J. A., III; Logue, M. W. Amine hydrochlorides by reduction in the presence of chloroform. *J. Org. Chem.* **1972**, *2*, 335-336.
95. Hirose, K. A Practical Guide for the Determination of Binding Constants. *J. Inclusion Phenom. Macrocyclic Chem.* **2001**, *3*, 193-209.
96. Emenike, B. U.; Bey, S. N.; Bigelow, B. C.; Chakravartula, S. V. S. Quantitative model for rationalizing solvent effect in noncovalent CH–Aryl interactions. *Chem. Sci.* **2016**, *2*, 1401-1407.
97. Allinger, N. L.; Yuh, Y. H.; Lii, J. H. Molecular mechanics. The MM3 force field for hydrocarbons. 1. *J. Am. Chem. Soc.* **1989**, *23*, 8551-8566.
98. Halgren, T. A. MMFF VI. MMFF94s option for energy minimization studies. *J. Comput. Chem.* **1999**, *7*, 720-729.
99. Harder, E.; Damm, W.; Maple, J.; Wu, C.; Reboul, M.; Xiang, J. Y.; Wang, L.; Lupyan, D.; Dahlgren, M. K.; Knight, J. L.; Kaus, J. W.; Cerutti, D. S.; Krilov, G.; Jorgensen, W. L.; Abel, R.; Friesner, R. A. OPLS3: A Force Field Providing Broad Coverage of Drug-like Small Molecules and Proteins. *J. Chem. Theory Comput.* **2016**, *1*, 281-296.
100. Roos, K.; Wu, C.; Damm, W.; Reboul, M.; Stevenson, J. M.; Lu, C.; Dahlgren, M. K.; Mondal, S.; Chen, W.; Wang, L.; Abel, R.; Friesner, R. A.; Harder, E. D. OPLS3e: Extending Force Field Coverage for Drug-Like Small Molecules. *J. Chem. Theory Comput.* **2019**, *3*, 1863-1874.
101. Zhao, Y.; Truhlar, D. G. The M06 suite of density functionals for main group thermochemistry, thermochemical kinetics, noncovalent interactions, excited states, and transition elements: two new functionals and systematic testing of four M06-class functionals and 12 other functionals. *Theor. Chem. Acc.* **2008**, *1*, 215-241.
102. Chai, J.-D.; Head-Gordon, M. Long-range corrected hybrid density functionals with damped atom–atom dispersion corrections. *Phys. Chem. Chem. Phys.* **2008**, *44*, 6615-6620.
103. Cortis, C. M.; Friesner, R. A. An automatic three-dimensional finite element mesh generation system for the Poisson–Boltzmann equation. *J. Comput. Chem.* **1997**, *13*, 1570-1590.
104. Keeler, J., *Understanding NMR spectroscopy*. 2nd ed. 2010: John Wiley and Sons. p. 241-312.

105. Fattori, J.; Rodrigues, F. H. S.; Pontes, J. G. M.; Paula Espíndola, A.; Tasic, L., *Monitoring Intermolecular and Intramolecular Interactions by NMR Spectroscopy*, in *Applications of NMR Spectroscopy, Vol. 3*, A. ur-Rahman;M. I. Choudhary (ed.), 2015, Bentham Science Publishers. p. 180-266.
106. Warshel, A. Electrostatic basis of structure-function correlation in proteins. *Acc. Chem. Res.* **1981**, *9*, 284-290.
107. Yoshida, K.; Kuroda, D.; Kiyoshi, M.; Nakakido, M.; Nagatoishi, S.; Soga, S.; Shirai, H.; Tsumoto, K. Exploring designability of electrostatic complementarity at an antigen-antibody interface directed by mutagenesis, biophysical analysis, and molecular dynamics simulations. *Sci. Rep.* **2019**, *1*, 4482.
108. Shokri, A.; Ramezani, M.; Fattahi, A.; Kass, S. R. Electrostatically Defying Cation–Cation Clusters: Can Likes Attract in a Low-Polarity Environment? *J. Phys. Chem. A* **2013**, *38*, 9252-9258.
109. Gao, J.; Boudon, S.; Wipff, G. Ab initio and crystal structure analysis of like-charged ion pairs. *J. Am. Chem. Soc.* **1991**, *25*, 9610-9614.
110. Dalla Favera, N.; Kiehne, U.; Bunzen, J.; Hytteballe, S.; Lützen, A.; Piguet, C. Intermetallic Interactions Within Solvated Polynuclear Complexes: A Misunderstood Concept. *Angew. Chem. Int. Ed.* **2010**, *1*, 125-128.
111. Grolier, J.-P. E.; del Río, J. M. Isothermal titration calorimetry: A thermodynamic interpretation of measurements. *J. Chem. Thermodyn.* **2012**, 193-202.
112. Turnbull, W. B.; Daranas, A. H. On the Value of c: Can Low Affinity Systems Be Studied by Isothermal Titration Calorimetry? *J. Am. Chem. Soc.* **2003**, *48*, 14859-14866.
113. Perlmutter-Hayman, B. Cooperative binding to macromolecules. A formal approach. *Acc. Chem. Res.* **1986**, *3*, 90-96.
114. Rogers, B. A.; Okur, H. I.; Yan, C.; Yang, T.; Heyda, J.; Cremer, P. S. Weakly hydrated anions bind to polymers but not monomers in aqueous solutions. *Nat. Chem.* **2022**, *1*, 40-45.
115. Tesei, G.; Aspelin, V.; Lund, M. Specific Cation Effects on SCN– in Bulk Solution and at the Air–Water Interface. *J. Phys. Chem. B* **2018**, *19*, 5094-5105.
116. Seiler, P.; Dobler, M.; Dunitz, J. D. Potassium Thiocyanate Complex of 1,4,7,10,13,16-Hexaoxacyclooctadecane. *Acta Crystallogr. Sect. B: Struct. Sci.* **1974**, *Nov15*, 2744-2745.
117. Zhou, D.; Hao, H.; Ma, Y.; Zhong, H.; Dai, Y. n.; Cai, K.; Mukherjee, S.; Liu, J.; Bian, H. Specific Host–Guest Interactions in the Crown Ether Complexes with K+ and NH4+ Revealed from the Vibrational Relaxation Dynamics of the Counteranion. *J. Phys. Chem. B* **2020**, *41*, 9154-9162.
118. Owen, B. B.; Miller, R. C.; Milner, C. E.; Cogan, H. L. The Dielectric Constant of Water as a Function of Temperature and Pressure. *J. Phys. Chem.* **1961**, *11*, 2065-2070.
119. Canard, G.; Piguet, C. The Origin of the Surprising Stabilities of Highly Charged Self-Assembled Polymetallic Complexes in Solution. *Inorg. Chem.* **2007**, *9*, 3511-3522.

120. Arunan, E.; Desiraju, G. R.; Klein, R. A.; Sadlej, J.; Scheiner, S.; Alkorta, I.; Clary, D. C.; Crabtree, R. H.; Dannenberg, J. J.; Hobza, P.; Kjaergaard, H. G.; Legon, A. C.; Mennucci, B.; Nesbitt, D. J. Definition of the hydrogen bond (IUPAC Recommendations 2011). *Pure Appl. Chem.* **2011**, *8*, 1637-1641.

121. Zhang, D.-W.; Wang, H.; Li, Z.-T., *Hydrogen Bonding Motifs: New Progresses*, in *Hydrogen Bonded Supramolecular Structures*, Z.-T. Li;L.-Z. Wu (ed.), 2015, Springer Berlin Heidelberg: Berlin, Heidelberg. p. 1-36.

122. Dannenberg, J. J.; Haskamp, L.; Masunov, A. Are Hydrogen Bonds Covalent or Electrostatic? A Molecular Orbital Comparison of Molecules in Electric Fields and H-Bonding Environments. *J. Phys. Chem. A* **1999**, *35*, 7083-7086.

123. van der Lubbe, S. C. C.; Fonseca Guerra, C. The Nature of Hydrogen Bonds: A Delineation of the Role of Different Energy Components on Hydrogen Bond Strengths and Lengths. *Chem. – Asian J.* **2019**, *16*, 2760-2769.

124. Jorgensen, W. L.; Pranata, J. Importance of secondary interactions in triply hydrogen bonded complexes: guanine-cytosine vs uracil-2,6-diaminopyridine. *J. Am. Chem. Soc.* **1990**, *5*, 2008-2010.

125. Pranata, J.; Wierschke, S. G.; Jorgensen, W. L. OPLS potential functions for nucleotide bases. Relative association constants of hydrogen-bonded base pairs in chloroform. *J. Am. Chem. Soc.* **1991**, *8*, 2810-2819.

126. Murray, T. J.; Zimmerman, S. C. New triply hydrogen bonded complexes with highly variable stabilities. *J. Am. Chem. Soc.* **1992**, *10*, 4010-4011.

127. Beijer, F. H.; Kooijman, H.; Spek, A. L.; Sijbesma, R. P.; Meijer, E. W. Self-Complementarity Achieved through Quadruple Hydrogen Bonding. *Angew. Chem. Int. Ed.* **1998**, *1-2*, 75-78.

128. Beijer, F. H.; Sijbesma, R. P.; Kooijman, H.; Spek, A. L.; Meijer, E. W. Strong Dimerization of Ureidopyrimidones via Quadruple Hydrogen Bonding. *J. Am. Chem. Soc.* **1998**, *27*, 6761-6769.

129. Söntjens, S. H. M.; Sijbesma, R. P.; van Genderen, M. H. P.; Meijer, E. W. Stability and Lifetime of Quadruply Hydrogen Bonded 2-Ureido-4[1H]-pyrimidinone Dimers. *J. Am. Chem. Soc.* **2000**, *31*, 7487-7493.

130. Zhang, J.; Qi, S.; Zhang, C.; Fan, Z.; Ding, Q.; Mao, S.; Dong, Z. Controlling Keto–Enol Tautomerism of Ureidopyrimidinone to Generate a Single-Quadruple AADD-DDAA Dimeric Array. *Org. Lett.* **2020**, *18*, 7305-7309.

131. Kheria, S.; Rayavarapu, S.; Kotmale, A. S.; Sanjayan, G. J. Three in one: prototropy-free highly stable AADD-type self-complementary quadruple hydrogen-bonded molecular duplexes with a built-in fluorophore. *Chem. Commun.* **2017**, *18*, 2689-2692.

132. Lafitte, V. G. H.; Aliev, A. E.; Horton, P. N.; Hursthouse, M. B.; Bala, K.; Golding, P.; Hailes, H. C. Quadruply Hydrogen Bonded Cytosine Modules for Supramolecular Applications. *J. Am. Chem. Soc.* **2006**, *20*, 6544-6545.

133. Aparicio, F.; Mayoral, M. J.; Montoro-García, C.; González-Rodríguez, D. Guidelines for the assembly of hydrogen-bonded macrocycles. *Chem. Commun.* **2019**, *51*, 7277-7299.

134. Marsh, A.; Silvestri, M.; Lehn, J.-M. Self-complementary hydrogen bonding heterocycles designed for the enforced self-assembly into supramolecular macrocycles. *Chem. Commun.* **1996**, *13*, 1527-1528.
135. Mascal, M.; Hext, N. M.; Warmuth, R.; Arnall-Culliford, J. R.; Moore, M. H.; Turkenburg, J. P. The G−C DNA Base Hybrid: Synthesis, Self-Organization and Structural Analysis. *J. Org. Chem.* **1999**, *23*, 8479-8484.
136. Mascal, M.; Hext, N. M.; Warmuth, R.; Moore, M. H.; Turkenburg, J. P. Programming a Hydrogen-Bonding Code for the Specific Generation of a Supermacrocycle. *Angew. Chem. Int. Ed. Engl.* **1996**, *19*, 2204-2206.
137. Asadi, A.; Patrick, B. O.; Perrin, D. M. G^C Quartet — A DNA-Inspired Janus-GC Heterocycle: Synthesis, Structural Analysis, and Self-Organization. *J. Am. Chem. Soc.* **2008**, *39*, 12860-12861.
138. Catti, L.; Zhang, Q.; Tiefenbacher, K. Advantages of Catalysis in Self-Assembled Molecular Capsules. *Chem. – Eur. J.* **2016**, *27*, 9060-9066.
139. Galan, A.; Ballester, P. Stabilization of reactive species by supramolecular encapsulation. *Chem. Soc. Rev.* **2016**, *6*, 1720-1737.
140. Wyler, R.; de Mendoza, J.; Rebek Jr., J. A Synthetic Cavity Assembles Through Self-Complementary Hydrogen Bonds. *Angew. Chem. Int. Ed. Engl.* **1993**, *12*, 1699-1701.
141. Meissner, R. S.; Rebek, J.; de Mendoza, J. Autoencapsulation Through Intermolecular Forces: A Synthetic Self-Assembling Spherical Complex. *Science* **1995**, *5241*, 1485-1488.
142. Heinz, T.; Rudkevich, D. M.; Rebek, J. Pairwise selection of guests in a cylindrical molecular capsule of nanometre dimensions. *Nature* **1998**, *6695*, 764-766.
143. Montà-González, G.; Sancenón, F.; Martínez-Máñez, R.; Martí-Centelles, V. Purely Covalent Molecular Cages and Containers for Guest Encapsulation. *Chem. Rev.* **2022**, *16*, 13636-13708.
144. Beaudoin, D.; Rominger, F.; Mastalerz, M. Chirality-Assisted Synthesis of a Very Large Octameric Hydrogen-Bonded Capsule. *Angew. Chem. Int. Ed.* **2016**, *50*, 15599-15603.
145. Merget, S.; Catti, L.; Zev, S.; Major, D. T.; Trapp, N.; Tiefenbacher, K. Concentration-Dependent Self-Assembly of an Unusually Large Hexameric Hydrogen-Bonded Molecular Cage. *Chem. – Eur. J.* **2021**, *13*, 4447-4453.
146. Eisenberg, B. Ionic Channels in Biological Membranes: Natural Nanotubes. *Acc. Chem. Res.* **1998**, *3*, 117-123.
147. Mario Borgnia; Søren Nielsen; Andreas Engel; Agre, P. Cellular and Molecular Biology of the Aquaporin Water Channels. *Annu. Rev. Biochem* **1999**, *1*, 425-458.
148. Horwich, A. L.; Weber-Ban, E. U.; Finley, D. Chaperone rings in protein folding and degradation. *Proc. Natl. Acad. Sci. U. S. A.* **1999**, *20*, 11033-11040.
149. Sigler, P. B.; Xu, Z.; Rye, H. S.; Burston, S. G.; Fenton, W. A.; Horwich, A. L. STRUCTURE AND FUNCTION IN GroEL-MEDIATED PROTEIN FOLDING. *Annu. Rev. Biochem* **1998**, *1*, 581-608.

150. D. Voges; P. Zwickl, a.; Baumeister, W. The 26S Proteasome: A Molecular Machine Designed for Controlled Proteolysis. *Annu. Rev. Biochem* **1999**, *1*, 1015-1068.
151. Hunt, R. T.; Nasmyth, K. A.; Diffley, J.; Zwickl, P.; Voges, D.; Baumeister, W. The proteasome: a macromolecular assembly designed for controlled proteolysis. *Philos. Trans. R. Soc., B* **1999**, *1389*, 1501-1511.
152. Bong, D. T.; Clark, T. D.; Granja, J. R.; Ghadiri, M. R. Self-Assembling Organic Nanotubes. *Angew. Chem. Int. Ed.* **2001**, 988-1011.
153. Neniškis, A.; Račkauskaitė, D.; Shi, Q.; Robertson, A. J.; Marsh, A.; Ulčinas, A.; Valiokas, R.; Brown, S. P.; Wärnmark, K.; Orentas, E. A Tautoleptic Approach to Chiral Hydrogen-Bonded Supramolecular Tubular Polymers with Large Cavity. *Chem. – Eur. J.* **2018**, *53*, 14028-14033.
154. Appella, D. H.; Christianson, L. A.; Karle, I. L.; Powell, D. R.; Gellman, S. H. β-Peptide Foldamers: Robust Helix Formation in a New Family of β-Amino Acid Oligomers. *J. Am. Chem. Soc.* **1996**, *51*, 13071-13072.
155. Appella, D. H.; Christianson, L. A.; Klein, D. A.; Powell, D. R.; Huang, X.; Barchi, J. J.; Gellman, S. H. Residue-based control of helix shape in β-peptide oligomers. *Nature* **1997**, *6631*, 381-384.
156. Pantoş, G. D.; Pengo, P.; Sanders, J. K. M. Hydrogen-Bonded Helical Organic Nanotubes. *Angew. Chem. Int. Ed.* **2007**, *1-2*, 194-197.
157. Ponnuswamy, N.; Pantoş, G. D.; Smulders, M. M. J.; Sanders, J. K. M. Thermodynamics of Supramolecular Naphthalenediimide Nanotube Formation: The Influence of Solvents, Side Chains, and Guest Templates. *J. Am. Chem. Soc.* **2012**, *1*, 566-573.
158. Pantoş, G. D.; Wietor, J.-L.; Sanders, J. K. M. Filling Helical Nanotubes with C60. *Angew. Chem. Int. Ed.* **2007**, *13*, 2238-2240.
159. De Santis, P.; Morosetti, S.; Rizzo, R. Conformational Analysis of Regular Enantiomeric Sequences. *Macromolecules* **1974**, *1*, 52-58.
160. Ghadiri, M. R.; Granja, J. R.; Milligan, R. A.; McRee, D. E.; Khazanovich, N. Self-assembling organic nanotubes based on a cyclic peptide architecture. *Nature* **1993**, *6453*, 324-327.
161. Rodríguez-Vázquez, N.; García-Fandiño, R.; Amorín, M.; Granja, J. R. Self-assembling α,γ-cyclic peptides that generate cavities with tunable properties. *Chem. Sci.* **2016**, *1*, 183-187.
162. Ghadiri, M. R.; Granja, J. R.; Buehler, L. K. Artificial transmembrane ion channels from self-assembling peptide nanotubes. *Nature* **1994**, *6478*, 301-304.
163. Granja, J. R.; Ghadiri, M. R. Channel-Mediated Transport of Glucose across Lipid Bilayers. *J. Am. Chem. Soc.* **1994**, *23*, 10785-10786.
164. Sánchez-Quesada, J.; Sun Kim, H.; Ghadiri, M. R. A Synthetic Pore-Mediated Transmembrane Transport of Glutamic Acid. *Angew. Chem. Int. Ed.* **2001**, *13*, 2503-2506.

165. Fernandez-Lopez, S.; Kim, H.-S.; Choi, E. C.; Delgado, M.; Granja, J. R.; Khasanov, A.; Kraehenbuehl, K.; Long, G.; Weinberger, D. A.; Wilcoxen, K. M.; Ghadiri, M. R. Antibacterial agents based on the cyclic d,l-α-peptide architecture. *Nature* **2001**, *6845*, 452-455.

166. Motiei, L.; Rahimipour, S.; Thayer, D. A.; Wong, C.-H.; Ghadiri, M. R. Antibacterial cyclic d,l-α-glycopeptides. *Chem. Commun.* **2009**, *25*, 3693-3695.

167. Vázquez-González, V.; Mayoral, M. J.; Chamorro, R.; Hendrix, M. M. R. M.; Voets, I. K.; González-Rodríguez, D. Noncovalent Synthesis of Self-Assembled Nanotubes through Decoupled Hierarchical Cooperative Processes. *J. Am. Chem. Soc.* **2019**, *41*, 16432-16438.

168. Vázquez-González, V.; Mayoral, M. J.; Aparicio, F.; Martínez-Arjona, P.; González-Rodríguez, D. The Role of Peripheral Amide Groups as Hydrogen-Bonding Directors in the Tubular Self-Assembly of Dinucleobase Monomers. *ChemPlusChem* **2021**, *8*, 1087-1096.

169. Orentas, E.; Wallentin, C.-J.; Bergquist, K.-E.; Lund, M.; Butkus, E.; Wärnmark, K. Topology Selection and Tautoleptic Aggregation: Formation of an Enantiomerically Pure Supramolecular Belt over a Helix. *Angew. Chem. Int. Ed.* **2011**, *9*, 2071-2074.

170. Shi, Q.; Bergquist, K.-E.; Huo, R.; Li, J.; Lund, M.; Vácha, R.; Sundin, A.; Butkus, E.; Orentas, E.; Wärnmark, K. Composition- and Size-Controlled Cyclic Self-Assembly by Solvent- and C60-Responsive Self-Sorting. *J. Am. Chem. Soc.* **2013**, *40*, 15263-15268.

171. Jozeliūnaitė, A.; Neniškis, A.; Bertran, A.; Bowen, A. M.; Di Valentin, M.; Raišys, S.; Baronas, P.; Kazlauskas, K.; Vilčiauskas, L.; Orentas, E. Fullerene Complexation in a Hydrogen-Bonded Porphyrin Receptor via Induced-Fit: Cooperative Action of Tautomerization and C–H···π Interactions. *J. Am. Chem. Soc.* **2023**, *1*, 455-464.

172. Račkauskaitė, D.; Bergquist, K.-E.; Shi, Q.; Sundin, A.; Butkus, E.; Wärnmark, K.; Orentas, E. A Remarkably Complex Supramolecular Hydrogen-Bonded Decameric Capsule Formed from an Enantiopure C2-Symmetric Monomer by Solvent-Responsive Aggregation. *J. Am. Chem. Soc.* **2015**, *33*, 10536-10546.

173. Shi, Q.; Javorskis, T.; Bergquist, K.-E.; Ulčinas, A.; Niaura, G.; Matulaitienė, I.; Orentas, E.; Wärnmark, K. Stimuli-controlled self-assembly of diverse tubular aggregates from one single small monomer. *Nat. Commun.* **2017**, *1*, 14943.

174. Jozeliūnaitė, A.; Javorskis, T.; Vaitkevičius, V.; Klimavičius, V.; Orentas, E. Fully Supramolecular Chiral Hydrogen-Bonded Molecular Tweezer. *J. Am. Chem. Soc.* **2022**, *18*, 8231-8241.

175. Račkauskaitė, D.; Gegevičius, R.; Matsuo, Y.; Wärnmark, K.; Orentas, E. An Enantiopure Hydrogen-Bonded Octameric Tube: Self-Sorting and Guest-Induced Rearrangement. *Angew. Chem. Int. Ed.* **2016**, *1*, 208-212.

176. Kozlowska, M.; Goclon, J.; Rodziewicz, P. Intramolecular Hydrogen Bonds in Low-Molecular-Weight Polyethylene Glycol. *ChemPhysChem* **2016**, *8*, 1143-1153.

177. Parray, Z. A.; Hassan, M. I.; Ahmad, F.; Islam, A. Amphiphilic nature of polyethylene glycols and their role in medical research. *Polym. Test.* **2020**, 106316.

178. Li, W.; Zhan, P.; De Clercq, E.; Lou, H.; Liu, X. Current drug research on PEGylation with small molecular agents. *Prog. Polym. Sci.* **2013**, *3*, 421-444.

179. Veronese, F. M.; Pasut, G. PEGylation, successful approach to drug delivery. *Drug Discovery Today* **2005**, *21*, 1451-1458.
180. Webber, M. J.; Appel, E. A.; Vinciguerra, B.; Cortinas, A. B.; Thapa, L. S.; Jhunjhunwala, S.; Isaacs, L.; Langer, R.; Anderson, D. G. Supramolecular PEGylation of biopharmaceuticals. *Proc. Natl. Acad. Sci. U. S. A.* **2016**, *50*, 14189-14194.
181. Bottini, M.; Rosato, N.; Bottini, N. PEG-Modified Carbon Nanotubes in Biomedicine: Current Status and Challenges Ahead. *Biomacromolecules* **2011**, *10*, 3381-3393.
182. Ravelli, D.; Merli, D.; Quartarone, E.; Profumo, A.; Mustarelli, P.; Fagnoni, M. PEGylated carbon nanotubes: preparation, properties and applications. *RSC Advances* **2013**, *33*, 13569-13582.
183. Obert, E.; Bellot, M.; Bouteiller, L.; Andrioletti, F.; Lehen-Ferrenbach, C.; Boué, F. Both Water- and Organo-Soluble Supramolecular Polymer Stabilized by Hydrogen-Bonding and Hydrophobic Interactions. *J. Am. Chem. Soc.* **2007**, *50*, 15601-15605.
184. Kieltyka, R. E.; Pape, A. C. H.; Albertazzi, L.; Nakano, Y.; Bastings, M. M. C.; Voets, I. K.; Dankers, P. Y. W.; Meijer, E. W. Mesoscale Modulation of Supramolecular Ureidopyrimidinone-Based Poly(ethylene glycol) Transient Networks in Water. *J. Am. Chem. Soc.* **2013**, *30*, 11159-11164.
185. Leenders, C. M. A.; Albertazzi, L.; Mes, T.; Koenigs, M. M. E.; Palmans, A. R. A.; Meijer, E. W. Supramolecular polymerization in water harnessing both hydrophobic effects and hydrogen bond formation. *Chem. Commun.* **2013**, *19*, 1963-1965.
186. Wallentin, C. J.; Orentas, E.; Butkus, E.; Wärnmark, K. Baker's Yeast for Sweet Dough Enables Large-Scale Synthesis of Enantiomerically Pure Bicyclo[3.3.1]nonane-2,6-dione. *Synthesis* **2009**, *05*, 864-867.
187. Alkauskas, A.; Ceponkus, J.; Mikulskiene, B.; Aleksa, V.; Butkus, E.; Sablinskas, V. Conformational stability of bicyclo[3.3.1]nonane-2,6-dione and bicyclo[3.3.1]nonane-2,9-dione: ab initio calculations and vibrational spectroscopy studies. *J. Mol. Struct.* **2001**, 517-521.
188. Vellekoop, A. S.; Smith, R. A. J. The Mechanism of Organocuprate 1,4-Addition Reactions with .alpha.,.beta.-Unsaturated Ketones: Formation of Cuprate-Enone Complexes with Lithium Dimethylcuprate. *J. Am. Chem. Soc.* **1994**, *7*, 2902-2913.
189. Lipshutz, B. H.; Sengupta, S., *Organocopper Reagents: Substitution, Conjugate Addition, Carbo/Metallocupration, and Other Reactions*, in *Organic Reactions*, L. A. Paquette (ed.), 1992, John Wiley & Sons. p. 135-631.
190. Lipshutz, B. H. Applications of Higher-Order Mixed Organocuprates to Organic Synthesis. *Synthesis* **1987**, *04*, 325-341.
191. Lipshutz, B. H.; Wilhelm, R. S.; Kozlowski, J. A. The chemistry of higher order organocuprates. *Tetrahedron* **1984**, *24*, 5005-5038.
192. Davies, R. P. The structures of lithium and magnesium organocuprates and related species. *Coord. Chem. Rev.* **2011**, *11*, 1226-1251.
193. Krause, N. New Results Regarding the Structure and Reactivity of Cyanocuprates—The End of an Old Controversy. *Angew. Chem. Int. Ed.* **1999**, *1-2*, 79-81.

194. Harutyunyan, S. R.; López, F.; Browne, W. R.; Correa, A.; Peña, D.; Badorrey, R.; Meetsma, A.; Minnaard, A. J.; Feringa, B. L. On the Mechanism of the Copper-Catalyzed Enantioselective 1,4-Addition of Grignard Reagents to α,β-Unsaturated Carbonyl Compounds. *J. Am. Chem. Soc.* **2006**, *28*, 9103-9118.
195. Jerphagnon, T.; Pizzuti, M. G.; Minnaard, A. J.; Feringa, B. L. Recent advances in enantioselective copper-catalyzed 1,4-addition. *Chem. Soc. Rev.* **2009**, *4*, 1039-1075.
196. Woodward, S. Decoding the 'black box' reactivity that is organocuprate conjugate addition chemistry. *Chem. Soc. Rev.* **2000**, *6*, 393-401.
197. Van Heerden, P. S.; Bezuidenhoudt, B. C. B.; Steenkamp, J. A.; Ferreira, D. Conjugate addition of benzyl copper reagents to α,α-enoates and -enones. *Tetrahedron Lett.* **1992**, *17*, 2383-2386.
198. Linderman, R. J.; Godfrey, A.; Horne, K. Applications of α-alkoxyorganocuprate reagents in the regiospecific synthesis of cyclic homoaldol products. *Tetrahedron* **1989**, *2*, 495-506.
199. Berk, S. C.; Knochel, P.; Yeh, M. C. P. General approach to highly functionalized benzylic organometallics of zinc and copper. *J. Org. Chem.* **1988**, *24*, 5789-5791.
200. van Heerden, P. S.; Bezuidenhoudt, B. C. B.; Ferreira, D. Tetramethylethylene diamine/trimethylsilyl chloride mediated addition of benzyl copper reagents to α,β-unsaturated esters. *Tetrahedron* **1996**, *37*, 12313-12322.
201. Parham, W. E.; Jones, L. D.; Sayed, Y. A. Selective halogen-lithium exchange in bromophenylalkyl halides. *J. Org. Chem.* **1976**, *7*, 1184-1186.
202. Knochel, P.; Rozema, M. J.; Tucker, C. E.; Retherford, C.; Furlong, M.; AchyuthaRao, S. The chemistry of polyfunctional organozinc and copper reagents. *Pure Appl. Chem.* **1992**, *3*, 361-369.
203. Levin, V. V.; Zemtsov, A. A.; Struchkova, M. I.; Dilman, A. D. Reactions of Difluorocarbene with Organozinc Reagents. *Org. Lett.* **2013**, *4*, 917-919.
204. Zarycz, M. N. C.; Fonseca Guerra, C. NMR 1H-Shielding Constants of Hydrogen-Bond Donor Reflect Manifestation of the Pauli Principle. *J. Phys. Chem. Lett.* **2018**, *13*, 3720-3724.
205. García de la Torre, J.; del Rio Echenique, G.; Ortega, A. Improved Calculation of Rotational Diffusion and Intrinsic Viscosity of Bead Models for Macromolecules and Nanoparticles. *J. Phys. Chem. B* **2007**, *5*, 955-961.
206. Garcia de la Torre, J.; Navarro, S.; Lopez Martinez, M. C.; Diaz, F. G.; Lopez Cascales, J. J. HYDRO: a computer program for the prediction of hydrodynamic properties of macromolecules. *Biophys. J.* **1994**, *2*, 530-531.
207. de Greef, T. F. A.; Nieuwenhuizen, M. M. L.; Stals, P. J. M.; Fitié, C. F. C.; Palmans, A. R. A.; Sijbesma, R. P.; Meijer, E. W. The influence of ethylene glycol chains on the thermodynamics of hydrogen-bonded supramolecular assemblies in apolar solvents. *Chem. Commun.* **2008**, *36*, 4306-4308.
208. de Greef, T. F. A.; Nieuwenhuizen, M. M. L.; Sijbesma, R. P.; Meijer, E. W. Competitive Intramolecular Hydrogen Bonding in Oligo(ethylene oxide) Substituted Quadruple Hydrogen Bonded Systems. *J. Org. Chem.* **2010**, *3*, 598-610.

209. Stals, P. J. M.; Haveman, J. F.; Martín-Rapún, R.; Fitié, C. F. C.; Palmans, A. R. A.; Meijer, E. W. The influence of oligo(ethylene glycol) side chains on the self-assembly of benzene-1,3,5-tricarboxamides in the solid state and in solution. *J. Mater. Chem.* **2009**, *1*, 124-130.
210. Jozeliūnaitė, A. *Dynamic Hydrogen-Bonded Tubular Supramolecular Assemblies*. 2022, Vilnius University, Doctoral dissertation